

# Quantum entanglement in condensed matter systems

Nicolas Laflorencie

*Laboratoire de Physique Théorique, Université de Toulouse, CNRS, UPS, France*

---

## Abstract

This review focuses on the field of quantum entanglement applied to condensed matter physics systems with strong correlations, a domain which has rapidly grown over the last decade. By tracing out part of the degrees of freedom of correlated quantum systems, useful and non-trivial informations can be obtained through the study of the reduced density matrix, whose eigenvalue spectrum (the entanglement spectrum) and the associated Rényi entropies are now well recognized to contains key features. In particular, the celebrated area law for the entanglement entropy of ground-states will be discussed from the perspective of its subleading corrections which encode universal details of various quantum states of matter, *e.g.* symmetry breaking states or topological order. Going beyond entropies, the study of the low-lying part of the entanglement spectrum also allows to diagnose topological properties or give a direct access to the excitation spectrum of the edges, and may also raise significant questions about the underlying entanglement Hamiltonian. All these powerful tools can be further applied to shed some light on disordered quantum systems where impurity/disorder can conspire with quantum fluctuations to induce non-trivial effects. Disordered quantum spin systems, the Kondo effect, or the many-body localization problem, which have all been successfully (re)visited through the prism of quantum entanglement, will be discussed in details. Finally, the issue of experimental access to entanglement measurement will be addressed, together with its most recent developments.

---

## Contents

<b>1</b>	<b>Introduction</b>	<b>4</b>
<b>2</b>	<b>Universality beyond the area law</b>	<b>6</b>
2.1	The area law . . . . .	6
2.1.1	One dimension . . . . .	6
2.1.2	$d > 1$ fermions . . . . .	8
2.1.3	Non-interacting bosons . . . . .	9
2.2	Corrections to the area law for various states of matter . . . . .	10
2.2.1	State of the art . . . . .	10
2.2.2	Corner contributions in dimension $d = 2$ . . . . .	12
2.3	Continuous symmetry breaking . . . . .	16
2.3.1	Large $s$ approach for $d = 2$ . . . . .	16
2.3.2	Quantum Monte Carlo simulations . . . . .	21
2.3.3	Summary and outlook . . . . .	24
2.4	Long-range entanglement in topologically ordered phases . . . . .	25
2.4.1	Topological entanglement entropy . . . . .	25
2.4.2	Numerical results . . . . .	26
<b>3</b>	<b>Entanglement spectroscopy</b>	<b>30</b>
3.1	Entanglement spectrum in one dimension and beyond . . . . .	30
3.1.1	Quantum spin chains and ladders . . . . .	30
3.1.2	Conventional ordered and gapped states in $d > 1$ . . . . .	38
3.2	Entanglement spectroscopy of topological order . . . . .	40
3.2.1	Identify topological order with entanglement spectra . . . . .	41
3.2.2	Correspondence between edge and entanglement spectra . . . . .	43
3.2.3	Chiral spin liquid state . . . . .	44
3.3	Entanglement Hamiltonian . . . . .	45
3.3.1	Boundary theories for gapped phases . . . . .	45
3.3.2	Participation spectroscopy . . . . .	48
3.3.3	Gapless states . . . . .	51

<b>4</b>	<b>Impurity and disorder effects</b>	<b>55</b>
4.1	Disordered quantum spin systems . . . . .	55
4.1.1	Entanglement in random spin chains . . . . .	56
4.1.2	Entanglement, disorder, and RG flows . . . . .	59
4.1.3	$d > 1$ Infinite randomness . . . . .	61
4.2	Entanglement and Kondo physics . . . . .	63
4.2.1	Generalities . . . . .	63
4.2.2	Impurity entanglement in the one-channel Kondo problem	64
4.2.3	Boundary effects . . . . .	68
4.2.4	Other examples of quantum impurity problems probed by entanglement . . . . .	71
4.3	Many-body localization . . . . .	72
4.3.1	General properties . . . . .	72
4.3.2	Area <i>vs.</i> volume law for highly excited states . . . . .	75
4.3.3	Entanglement growth after global quantum quenches . . .	78
4.3.4	Open questions . . . . .	83
<b>5</b>	<b>Towards entanglement measurement</b>	<b>85</b>
5.1	Quantum noise and bipartite fluctuations . . . . .	86
5.1.1	Bipartite fluctuation as an entanglement meter . . . . .	86
5.1.2	Bipartite fluctuations to detect quantum criticality . . . .	89
5.1.3	Experimental proposal . . . . .	95
5.2	Entanglement detection and measure in cold atom experiments .	97
5.2.1	Theoretical proposals using SWAP-based protocols . . . .	97
5.2.2	First measurements . . . . .	98
<b>6</b>	<b>Conclusion</b>	<b>100</b>
6.1	Summary . . . . .	100
6.2	Open questions . . . . .	100
<b>7</b>	<b>Bibliography</b>	<b>103</b>

## 1. Introduction

The "spooky" nature of quantum entanglement has been a subject of several and intense debates since the early days of quantum mechanics [1, 2]. At first attached to fundamental questions regarding the formulation and the foundations of quantum mechanics, in particular after Bell's theorem [3, 4], the concept of entanglement has recently generated an enormous interest in several communities [5, 6, 7, 8, 9, 10, 11, 12, 13, 14, 15], *e.g.* atomic physics and quantum optics, condensed matter, mathematical physics, high energy physics, quantum information and quantum cryptography, cosmology, etc.

Shortly after the seminal works of Bennett and co-workers [5] on quantum teleportation, the study of entanglement in condensed matter model systems has strongly benefited from the rapid development of quantum information [16, 17]. Built at the interface of quantum information science, condensed matter theory, statistical physics, quantum field theory, the study of many-body entangled states rapidly has become a very active topic, in particular triggered by the discovery that entanglement could serve as a new smoking gun for quantum critical phenomena [18, 19, 20, 21]. In parallel, numerical approaches for quantum many-body systems have also taken advantage of such progresses, with the impressive development of very efficient variational techniques such as matrix-product-state and tensor network methods [22].

The framework of quantum entanglement for condensed matter physics is nowadays very wide, and this topic has certainly acquired now a robust and mature status. It is therefore quite ambitious and perhaps illusory to pretend giving an exhaustive overview. Consequently, some aspects of quantum entanglement in condensed matter systems will not be discussed here. For instance, we will not address multipartite entanglement, focusing on the bipartite case, as exemplified in Fig. 1 for a two-dimensional ( $d = 2$ ) system. In such a case, assuming  $|\Psi\rangle$  is a pure state defined over degrees of freedom of  $A \cup B$ , the central object of interest in this review article will be the reduced density matrix



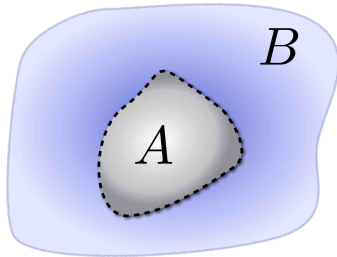


Figure 1: Real space bipartition of a physical system (here in dimension  $d = 2$ ) in two parts.

(RDM) associated with such a real space bipartition<sup>1</sup>, defined by

$$\rho_A = \text{Tr}_B |\Psi\rangle\langle\Psi|. \quad (1)$$

The eigenvalues of  $\rho_A$  (the entanglement spectrum) and the corresponding Rényi entanglement entropy

$$S_q(A) = \frac{1}{1-q} \ln \text{Tr}(\rho_A^q) \quad (2)$$

will be the main targets of this overview.

In a first part (Section 2) the celebrated area law for the ground-state entanglement entropy will be briefly discussed, preferring to focus on sub-leading correcting terms which carry universality for various quantum states of matter, broken symmetries and topological properties. In Section 3, entanglement spectroscopy results will be presented for a large variety of low-dimensional correlated ground-states, *e.g.* gapped and gapless spin chains and ladders, topological ordered phases such as fractional quantum Hall states or spin liquids, broken continuous symmetry states such as superfluids. Disorder quantum systems will then be considered in Section 4, focusing on three important cases. First we address ground-state entanglement for disordered quantum spin models and Kondo impurity problems. Then the many-body localization of excited states will be discussed through entanglement features. Finally, Section 5 will address the crucial issue of experimental detection and measure of entanglement. Finally, conclusions and some open questions will be listed in Section 6.

---

<sup>1</sup>Other types of bipartitions (momentum or orbital) will also be considered, see Section 3.

## 2. Universality beyond the area law

### 2.1. The area law

As originally studied by Bombelli *et al.* [23], Srednicki [24], Callan and Wilczek [25], Holzhey *et al.* [26] in the context of black-hole physics [27], the geometric, or entanglement entropy in the ground-state of a free scalar bosonic field is well-known to obey the so-called area law, *i.e.* in dimension  $d$  it scales with the surface of the subsystem  $A$ :

$$S_q(A) \propto L^{d-1}. \quad (3)$$

In this section, we simply give a short survey of this topic, which has been recently reviewed in a thorough way by Eisert, Cramer, and Plenio [13].

#### 2.1.1. One dimension

For one dimensional quantum systems, one has to make a distinction between critical and non-critical ground-states. Indeed, strictly speaking the area law for  $d = 1$  yields a constant entropy, independent of the subsystem size. As proved by Hastings [28] this only occurs for non-critical ground-states having a finite correlation length. This is exemplified in Fig. 2 (a) where we show exact diagonalization results obtained for the dimerized quantum spin-1/2 chain model

$$\mathcal{H}_{\text{1dxy}}(\delta) = \sum_{i=1}^L [1 + \delta(-1)^i] (S_i^x S_{i+1}^x + S_i^y S_{i+1}^y). \quad (4)$$

This system, equivalent to a free-fermion problem after a Jordan-Wigner transformation [29], has a gap above its short-range correlated dimerized ground-state for any  $\delta \neq 0$  [30], and is critical with power-law decaying correlations in the absence of modulation  $\delta = 0$ . The uniform part of the von-Neumann ( $q = 1$ ) entanglement entropy is plotted against the subsystem length  $\ell_A$  for increasing dimerization strengths in Fig. 2 (a) where we clearly see that  $S_1$  gets saturated to a constant, as expected for  $d = 1$  with short-range correlations [28, 31]. On the other hand, critical chains described by conformal field theory (CFT) [26, 21]

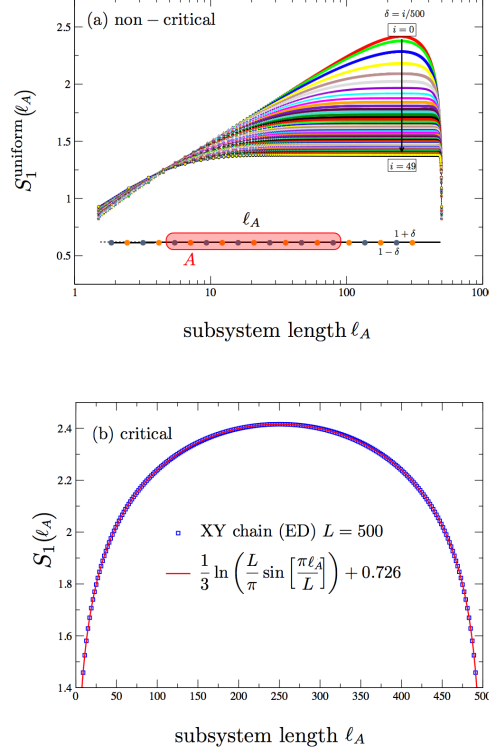


Figure 2: Left (a): Uniform part of the entanglement entropy  $S_1^{\text{uniform}}(\ell_A)$  of a non-critical dimerized spin- $\frac{1}{2}$  XY chain plotted against the subsystem length  $\ell_A$  for various dimerization strengths  $\delta = i/500$ ,  $i = 0, \dots, 49$ . Exact diagonalization results for periodic chains of  $L = 500$  sites. Right (b): Critical (gapless) spin- $\frac{1}{2}$  XY chain ED results compared to the log scaling from conformal field theory Eq. (5) with the exact additive constant calculated by Jin and Korepin [32].

display a logarithmic violation of the strict area law, as Rényi entropies grow with the subsystem length  $\ell_A$  following the universal form

$$S_q(A) = \frac{c}{6} \left( 1 + \frac{1}{q} \right) \ln \left( \frac{L}{\pi} \sin \left[ \frac{\pi \ell_A}{L} \right] \right) + s_q + \dots \quad (5)$$

for periodic chains of length  $L$ . The constant term  $s_q$  is non-universal but can be evaluated exactly in some cases [32], see Fig. 2 (b). The ellipses in Eq. (5) represent subleading corrections to scaling, vanishing as power-laws of the subsystem size involving the Luttinger liquid exponent [33, 34].

### 2.1.2. $d > 1$ fermions

Conventional metals, described as free fermions or Fermi liquids are known to weakly violate the area law by a multiplicative logarithmic correction [35, 36, 37, 38] if there is a well-defined Fermi surface, while for non-critical fermions the entropy obeys a strict area law. This logarithmic enhancement can be related to the topology of the Fermi surface [36, 39, 40, 41] through

$$S_q(A) = \frac{q+1}{24q} \iint d\mathcal{A}_x d\mathcal{A}_k |n_x \cdot n_k| \left( \frac{\ell_A}{2\pi} \right)^{d-1} \times \ln \ell_A + o(\ell_A^{d-1} \ln \ell_A), \quad (6)$$

where  $n_x$  and  $n_k$  are units normal to the real space boundary  $\mathcal{A}_x$  and the Fermi surface  $\mathcal{A}_k$ . One can also understand such a weak violation of the area law using a low-energy description of the Fermi surface like an ensemble of one dimensional gapless modes, as proposed by Swingle [40, 42]. A multidimensional bosonization approach gives essentially similar results for Fermi liquids [43].

Another very interesting result for free fermions came with the seminal works by Klich and co-workers on quantum noise [44, 45]. They found a direct link between entanglement entropies and the fluctuations of a globally conserved quantity within a subsystem, for instance the particle number for Fermi gases or the subsystem magnetization for quantum magnets. This has motivated a large number of subsequent studies [46, 47, 48, 49, 50, 51, 52, 53, 54, 55, 56, 57]. Remarkably, using the full counting statistics [58] there is an exact expression for all Rényi entropies [49]. This is further discussed below in Section 5.1.1.

Particle number fluctuations and entanglement entropies have also been explored in the context of ultracold Fermi gases [59, 54, 50, 60]. Note also that in a similar context, connections to random matrix theory have been recently discussed [61, 55, 62, 63] to obtain analytic expressions in various regimes of a one dimensional gas confined by a harmonic trap.

On the numerical side, recent progresses have also been made using quantum Monte Carlo (QMC) techniques for accessing entanglement properties of interacting fermions [64, 65, 66, 67, 68, 69, 70]. In particular, emergent fermions (spinons) with a Fermi surface have been detected through the logarithmic enhancement of the area law in a critical quantum spin liquid state using vari-

ational Monte Carlo [64]. Nevertheless, a relatively unexplored field concerns non-Fermi liquids for which Swingle and Senthil argued for a similar logarithmically enhanced area law [71]. Using a variational Monte Carlo approach the composite fermion wave function [72] for half-filled Landau level  $\nu = 1/2$ , a non-Fermi liquid state, has been shown to indeed exhibit a logarithmically enhanced area law, but with a prefactor twice larger [73].

Another interesting example is the Bose metal state, the so-called exciton Bose liquid [74] which displays a "Bose surface" with gapless excitations, for which a logarithmic enhancement of the area law was found [75, 76].

Let us finally mention that free fermions in a weak random potential, but still in a metallic (diffusive) regime, loose logarithmic enhancement and obey a strict area law for the mean entropy [77, 78, 79]. This can be understood from the smearing of the sharp Fermi surface by disorder, despite a finite density of gapless states [78].

### 2.1.3. *Non-interacting bosons*

We now turn to the case of non-interacting bosonic models. In contrast with the free fermions case, free bosons with non-relativistic quadratic dispersion display Bose-Einstein condensation. In this context, the area law term is suppressed, and the dominant scaling of the Rényi entropy is logarithmic with the number of particles [80, 81]. This situation is somehow unphysical, and can be understood as a mean-field limit for which we do not expect a well-defined "area". Below we will see in Sec. 2.3 that any interaction will restore the area law term, while additional logarithmic corrections associated to Nambu-Goldstone modes are expected.

For a relativistic free bosonic field theory, which is equivalent to a system of coupled harmonic oscillators, Rényi entropies scale with the area in dimension  $d > 1$  [23, 24, 25, 26]. This was clearly confirmed numerically for critical and non-critical regimes where, contrary to free fermions, a strict area law is observed in both cases [82, 38]. Numerical evaluation for lattice quadratic Hamiltonians is made possible using Wick's theorem, as shown by Chung and Peschel [83].

## 2.2. Corrections to the area law for various states of matter

### 2.2.1. State of the art

The area law term discussed above does not a priori carry information regarding a given phase of matter. Nevertheless, it has been shown to display critical behavior when a quantum phase transition is crossed, developing a local extremum at a critical point  $g = g_c$  [84, 85, 86, 87, 88], with  $a_q(g_c) - a_q(g) \propto |g - g_c|^{\nu(d-1)}$ , where  $\nu$  is the correlation length exponent associated to the critical point. Fig. 3 shows such cusp singularities for O(3) [87] and O(2) [88] quantum critical points. This singular behavior is natural if one interprets the entropy as a surface or boundary free energy [89].

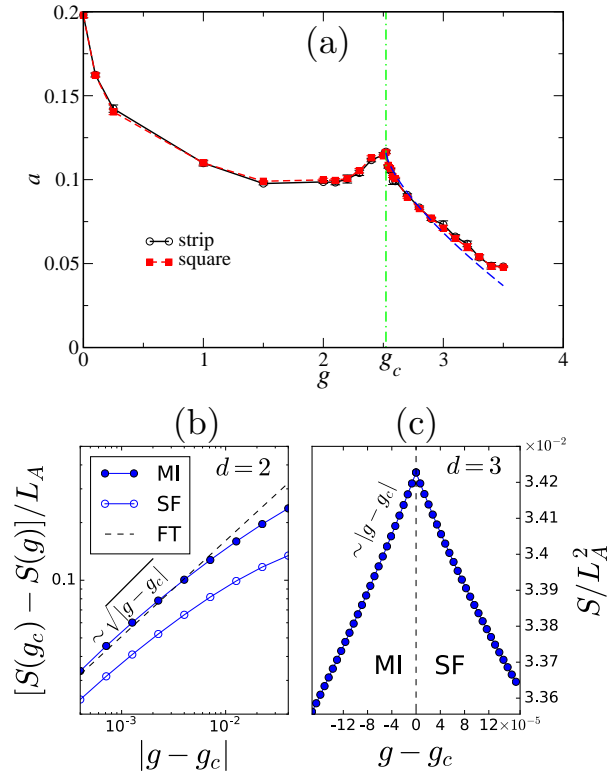


Figure 3: Cusp singularity for the area law prefactor across a quantum phase transition. (a) QMC results for a  $s = 1/2$  Heisenberg bilayer, from [87]. (b) Schwinger-boson results for the superfluid - insulator transition in  $d = 2$  and (c)  $d = 3$ , from [88].

Going beyond the leading area law term, universal signatures are expected for various quantum phases of matter. The first discussed and celebrated example is for (1+1) CFT which describes critical interacting  $d = 1$  quantum chains [20, 21, 90], with the logarithmic growth Eq. (5) involving the central charge  $c$  of the underlying CFT. In higher dimension, several authors have studied the problem which turns out to be much richer [89, 91, 84, 92, 93, 94, 95, 96, 97, 98, 99, 86, 100, 87, 101, 102, 103].

In Table 1, we give a simplified overview of different quantum states of matter with their associated entanglement entropy scalings, and physical examples of realizations. Generally speaking, ordered states can be classified in three main families. For discrete symmetry breaking, a trivial additive constant depending only on the degeneracy of the ground-state is expected  $\ln(\text{deg})$  [92]. In the case of continuous symmetry breaking, *e.g.*  $U(1)$  for superfluids or  $SU(2)$  for Heisenberg antiferromagnets, additional logarithmic corrections due to Nambu-Goldstone modes are present [104, 96], as we discuss in detail below in Section 2.3. For topological ordered phases, there is a negative constant [105, 106], as will be discussed in Section 2.4. At quantum critical points, for instance  $O(N)$ , an additive constant appears [84]. Note also the numerical study on cubic subsystems for the  $d = 3$  quantum Ising model [107].

Physical state	Entropy	Example
Gapped (brok. disc. sym.)	$aL^{d-1} + \ln(\text{deg})$	Gapped XXZ [92]
$d = 1$ CFT	$\frac{c}{3} \ln L$	$s = \frac{1}{2}$ Heisenberg chain [21]
$d \geq 2$ QCP	$aL^{d-1} + \gamma_{\text{QCP}}$	Wilson-Fisher $O(N)$ [84]
Ordered (brok. cont. sym.)	$aL^{d-1} + \frac{n_G}{2} \ln L$	Superfluid, Néel order [96]
Topological order	$aL^{d-1} - \gamma_{\text{top}}$	$\mathbb{Z}_2$ spin liquid [108]

Table 1: Entanglement entropy scaling for various examples of states of matter, either disordered, ordered, or critical, with smooth boundaries (no corners).

### 2.2.2. Corner contributions in dimension $d = 2$

We first focus on the issue of subsystems having non-smooth boundaries with the particular example of sharp corners in two dimensions which are responsible for additive logarithmic corrections to the area law, as studied in several works [89, 109, 94, 110, 86, 100, 87, 101, 111, 112, 113, 114, 115]. The area law is indeed corrected as follows

$$\Delta S_q^c = \left( \sum_c l_q^c \right) \ln L, \quad (7)$$

where the sum is taken over sharp corner angles. With smooth boundaries, such a logarithmic divergence occurs only for odd dimensions [10, 116]. For even values of  $d$ , sharp angles lead to logarithmic corrections which are expected to be universal for all systems with the same type of symmetry breaking/phase transition. In  $d = 2$  it has been studied in several situations, such as CFT with  $z \neq 1$  where the prefactor was shown to be directly proportional to the central charge [89]. For free scalar field theory, Casini and Huerta have provided an analytical solution [109] for integer  $q \geq 2$  while it involves a tricky numerical solution of a set of non-linear differential equations, valid for  $\varphi_c \in [0, \pi]$  ( $l_q(\varphi) = l_q(2\pi - \varphi)$ ). Below in Fig. 4 we show numerical results obtained in Ref. [112] for non-interacting relativistic bosons on a square lattice, reproducing the free scalar field results of Casini and Huerta.

In order to extract the corner corrections, we study square subsystems (having 4 corners, each with  $\varphi = \pi/2$ ) of perimeter  $2L$  (embedded in a  $L \times L$  torus) at which one subtracts the entropies from corner-free strips  $\ell \times L$  having the same perimeter so that the area law contribution cancels, as well as other potential corrections (*e.g.* Goldstone modes for continuous symmetry breakings, see also below in Section 2.3).

Working with spin-wave (SW) corrections of an  $SU(2)$  model [112], there are two Nambu-Goldstone modes from which we expect the leading term of this difference to be given by

$$S_q^{\text{square}} - S_q^{\text{strip}} = 8l_q(\pi/2) \ln L + \dots \quad (8)$$



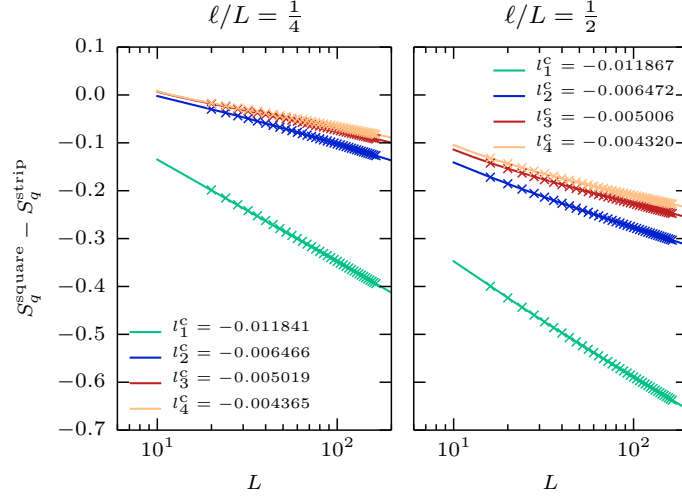


Figure 4: Difference of entanglement entropies for  $d = 2$  relativistic spin-waves (free bosons) between square and strip geometries, yielding the logarithmic corrections Eq. (8). Fits (full lines) to the form  $8l_q(\pi/2) \ln(L) + b_q + c_q/L + d_q/L^2$  are shown by full lines. Exact diagonalization results (symbols) are displayed for two different aspect ratios of the strips and various Rényi parameters  $q = 1, 2, 3, 4$ . Reprinted from [112].

Numerical diagonalization results of the non-interacting SWs Hamiltonian [112] are plotted in Fig. 4 where we clearly see that the above difference Eq. (8) is clearly dominated by a logarithmic scaling which allows us to extract  $l_q(\pi/2)$ . Small variations of the results for different aspects ratios of the strips (see left and right panels of Fig. 4) can be used as a measure of the error due to finite size effects and fitting procedure. Our results, in perfect agreement with those of Casini and Huerta [109], are displayed in Table 2 together with other estimates for interacting field theories obtained from numerical simulations using series expansion [117], numerical linked cluster expansion [86, 100, 101] or QMC [118]. Note that extracting such small log corrections is very challenging for interacting fixed points and series or numerical linked cluster expansion turns out to be more controlled than QMC for this task.

The fact that universality emerges in the corner logarithmic terms is remarkable. It was then proposed that the prefactor of the logarithmic correction is an

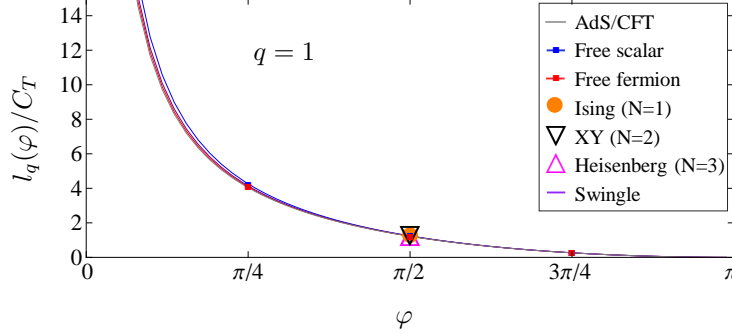


Figure 5: Universal ratio  $l_q(\varphi)/C_T$  for various  $2+1$  CFT at  $q=1$ : holography (gray), free Dirac fermion (red), scalar field (blue). Numerical results for Wilson-Fisher  $O(N)$  fixed points: Ising [86], XY [101], and Heisenberg [100] are shown at  $\varphi = \pi/2$ , as well as Swingle’s [110] trial function  $\pi^2/8 [1 + (\pi - \varphi) \cot(\varphi)]$ . Reprinted from Ref. [111].

effective measure of the degrees of freedom of the underlying CFT [109, 116, 100]. Using CFT and holographic calculations, Bueno and co-workers have suggested that the ratio  $l_q(\varphi)/C_T$  is universal for a broad range of CFT, including Wilson-Fisher fixed points of the  $O(N)$  model [111, 113, 114] (see Fig. 5), where  $C_T$  is the central charge of the stress tensor correlator. Various estimates of this ratio are reported in Table 2 for  $q=1, 2$  at angle  $\varphi = \pi/2$ , using the central charge obtained from conformal bootstrap methods [119]. One sees that the agreement is reasonably good, in particular for  $q=2$ . Note however a recent numerical work [115] where the inclusion of unusual scaling corrections improves infinite size extrapolations of the corner coefficients, yielding in particular a smaller value for  $O(1)$  at  $q=1$ , in better agreement with the predicted universal ratio.

Finally, we can also investigate the Rényi index dependence for non-integer values of  $q$ . In Fig. 6 we report numerical linked expansions results for (a)  $O(2)$  [101] and (b)  $O(3)$  [100] together with different estimates for the Ising fixed point, as well as our estimate for free scalar [112]. The non-trivial  $q$ -dependences are qualitatively similar, and the ratio between  $O(2)$  and  $O(1)$  is well compatible with 2, although indistinguishable from the CFT prediction  $\simeq 2.00625$  of Bueno *et al.* [111], as well as for  $O(3)$  with a factor 3, again perfectly compatible with the CFT result  $\simeq 3.0077$  [111].

	$-l_1(\pi/2)$	$-\frac{l_1(\pi/2)}{C_T}$	$-l_2(\pi/2)$	$-\frac{l_2(\pi/2)}{C_T}$
O(1)	0.013(1) [86, 101]	1.4(1)	0.0055(5) [117, 86]	0.61(5)
O(2)	0.024(1) [101]	1.34(6)	0.011(1) [101, 118]	0.61(6)
O(3)	0.036(2) [100]	1.34(8)	0.017(1) [100, 87]	0.63(4)
Free scalar	0.0118(1) [109, 112]	1.24(1)	0.0064(1) [109, 112]	0.67(1)

Table 2: Prefactor  $l_q(\pi/2)$  of the corner logarithmic correction in Eq. (7). Most of these results come from numerical simulations for Wilson-Fisher fixed points of the  $O(N)$  models. The putative universal ratio  $l_q/C_T$  [111, 113] is also reported.

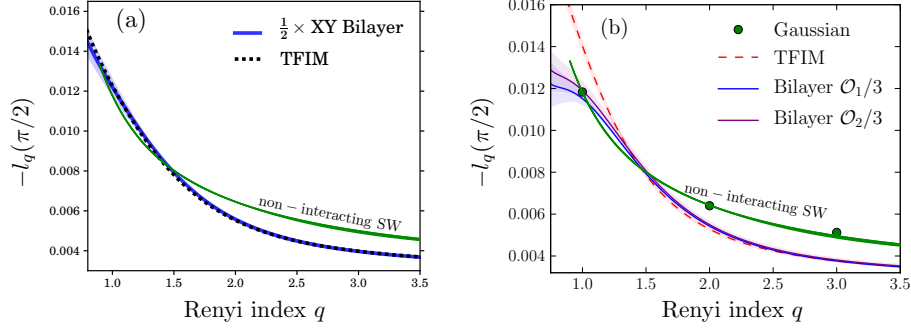


Figure 6: Corner coefficient of the logarithmic correction in Eq. (7) for a  $\pi/2$  angle, plotted as a function of the Rényi index  $q$  for various critical theories in  $2+1$  dimensions. (a) Estimates for an  $O(2)$  critical point obtained with numerical linked cluster expansion calculations on an XY bilayer are twice the coefficient of the  $O(1)$  Ising fixed point. Reprinted from [101]. (b) The Heisenberg  $O(3)$  case studied with numerical linked cluster expansion with two types of cluster expansions ( $\mathcal{O}_1$  and  $\mathcal{O}_2$ ), is seemingly thrice the  $O(1)$  result, at least for  $q \geq 1.3$ . Reprinted from [100]. For both cases, the free scalar result from non-interacting SW [112] is shown (green line) for comparison. Note the difference in the estimates for Ising between the two panels, as commented in Ref. [101] where larger clusters were used (left panel).

### 2.3. Continuous symmetry breaking

For condensed matter systems presenting a spontaneous breaking of continuous symmetry at zero temperature in the thermodynamic limit, such as Bose-condensed superfluids or ordered antiferromagnets, additive logarithmic corrections have been originally observed using modified SW theory [104] and numerical simulations [120] on  $d = 2$  quantum antiferromagnets. Shortly after, Metlitski and Grover [96] proposed an analytical interpretation based on quantum rotor and non-linear sigma models where both SW excitations and the "tower of states" (TOS) due to the symmetry restoration in a finite volume [121, 122] are responsible for a logarithmic correction, proportional to the number of Nambu-Goldstone modes  $n_G$  associated with the symmetry breaking, thus yielding

$$S_q = a_q L^{d-1} + \frac{n_G}{2} \ln \left( \frac{\rho_s}{v} L^{d-1} \right) + \gamma_q^{\text{ord}}, \quad (9)$$

where  $\rho_s$  is the stiffness,  $v$  the SW velocity, and  $\gamma_q^{\text{ord}}$  a universal geometric constant (see below).

#### 2.3.1. Large $s$ approach for $d = 2$

*Logarithmic corrections due to Nambu-Goldstone modes*—. As developed in Refs. [104, 123, 112] for ordered phases where a continuous symmetry is broken, a SW (SW) treatment allows to capture subleading corrections in Eq. (9). A canonical example is the so-called  $J_1 - J_2$  spin- $s$  antiferromagnet [124], governed on the square lattice by the Hamiltonian

$$\mathcal{H} = J_1 \sum_{\langle ij \rangle} \vec{S}_i \cdot \vec{S}_j + J_2 \sum_{\langle\langle ij \rangle\rangle} \vec{S}_i \cdot \vec{S}_j + h \sum_i (-1)^i S_i^z. \quad (10)$$

When the external staggered field  $h = 0$ , this model exhibits Néel order with a spontaneous breaking of  $\text{SU}(2)$  symmetry in the thermodynamic limit at  $T = 0$  if  $J_2 < J_c(s)$  [124], with  $J_c \rightarrow J_1/2$  for  $s \gg 1$ . Replacing spin- $s$  operators by Holstein-Primakoff bosonic deviations about the classically ordered moment allows to expand the above  $J_1 - J_2$  model as  $\mathcal{H}/s^2 = E_{\text{cl.}} + \mathcal{H}^{(2)}/s + \mathcal{H}^{(4)}/s^2 + \dots$ , where  $E_{\text{cl.}}$  is the classical energy of the ordered ground-state,  $\mathcal{H}^{(2)}$  is a quadratic

Hamiltonian in term of Holstein-Primakoff bosons, and  $\mathcal{H}^{(4)}$  is quartic. Truncating the above expansion at the quadratic ( $1/s$ ) level usually captures most of the low-energy physics of quantum antiferromagnets [125], and we further expect better accuracy for  $s \gg 1$ . Such a treatment leads to the quadratic bosonic model

$$\mathcal{H}^{(2)} = \sum_{\mathbf{k}} A_{\mathbf{k}}(b_{\mathbf{k}}^{\dagger} b_{\mathbf{k}} + b_{-\mathbf{k}}^{\dagger} b_{-\mathbf{k}}) + B_{\mathbf{k}}(b_{\mathbf{k}}^{\dagger} b_{-\mathbf{k}}^{\dagger} + b_{\mathbf{k}} b_{-\mathbf{k}}), \quad (11)$$

where  $A_{\mathbf{k}} = 2s(J_2 \cos k_x \cos k_y + J_1 - J_2) + \frac{h}{2}$  and  $B_{\mathbf{k}} = -sJ_1(\cos k_x + \cos k_y)$  that we solve using a standard Bogoliubov transformation, yielding a quasi-particle dispersion  $\Omega_{\mathbf{k}} = 2\sqrt{A_{\mathbf{k}}^2 - B_{\mathbf{k}}^2}$ . In the vicinity of its two minima at  $\mathbf{k}_0 = (0, 0)$  and  $(\pi, \pi)$  the SW dispersion takes the relativistic form

$$\Omega_{\mathbf{k}} \approx v\sqrt{|\mathbf{k} - \mathbf{k}_0|^2 + m^2}, \quad (12)$$

with a velocity  $v = 2\sqrt{2}s\sqrt{J_1(J_1 - 2J_2)}$  and a mass gap  $m = \sqrt{\frac{h}{s(J_1 - 2J_2)}}$ . Such a (small) gap plays a crucial role for finite lattice calculations. Indeed, in order to correct the fact that spin rotational symmetry is broken on finite lattices within the SW framework, one can artificially proceed to a fictitious restoration by adjusting the staggered field  $h$  in Eq. (10) so that the (SW-corrected) sublattice magnetization vanishes, following Refs. [126, 127]. As discussed in Refs. [104, 123, 112], such a (size-dependent) artificial staggered field has to scale as  $h^* \approx \frac{2J_1}{sL^4}$  for  $L \times L$  lattices in the large  $s$  limit. Interestingly, the induced gap has precisely the Anderson TOS scaling [121, 122]

$$m^*(L) = \sqrt{\frac{2J_1}{s^2(J_1 - 2J_2)}} \frac{1}{L^2}. \quad (13)$$

Such a finite size regularization allows to access Rényi entanglement entropies  $S_q(A)$  for various shapes of subsystem  $A$  [123, 112] by means of numerical diagonalization using the correlation matrix technique [128]. In Fig. 7 we show  $S_q(A)$  results for  $L \times \ell$  strip subsystems  $A$  (panel b) embedded in  $L \times L$

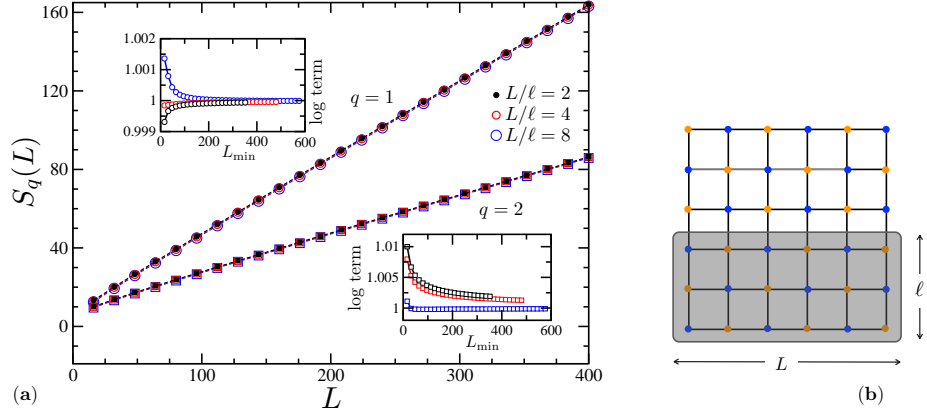


Figure 7: (a) SW results for the entanglement Rényi entropies ( $q = 1, 2$ ) of the square lattice Heisenberg model Eq. (10) with  $s = 100$  and  $J_2 = 0$  for strip subsystems (panel b) with different aspect ratios  $\ell/L$ , plotted against  $L$ . The insets of (a) show fit results for the prefactor of the log correction as a function of the minimal system size  $L_{\min}$  included in the fit. The log prefactor unambiguously converges to 1, independently of  $q$  and of the aspect ratio of the subsystem. Data taken from Ref. [112]

tori, up to  $600 \times 600^2$  with a large spin length  $s = 100$ . This plot shows that (i) the area law term does not depend on the aspect ratio of the subsystem, and (ii) the logarithmic correction in Eq. (9) is precisely governed by the prefactor  $n_G/2 = 1$ , independent of the Rényi index. The logarithmic corrections in Eq. (9) have been also captured within a similar SW formalism for  $d = 3$  U(1) and SU(2) cases [129], and also using a Schwinger boson formalism [88].

*Universal additive constant  $\gamma_q^{\text{ord}}$* —. In the case of  $d = 2$  strip subsystems with an aspect ratio  $\ell/L$ , Metlitski and Grover have also predicted the existence of an additive universal constant  $\gamma_q^{\text{ord}}(\ell/L)$  in the scaling of the Rényi entropies in Eq. (9). Using the large- $s$  expression for the stiffness  $\rho_s = s^2(J_1 - 2J_2)$  and the velocity  $v = 2\sqrt{2}s\sqrt{J_1(J_1 - 2J_2)}$ , one can extract  $\gamma_q^{\text{ord}}(\ell/L)$  by fitting our numerical data to the above form Eq. (9), as displayed in Fig. 8 against the

<sup>2</sup>Note that in order to access such large systems, translation symmetry of the subsystems was used for the strip geometry, thus optimizing the diagonalization procedure for large sizes.

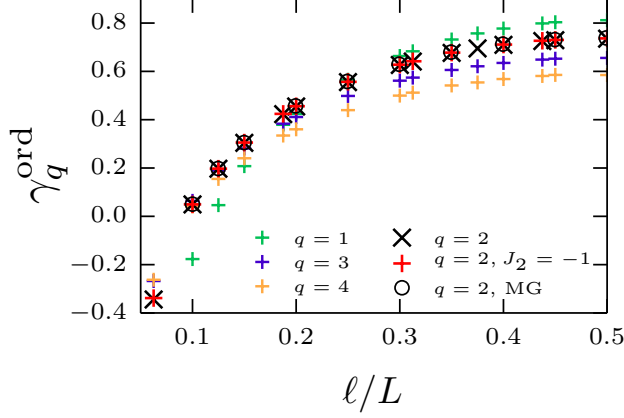


Figure 8: Additive constant  $\gamma_q^{\text{ord}}(\ell/L)$  for various Rényi parameters  $q$  as a function of  $\ell/L$  for  $s = 100$ , and  $J_2 = 0, -1$ . Perfect agreement with Metlitski and Grover (o) [96] is found for  $q = 2$ . Results for  $J_2/J_1 = -1$  at  $q = 2$  (+) agree perfectly with  $J_2 = 0$  (x), confirming universality. Reprinted from Ref. [112]

aspect ratio  $\ell/L$ . Results compare perfectly to those of Ref. [96] for Rényi  $q = 2$ . Universality is also confirmed by the fact that the results do not depend on the value of the second neighbor couplings  $J_2$ .

*Connection to free scalar field theory*— An attempt to directly connect this result to free scalar field theory has also been made in Refs. [96, 112]. On finite lattices, a diverging contribution from the zero mode has to be cut off by a small gap in the relativistic spectrum [38]. For a free scalar field, a small mass leads to a logarithmic correction to the entanglement entropy  $\sim \ln(\frac{1}{mL})$  [96]. However, an additional geometric constant  $\gamma_q^{\text{free}}(\ell/L)$ , which depends on the Rényi coefficient  $q$  and the aspect ratio  $\ell/L$  of strip subsystems, is also expected [96], thus yielding

$$S_q = a_q L - \frac{1}{2} \ln(mL) + \gamma_q^{\text{free}}(\ell/L). \quad (14)$$

This behavior can be checked numerically for relativistic bosons on a square lattice, described by Eq. (11) with  $A_{\mathbf{k}} = 2t - t(\cos k_x + \cos k_y)/2 - \Gamma/2$  and  $B_{\mathbf{k}} = t(\cos k_x + \cos k_y)/2$ . Using a very small (albeit size-independent) mass gap  $m = \sqrt{\Gamma/t} = 10^{-9}$ , exact diagonalization results for  $S_1 + \frac{1}{2} \ln(mL)$  are

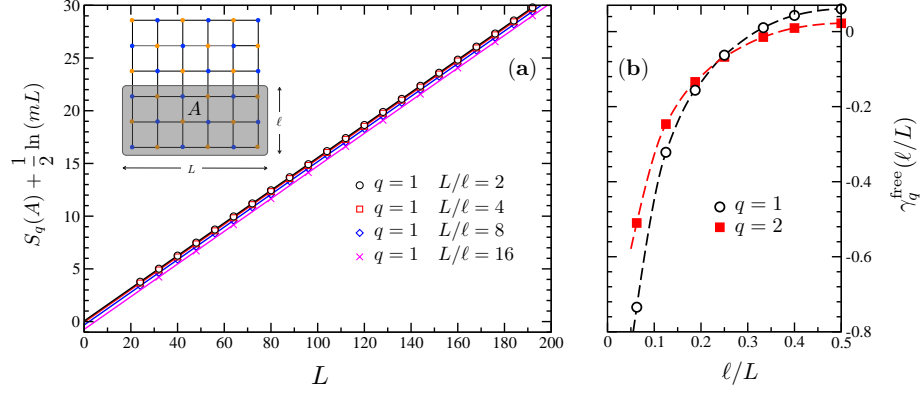


Figure 9: Rényi entanglement entropies of relativistic free bosons on the square lattice governed by the lattice Hamiltonian Eq. (11) with a small mass gap  $m = 10^{-9}$ . Subsystem  $A$  is a  $L \times \ell$  strip (grey region in the inset). Panel (a) shows the area law scaling for  $S_1(A) + \frac{1}{2} \ln(mL)$  for various aspect ratios. Panel (b) shows the geometric constant  $\gamma_q^{\text{free}}$  obtained from fits to the form Eq. (14) and plotted against  $\ell/L$ , the aspect ratio of subsystem  $A$ , for  $q = 1$  and  $q = 2$ . Lines are guides to the eyes.

displayed in panel (a) of Fig. 9 where, on top of the clear area law scaling, one see the aspect ratio dependence of the intercept at  $L \rightarrow 0$ , thus giving  $\gamma_q^{\text{free}}$ , displayed in the panel (b) against  $\ell/L$ .

Building on the result Eq. (14) for a single mode, the correction part for SU(2) antiferromagnets with  $n_G = 2$  relativistic Goldstone modes and a TOS gap given by the mass term  $m^*(L)$  in Eq. (13), can be expressed as  $\Delta S_q = \frac{n_G}{2} \ln\left(\frac{\rho_s}{v} L\right) + n_G (\ln \sqrt{2} + \gamma_q^{\text{free}})$ , where we have used the large  $s$  expression for the stiffness and the SW velocity. A direct comparison with Eq. (9) from Metlitski and Grover [96] yields

$$\gamma_q^{\text{ord su}(2)} = 2\gamma_q^{\text{free}} + \ln 2, \quad (15)$$

which agrees with them [96], but only at  $q = 2$ . Using similar arguments for the XY model with a single Goldstone mode [123], one gets

$$\gamma_q^{\text{ord u}(1)} = \gamma_q^{\text{free}} + \frac{5}{4} \ln 2, \quad (16)$$

which compares well to QMC results of Kulchytskyy *et al.* [130] (see below).



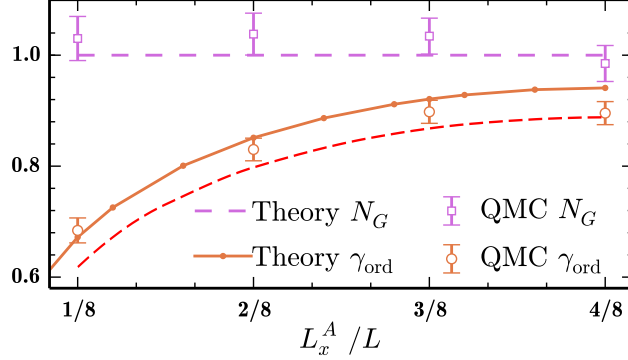


Figure 10: Subleading terms of the second Rényi entropy  $\frac{n_G}{2} \ln L$  and  $\gamma_2^{\text{ord}}$  from Eq. (9) obtained from QMC simulations of the  $d = 2$   $s = 1/2$  XY model at  $T = 0$ , up to  $L = 32$ . The red dashed line is the large- $s$  prediction Eq. (16). Reprinted from Ref. [130].

### 2.3.2. Quantum Monte Carlo simulations

*Entanglement entropies*—. One of the most efficient numerical method to diagnose continuous symmetry breaking in the entanglement scaling for dimension  $d \geq 2$  is based on QMC sampling, in particular after the work of Hastings *et al.* [131]. Density Matrix Renormalization Group (DMRG) studies of  $d = 2$  quantum spin or bosonic models where SU(2) [132, 133] or U(1) [81] symmetry may be broken are also available, but they did not focus on logarithmic corrections. The first QMC attempts [120, 134, 87] to check the Goldstone modes signature  $\frac{n_G}{2} \ln L$  in the entropy [96] have indeed found a logarithmic term for Heisenberg models, but estimated the prefactor in the range  $0.5 - 0.8$ , which is smaller than the predicted value of one (with  $n_G = 2$  for SU(2) symmetry).

More recently, Kulchytskyy *et al.* [130] have performed an improved measurement of the second Rényi entropy  $S_2$  for the square lattice  $s = 1/2$  XY model from which they could estimate both the log prefactor (here  $n_G = 1$  for U(1) symmetry), as well as the constant in Eq. (9)  $\gamma^{\text{ord}}$  for lattice up to  $32 \times 32$ . Their results for both quantities, shown in Fig. 10 as a function of the aspect ratio of the strip subsystem, appear to be in good agreement with the analytical prediction of Metlitski and Grover [96] as well as with the large- $s$  prediction Eq. (16) from Ref. [112].

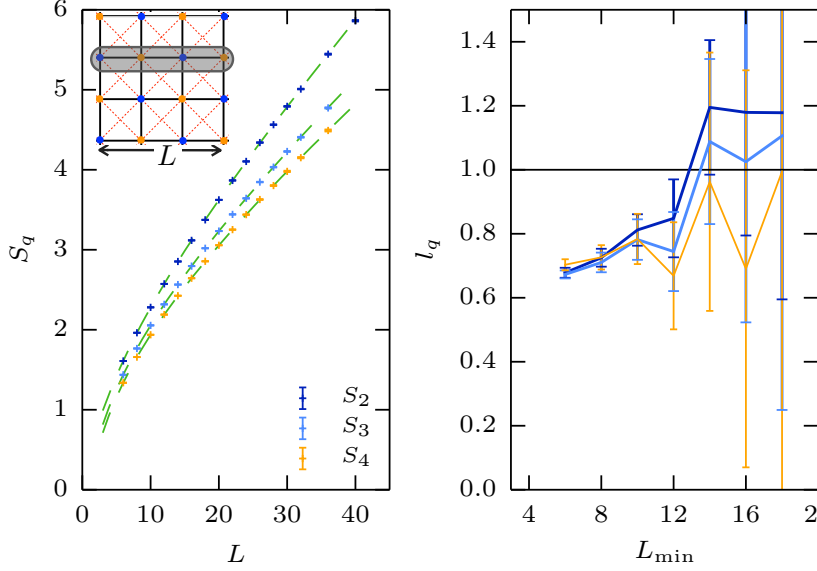


Figure 11: Left: QMC results for the entanglement Rényi entropies of the spin- $\frac{1}{2}$   $J_1 - J_2$  Heisenberg model for  $J_2/J_1 = -1$ , plotted against the length  $L$  of the subsystem line (depicted in the inset). Right: Prefactor of the logarithmic scaling term obtained by fits to the form  $S_q = a_q L + l_q \ln L + b_q + c_q/L$  over ranges  $[L_{\min}, L_{\max}]$  as a function of  $L_{\min}$ , with  $L_{\max} = 40$  for  $q = 2$  and  $L_{\max} = 36$  for  $q = 3, 4$ . Despite quite large error bars, these results are consistent with  $l_q = 1$  independent of  $J_2$  and  $q$ . Reprinted from Ref. [135].

In order to go beyond  $q = 2$ , building on the ratio trick proposed by Huhneniuk and Roscilde [134] one can improve the QMC estimate of Rényi (and also thermodynamic) entropies, as done in Ref. [135]. This method has been applied to the above  $s = 1/2$   $J_1 - J_2$  Heisenberg antiferromagnet on the square lattice Eq. (10), for which studying the Rényi entropies at  $q = 2, 3, 4$  of the simplest corner-free subsystem - a periodic one-dimensional line (see Fig. 11) - allowed to capture the logarithmic corrections with a prefactor close to unity, fully consistent with  $n_G = 2$  Goldstone bosons. The fact that universality can be captured for such a simple linear subsystem reinforces the idea that entanglement is dominated by boundary degrees of freedom.

*Shannon-Rényi entropies*—. Spontaneous breaking of a continuous symmetry also appears in the (basis-dependent) so-called "Shannon-Rényi" (SR) entropy computed in the ground-state of finite size systems. These wave-function entropies, recently introduced in series of works by Stéphan and co-workers [92, 95, 136], and further studied by other groups [137, 138, 139, 140, 141, 142, 143, 144, 145], can efficiently capture universal properties, *e.g.* Luttinger liquid physics, quantum criticality, symmetry breaking phases.

Expanding a given (ground-) state in a computational discrete orthonormal basis  $|\Phi\rangle = \sum_i a_i |i\rangle$ , the SR entropy of this wave-function is defined by

$$S_q^{\text{SR}} = \frac{1}{1-q} \ln \left( \sum_i |a_i|^{2q} \right), \quad (17)$$

where  $|a_i|^2$  is simply interpreted as the probability of occupying state  $|i\rangle$ , provided  $\sum_i |a_i|^2 = 1$ . Contrary to single particle problems such as the Anderson localization [146] where the SR entropy (related to the inverse participation ratio) does not grow with the number of sites, many-body states occupy a finite portion of the Hilbert space and therefore the leading term grows with the volume. However, as observed numerically using large scale QMC simulations [140], the first corrections to such a volume law are logarithmic for SU(2) and U(1) broken phases. This is exemplified in Fig. 12 where QMC data [140] for  $q = \infty$  (corresponding to the coefficient of the most probable state in the basis expansion) are shown for the ground-state of two different spin- $\frac{1}{2}$  models on a square lattice: the SU(2) Heisenberg antiferromagnet Eq. (10) with  $J_2/J_1 = -5$  and the U(1) XY model, both computed in the  $\{S^z\}$  basis. One clearly observes a volume law scaling as well as an additive logarithmic correction with a prefactor whose value depends on the symmetry.

An analytical explanation has been proposed recently by Misguich and co-workers [147], using a massless free-field description of the SW modes supplemented by a phase space argument treating the rotational symmetry in finite volume. They arrived at the following correction for  $q > 1$

$$\Delta S_q^{\text{SR}} = \frac{n_G}{4} \left( \frac{q+1}{q-1} \right) \ln N, \quad (18)$$

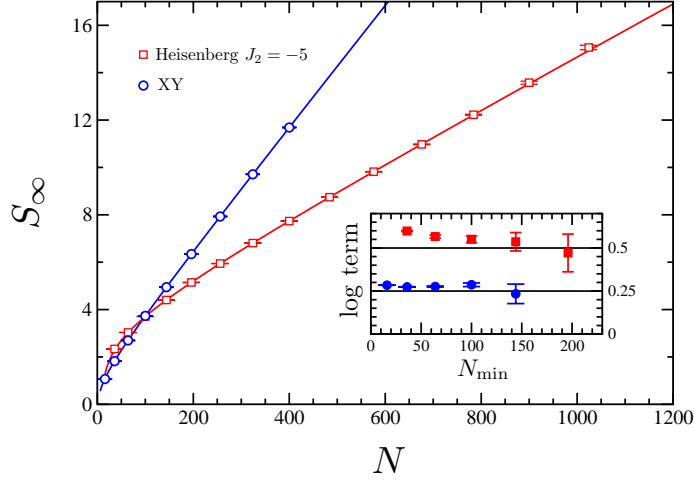


Figure 12: QMC results for the Shannon Rényi entropy  $S_\infty$  of two-dimensional symmetry breaking phases.  $T = 0$  QMC data for SU(2) Heisenberg antiferromagnet with second neighbor ferromagnetic coupling  $J_2/J_1 = -5$  (red squares) and U(1) symmetric XY model (blue circles) are shown both for  $s = 1/2$  versus the total number of lattice sites  $N$ . Inset: the prefactors of the logarithmic correction in Eq. (18), obtained after fitting over windows  $[N_{\min}, N_{\max}]$ , are plotted for the two models against  $N_{\min}$ . Data from [140].

which appears consistent with the numerics [140, 141].

### 2.3.3. Summary and outlook

Relativistic Nambu-Goldstone modes associated with continuous symmetry breaking show up as logarithmic corrections in the Rényi entanglement entropies, as written in Eq. (9). This was clearly verified using large- $s$  calculations, and QMC simulations for strip and line subsystems. Interestingly, the coefficients of the ground-state wave function expressed in a local computational basis also contain such a correction Eq. (18), as verified with large scale QMC.

Regarding the additive geometric constant  $\gamma_{\text{ord}}$  in Eq. (9), the discrepancy between the prediction of Metlitski and Grover and the large- $s$  result Eqs. (15)(16) remains to be understood. A QMC study for  $q > 2$ , while notoriously difficult, could perhaps resolve this issue. Another potentially interesting check would be to study other continuous symmetry breaking states, such as SU(N) for

instance using QMC [148] or flavor-wave theory [149]. Spin nematic ordered states [150] are also interesting exotic candidates where similar logarithmic corrections should occur.

#### 2.4. Long-range entanglement in topologically ordered phases

The current understanding of topological ordered phases has benefited from intensive works during the past 25 years [151, 152]. While a precise definition of topological order is still an active field of research [153], one can simply see it as a zero temperature disordered gapped state (*i.e.* with only short-range order of any local operators) which does not break any symmetry, and whose degeneracy is robust against local perturbations and depends on the topology of the space. This dependence implies that infinitely far boundaries can influence the ground-state properties, which seems to contradict the short-range nature of the correlations. Such a "robust hidden long-range structure" [154] has been diagnosed as "long-range entanglement" [155] (even though a topological ordered state is not necessarily more entangled than other states of matter).

##### 2.4.1. Topological entanglement entropy

One of the simplest way to characterize topological order relies on the entanglement entropy which displays a sub-leading constant beyond the conventional area law term, thus yielding

$$S = aL^{d-1} - \gamma, \quad (19)$$

as first identified by Hamma *et al.* [156], Kitaev and Preskill [105], and Levin and Wen [106]. This topological entropy  $\gamma$  is a universal number, characteristic of the topological order, which depends non-trivially on the quantum dimension of emergent quasi-particles above the degenerate ground-state [105, 106]:

$$\gamma = \ln \mathcal{D}, \quad (20)$$

where  $\mathcal{D}$  is the total quantum dimension.

Let us give a few examples: for  $\mathbb{Z}_2$  liquids, such as the toric code [157],  $\gamma = \ln 2$ , while for the chiral spin liquid state [158, 159]  $\gamma = \ln \sqrt{2}$ . For  $\nu = 1/m$

quantum Hall states,  $\gamma = \ln \sqrt{m}$  for the Laughlin fractional wave-function [160], while for the Moore-Read state [161]  $\gamma = \ln \sqrt{4m}$ . A very useful interpretation of this topological constant has been proposed by Stéphan and co-workers in a series of works [92, 95, 162] where they showed using CFT a correspondence between entanglement entropies of  $d = 2$  Rokhsar-Kivelson (RK) states and the (basis-dependent) Shannon-Rényi entropies associated to the coefficient of the wave-function of spin chains models. An interesting example is the  $d = 2$  eight-vertex RK state [163] which has  $\mathbb{Z}_2$  topological order, and corresponds to the Ising chain in transverse field in the ferromagnetic phase where the Shannon-Rényi entropies follows  $aL - \ln 2$ .

#### 2.4.2. Numerical results

$\mathbb{Z}_2$  spin liquids—. Considered to be the smoking gun of topological order, non-zero topological entanglement entropy may be hard to measure in numerical simulations. A construction in real space was proposed [105, 106] in order to cancel boundary and corner effects and get a better access to  $\gamma$ . This is illustrated in Fig. 13 for the  $\mathbb{Z}_2$  spin liquid phase of the quantum dimer model on the triangular lattice [164] at the RK point [165], computed using exact diagonalization by Furukawa and Misguich [108]. This subtraction trick has been used by several authors to measure the topological entanglement entropy [108, 167, 168, 162, 169], but it turns out that it is easier and more accurate to work with a cylinder geometry, as done for instance in Refs. [170, 162, 171, 132, 172, 173, 166, 174, 175, 176, 169]. In Fig. 14, we report  $d = 2$  DMRG results for  $\mathbb{Z}_2$  spin liquid states on (a) the frustrated  $J_1 - J_2$  spin- $\frac{1}{2}$  Heisenberg antiferromagnet on the square lattice Eq. (10) from [132], and (b) the Kagomé Heisenberg antiferromagnet<sup>3</sup> from [166]. In both cases one

---

<sup>3</sup>Note that there is still some debates regarding the nature of the ground-state due to the existence of various competing low-energy states. Among the three candidates, the gapped  $\mathbb{Z}_2$  spin liquid [177], the U(1) Dirac spin liquid [178], and the 36-site unit cell valence-bond solid [179], the most recent  $d = 2$  DMRG studies concluded for a  $\mathbb{Z}_2$  spin liquid [180, 166], with  $\mathbb{Z}_2$  topological order. For recent discussions, see also Refs. [181, 182].

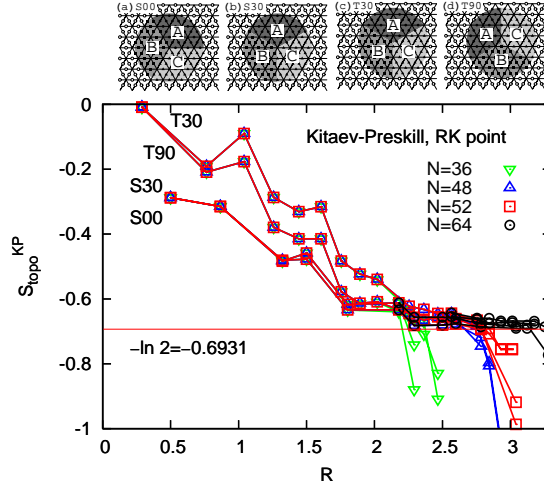


Figure 13: Topological entanglement entropy for the  $\mathbb{Z}_2$  spin liquid phase of the quantum dimer model on the triangular lattice at the RK point computed using exact diagonalization by Furukawa and Misguich [108], plotted as a function of the circle radius  $R$ . The 4 insets (top) show the 4 different Levin-Wen constructions used to extract  $\gamma$  which converges to the expected  $\ln 2$ . Reprinted from [108].

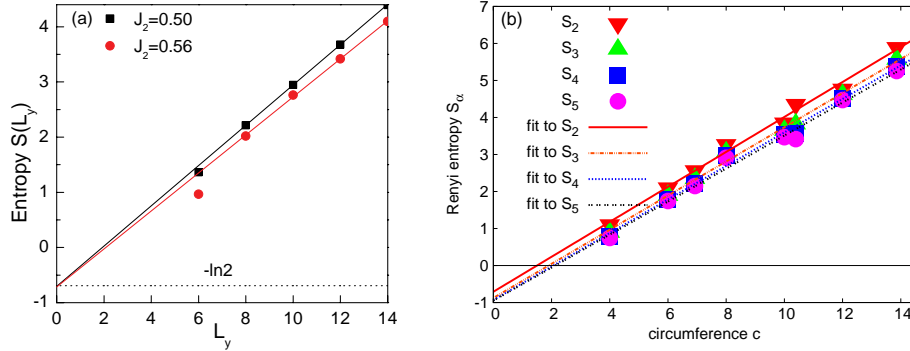


Figure 14: Entanglement entropy for  $\mathbb{Z}_2$  topological spin liquid states computed with DMRG on long cylinders of finite widths. Panel (a), reprinted from [132], shows the von Neuman entropy of the  $J_1 - J_2$  antiferromagnet on the square lattice as function of the perimeter of the cylinder  $L_y$  with an intercept  $\gamma = -\ln 2$  for  $L_y \rightarrow 0$ . Panel (b), reprinted from [166], shows various Rényi entropies  $S_q$  for the Kagomé antiferromagnet as function of the perimeter of the cylinder  $c$  with an intercept  $\gamma \rightarrow -\log_2(2) = -1$  for increasing values of  $q$ .

reads the topological entanglement entropy as the intercept when the cylinder circumference vanishes, in perfect agreement with the predicted quantum dimension  $\mathcal{D} = 2$  from Eq. (20). Note the better accord for the Kagomé model in Fig. 14 at larger Rényi parameters  $q$ , a consequence of the less good accuracy when computing lower weight entanglement modes. Surprisingly this numerical limitation seems to be at variance with the results obtained in Ref. [176].

*Fractional quantum Hall states*—. The topological entanglement entropy has also been measured with a great accuracy for Laughlin wave function at  $\nu = 1/m$  [183, 184, 170, 167] as well as for the non-abelian Moore-Read state [185, 186]. In Fig. 15 we report numerical results from Refs. [184, 185, 170]. More recently, non-abelian states such as fractional quantum Hall states at  $\nu = 13/5$  and  $\nu = 12/5$ , apparently captured by the  $k = 3$  parafermion Read-Rezayi state [187], have been studied in Refs. [188, 189]. The topological entanglement entropy of such a state  $\gamma = \frac{1}{2} \ln(5 + 5\phi^2) \simeq 1.45$  was successfully captured using large scale DMRG simulations. Note also the non-abelian phases in the two-component  $\nu = 2/3$  fractional quantum Hall states on a bilayer, with the emergence of Fibonacci anyons [190].

*Other examples*—. We now give a very short (and clearly non-exhaustive) list of recently discussed topological ordered phases characterized by their topological entropy. Using  $d = 2$  DMRG for the  $s = 1/2$  kagomé antiferromagnet in an external field, a magnetization plateau at filling  $1/9$  of saturation has been claimed to be a  $\mathbb{Z}_3$  spin liquid state [191]. The existence of this exotic plateau state had not been reported previously [192], but was diagnosed in a more recent study [193] to be a valence bond crystal coexisting with spin order, a phase where topological order is absent. Still on the kagomé lattice, hard-core bosons at  $\nu = 1/3$  filling have revealed an interesting  $\mathbb{Z}_2$  topological liquid state [194]. In Ref. [195] a frustrated spin- $\frac{1}{2}$  model on a square lattice was found to exhibit the same topological order as the spin chiral state. Note also the topological color code model [196] which exhibits a  $\mathbb{Z}_2 \times \mathbb{Z}_2$  spin liquid ground-state with  $\gamma = \ln 4$ , as studied numerically in [197].



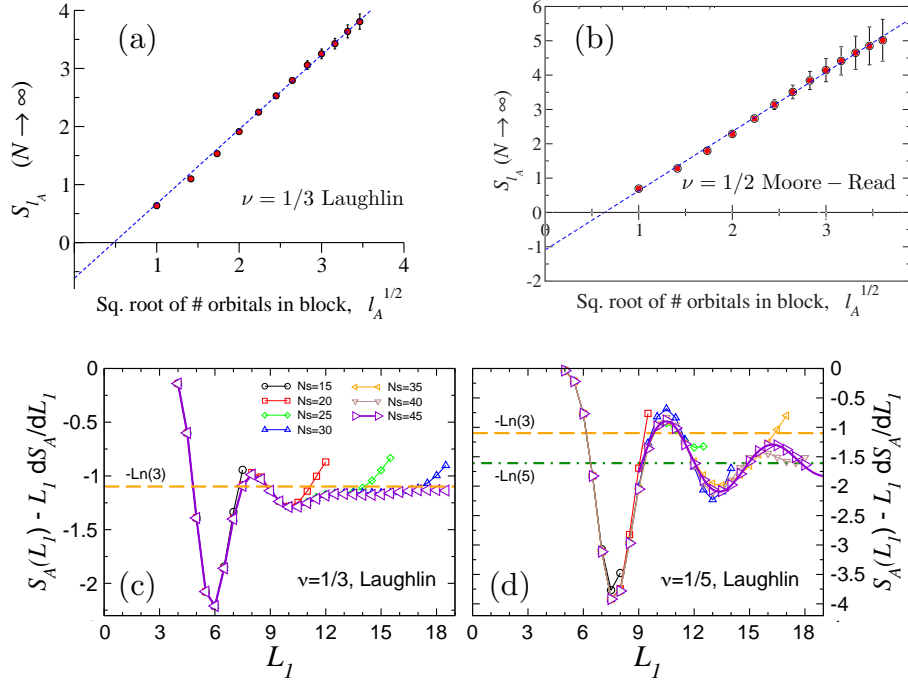


Figure 15: Entanglement entropies for fractional quantum Hall states computed (a,b) on a sphere with orbital partitions and (c,d) on a torus with real space cuts. (a) For the  $\nu = 1/3$  Laughlin wave-function the topological term is found in perfect agreement with  $\gamma = -\ln \sqrt{3} \simeq -0.55$ , reprinted from [184]. (b) For the  $\nu = 1/2$  Moore-Read state  $\gamma = -\ln \sqrt{8} \simeq -1.04$ , reprinted from [185]. For real space bipartitions on a torus (c,d), reprinted from [170],  $2 \times \gamma$  is plotted against the torus perimeter  $L_I$  for various magnetic flux quanta  $N_s = N/\nu$  with  $N$  electrons for  $\nu = 1/3$  and  $1/5$  Laughlin wave-functions. A good agreement is found with  $2\gamma = \ln \nu$ .

For extension to  $d > 2$ , we refer to the work of Grover *et al.* [198] (see also [199] for three-dimensional quantum spin liquids in iridate materials and [200] for U(1) quantum spin liquids). Finally, for topological order and topological entropy in classical systems, see *e.g.* Refs. [201, 202, 203].

### 3. Entanglement spectroscopy

Soon after the discovery of the DMRG algorithm for one dimensional quantum systems [204, 205], some attempts have been made to extend it to  $d = 2$  [206, 207, 208]. However, it was then quickly realized that such an extension is a quite difficult task, as observed through the study of the spectrum of the RDM, the entanglement spectrum (ES), for two dimensional non-interacting quantum systems [83]. Although such studies were first motivated by performance issues regarding the DMRG algorithm, some deeper investigations have later started to become a topic of increasing interest, in particular for quantum chains [209, 210, 211, 212, 213].

A breakthrough came in 2008 with the work of Li and Haldane [214] where they showed for  $\nu = 5/2$  fractional quantum Hall states that the low lying part of the RDM spectrum contains universal features regarding topological properties. This has triggered a huge interest, in particular for topological order that we discuss below in Section 3.2. Roughly at the same time, Calabrese and Lefèvre [215] focused on the eigenvalues distribution of the RDM for critical spin chains described by a CFT, which also raised a large inquisitiveness, as we review in Section 3.1. Among numerous fascinating properties of entanglement spectroscopy, the notion of entanglement Hamiltonian has been also intensively debated, as we discuss in Section 3.3.

#### 3.1. Entanglement spectrum in one dimension and beyond

##### 3.1.1. Quantum spin chains and ladders

*Quantum spin chains.* The ground-state of the spin  $s = 1/2$  XXZ chain, defined on a chain of  $L$  sites by the following Hamiltonian

$$\mathcal{H}_{xxz} = \sum_{i=1}^L (S_i^x S_{i+1}^x + S_i^y S_{i+1}^y + \Delta S_i^z S_{i+1}^z), \quad (21)$$

displays critical spin-spin correlations for  $-1 < \Delta \leq 1$  with a continuously varying Luttinger liquid parameter [216]

$$K = \frac{1}{2 \arccos(-\Delta)/\pi}. \quad (22)$$

This critical regime is described by a CFT [217] with central charge  $c = 1$ , yielding the logarithmic growth [21] of the Rényi entanglement entropies Eq. (5). Making a real-space bipartition, which defines a subsystem  $A$  (depicted in the inset of Fig. 16), its RDM  $\rho_A$  has eigenvalues  $\lambda_i$  which gives the ES  $\xi_i = -\ln \lambda_i$ . The eigenvalues distribution was first studied by Calabrese and Lefèvre [215] using CFT and exact diagonalization of Eq. (21) at  $\Delta = 0$ . Exploiting the fact that  $\text{Tr} \rho_A^q \sim L^{-\frac{c}{6}(q-\frac{1}{q})}$ , they derived an approximate expression for the mean number of eigenvalues larger than a given  $\lambda$ :

$$n(\lambda) = I_0 \left[ b \ln \left( \frac{\lambda_{\max}}{\lambda} \right) \right], \quad (23)$$

where  $I_0$  is the modified Bessel function of first kind,  $\lambda_{\max}$  is the largest eigenvalue, and  $b = -\ln \lambda_{\max}$ , nicely confirmed numerically for the XX point [215]. A good agreement was also found later by Pollmann and Moore using infinite time-evolved block decimation [218] for various XXZ anisotropies, albeit a fitting prefactor was used in Eq. (23). In the critical ferromagnetic regime  $-1 < \Delta < 0$ , Alba *et al.* [219] also observed a sizeable deviation from prediction Eq. (23).

Using large scale DMRG we have explored [220] the distribution of  $\lambda_i$  for various anisotropy parameters  $\Delta$  along the critical regime of the XXZ model. Numerical results for  $n(\lambda)$  with very large systems, up to  $L = 2000$  lattice sites and open boundary conditions, are shown in Fig. 16. There, we see that the prediction Eq. (23) works remarkably well at the XX point (free fermions), in agreement with Calabrese-Lefèvre, but with significant deviations appear for finite interaction  $\Delta \neq 0$ . Interestingly, attractive  $\Delta < 0$  and repulsive  $\Delta > 0$  interactions display opposite deviations, with a sign change at  $\Delta = 0$ . A finite size analysis, shown in Fig. 16 (Bottom) for the isotropic point  $\Delta = 1$ , reveals that finite size effects are responsible for the observed disagreement. Indeed, convergence to the asymptotic form Eq. (23) is slowed by logarithmic corrections  $\sim 1/\ln L$ , with a prefactor which change sign with the anisotropy  $\Delta^4$ . So far there is no analytical understanding for such finite size effects.

---

<sup>4</sup>These corrections exist on the entire critical regime and are not restricted to  $\Delta = 1$  [220].

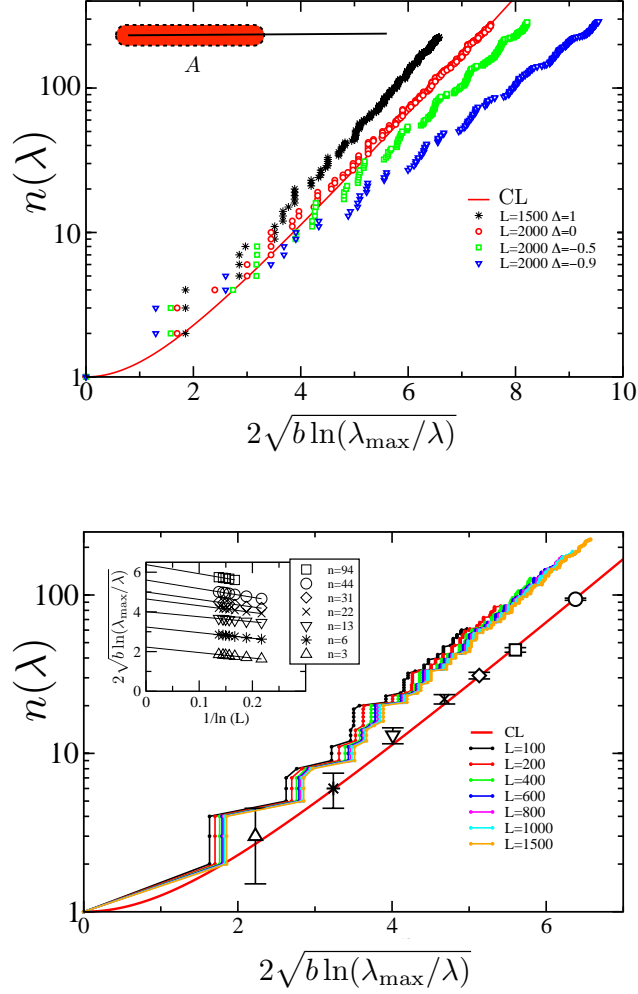


Figure 16: DMRG results for the entanglement eigenvalue distribution for open spin- $\frac{1}{2}$  XXZ chains with a real-space bipartition at half-chains  $L/2$  (inset). Top: Numerical results for  $n(\lambda)$  at various anisotropies  $\Delta$  for system sizes  $L \geq 1500$ , compared to the analytical prediction Eq. (23) from Calabrese and Lefèvre (CL) [215]. Bottom: Finite size convergence of  $n(\lambda)$  towards the CL formula Eq. (23). DMRG data for  $\Delta = 1$ . Inset: logarithmic convergence to the thermodynamic limit. Figure reprinted from Ref. [220].

The CFT description is also encoded in the microscopic structure of the entanglement levels, as discussed in Refs. [221, 220]. Indeed, for critical XXZ [221, 220], as well as for critical Bose-Hubbard chains [222, 221], the low lying part of

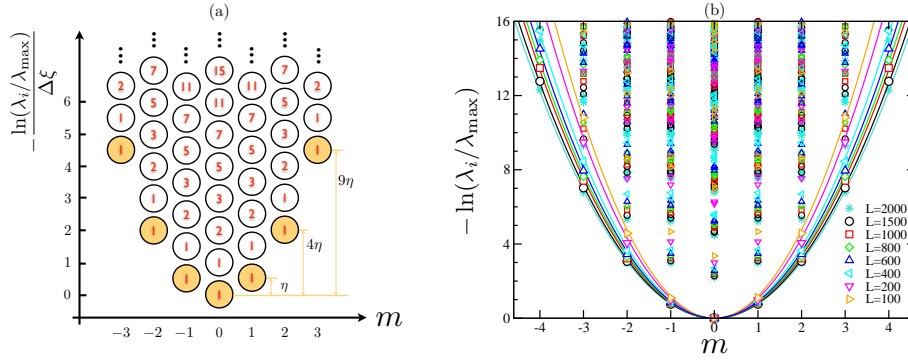


Figure 17: (a) Schematic representation of the CFT energy spectrum of a compactified boson ( $\eta = \frac{1}{2K}$ ) with open boundary conditions, reprinted from [221]. (b) Spin-resolved ES from DMRG calculations: results for open XXZ chains at  $\Delta = -0.5$  and various lengths  $L$ , as indicated on the plot. The lower part of the spectrum is fitted to the quadratic form Eq. (25), reprinted from [220].

the ES for subsystems of length  $\ell_A$  corresponds to the energy spectrum of open chains of length  $\ell_A$  with the same Luttinger parameter as the full system. This is shown in Fig. 17 (b) for XXZ chains at  $\Delta = -0.5$  where the low "energy" entanglement levels are perfectly described by the CFT prediction [217] for the low-energy spectrum of a critical open chain of  $\ell_A$  sites

$$E_0^m - E_0^0 = \frac{\pi u}{2K\ell_A} m^2, \quad (24)$$

where  $m$  is the  $S^z$  quantum number of the subsystem,  $E_0^m$  is the ground-state energy in a given magnetization sector  $m$ ,  $u$  the velocity of excitations, and  $K$  the Luttinger parameter. The entanglement levels in Fig. 17 can be identified with Eq. (24) using the correct "entanglement temperature" [220] (see also below in Section 3.3), thus yielding

$$-\ln \left( \lambda_i^{(m)} / \lambda_{\max}^{(m)} \right) = \frac{\pi^2}{K \ln(\ell_A / \ell_0)} m^2, \quad (25)$$

where  $\ell_0$  is a length scale of order 1. As a consistency check, one can extract the Luttinger parameter  $K$  from the quadratic envelope Eq. (25), which is shown in Fig. (51) (a) for Bose-Hubbard chains [221], and (b) for XXZ chains [220].

One should also mention some earlier results obtained by Peschel [223] on

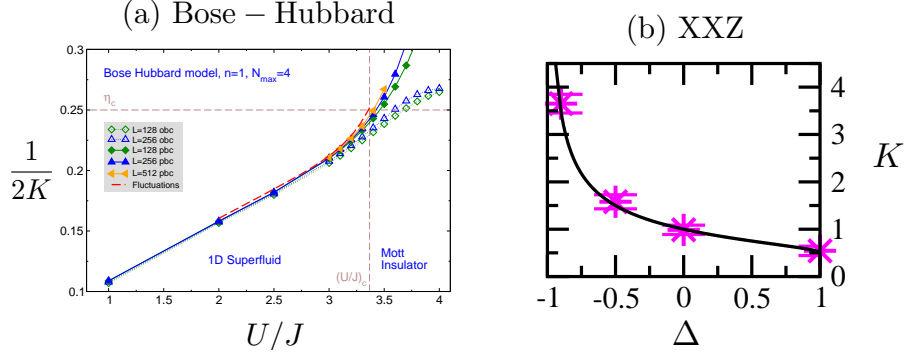


Figure 18: Luttinger  $K$  parameter estimated from the curvature of the low-energy part of the ES described by Eq. (25). (a) Bose-Hubbard chains at integer filling, reprinted from [221]. (b)  $s = 1/2$  XXZ chains compared to exact Bethe ansatz (full line) Eq. (22), reprinted from [220].

free electronic chains which suggest that the effective Hamiltonian is an open free fermion chain, but with non-homogeneous hopping terms vanishing at the boundaries. Such microscopic details should not change the above picture for quantum critical chains. However, in the gapped Ising regime of the XXZ chain ( $\Delta \gg 1$ ), the boundary-local nature of the ES has been clearly identified [224]. Note also that one could interpret the inhomogeneity in a local thermodynamic with a spatially varying local temperature [225, 226] decaying away from the boundary.

In Refs. [227, 228, 229, 230], the entanglement gap between the first two largest eigenvalues (the Schmidt gap) has been diagnosed as an order parameter to locate quantum phase transitions for quantum spin chain models, an idea further applied to quantum impurity problems [231]. One should however note that universal features captured by entanglement spectroscopy have been recently questioned when looking at momentum-space entanglement [232] where the closure of the Schmidt gap may not occur at the physical critical point. These second thoughts regarding universality are also supported by the recent discussion in Ref. [233].

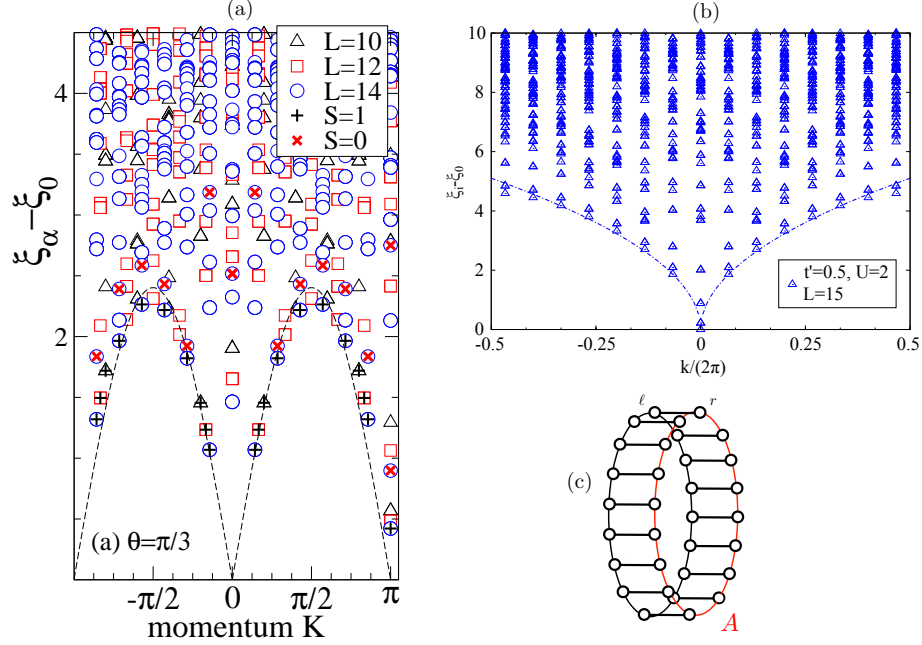


Figure 19: Exact diagonalization results for the momentum-resolved ES of 2-leg ladders, obtained after a real-space bipartition with one leg as subsystem  $A$  (c). (a)  $s = 1/2$  Heisenberg model which has a gapped ground-state, the dashed line being the de Cloiseaux - Pearson gapless dispersion (reprinted from [234]). (b) Interacting hard-core boson model with a single gapless mode, the dashed line being a  $\sqrt{k}$  dispersion (reprinted from [235]).

*Ladders*—. Ladder materials, originally introduced to study two-dimensional systems from a quasi- $d = 1$  perspective [236] are now well recognized to harbour many fascinating phenomena, and numerous experimental achievements [237, 238, 239]. A paradigmatic example is the two-leg ladder geometry (depicted in panel (c) of Fig. 19) for which the antiferromagnetic Heisenberg model presents a singlet ground-state separated from the first excited triplet state by a finite energy gap. Nevertheless, as first shown by Poilblanc [234] by tracing out a single leg (subsystem  $A$  in panel (c) of Fig. 19), the ES reveals an unexpected gapless feature when studied against the momentum quantum number  $k$  of the chain. Visible in Fig. 19 (a), the eigenvalues  $\lambda$  of the RDM, plotted as

$\xi = -\ln \lambda$  against the momentum  $k$  show a "low-energy" structure similar to the gapless des Cloizeaux - Pearson spectrum of a single Heisenberg chain [240]. It is quite remarkable that the ES appears to reflect the low-energy spectrum of each individual edge. This observation has then triggered further extensions and studies of quantum ladder systems [241, 242, 243, 244, 245, 235, 246, 135]. In particular, the authors of Ref. [235] analyzed in details, both analytically and numerically, the case of an interacting two-leg ladder of hard-core bosons with one gapless mode. The resulting momentum-resolved ES, displayed in Fig. 19 (b), features a  $\sqrt{k}$  low-energy dispersion, in contrast with the gapped ladder case [234, 241, 244, 245], thus reflecting the long-range nature of the boundary Hamiltonian (see also below Section 3.3).

*Quantum Monte Carlo approaches for entanglement spectroscopy*—. While exact diagonalization, DMRG, and tensor network approaches have been the most useful numerical techniques able to access ES of strongly correlated quantum systems, very recent developments have been made using QMC methods [67, 247, 135, 70]. For fermionic systems, Assaad and co-workers proposed a method based on the computation of spectral functions along the imaginary time [67, 70]. Another route was suggested for bosonic and quantum spin models [247, 135], using the fact that one can reconstruct the ES from higher-order Rényi entropies. This method, introduced in Ref. [49], and implemented in a QMC framework for Bose-Hubbard chains [247] and quantum spin ladders [135], relies on the Newton-Girard identities, which links the coefficients of a polynomial to the power sums of its roots.

However, in any practical QMC simulation, the knowledge of Rényi entanglement entropies is limited to some finite precision, and to not too large value of the Rényi parameter  $q \leq q_{\max}$ . For the extended Bose-Hubbard chain at unit filling, Chung *et al.* [247] have been able to reconstruct the low lying levels of the ES using  $q_{\max} = 4$ , as plotted in Fig. 20 (b). In Ref. [135] we have studied the isotropic  $s = 1/2$  Heisenberg ladder with  $J_{\text{leg}} = J_{\text{rung}}$  up to  $q_{\max} = 9$ . QMC results are shown in Fig. 20 (a) for a  $2 \times 10$  system (with the same bipartition as discussed



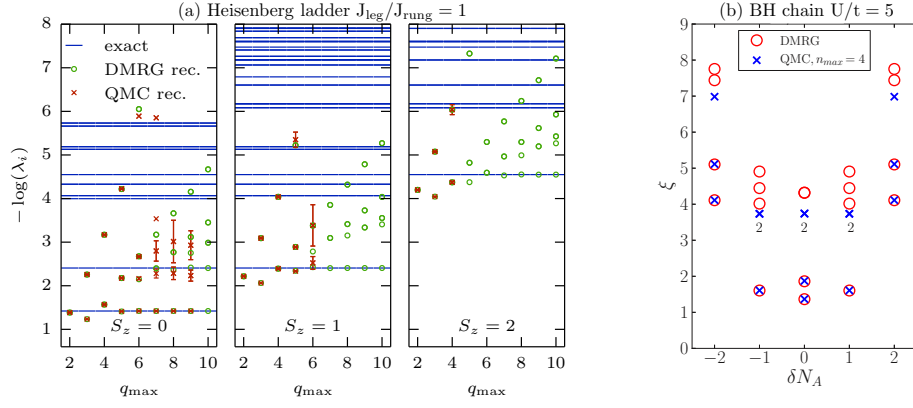


Figure 20: Reconstructed ES from QMC data. (a) Results for the  $2 \times 10$   $s = 1/2$  Heisenberg ladder with  $J_{\text{leg}} = J_{\text{rung}}$  plotted against  $q_{\text{max}}$ , and separated in spin sectors  $S_z$ . Exact and reconstructed DMRG data are also shown for comparison. Reprinted from [135]. (b) Results for a  $L = 48$  extended Bose - Hubbard chain at unit filling in the Mott insulating phase. Reprinted from [247].

previously in Fig. 19), and compared to exact DMRG results, as well as to the same reconstruction trick using DMRG data for  $S_{q \leq 10}$ . The convergence of the lowest entanglement level (in the  $S_z = 0$  sector) is very good, thus providing an efficient estimate of the single copy entanglement  $S_\infty = -\ln \lambda_{\text{max}}$  [248, 249] for which no direct QMC estimate is available, as it would rely on a Monte Carlo sampling of an infinite number of replicas. Nevertheless, despite the numerical gain using the spin-resolved structure of the RDM, we clearly see the limitations of this technique to access higher entanglement levels, even for exact DMRG data, while the reconstructed QMC spectrum carries additional errors due to the statistical uncertainty of the Rényi entanglement entropies.

Before switching to  $d = 2$ , one should mention an alternative spectroscopic tool relying on the participation spectrum [141, 142], which can be computed very efficiently within a QMC framework. This will be discussed below, when addressing the issue of entanglement Hamiltonian in Section 3.3.

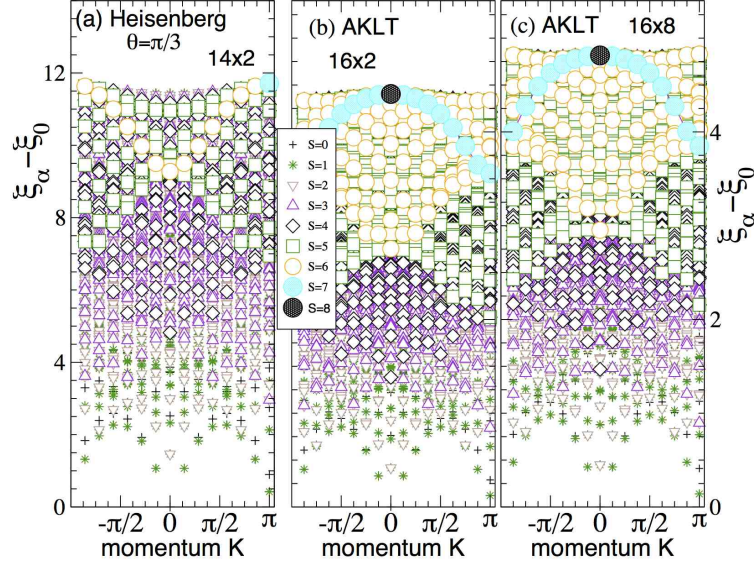


Figure 21: ES  $\xi_\alpha = -\ln \lambda_\alpha$  of Heisenberg and AKLT ladders (a,b) and  $d = 2$  AKLT cylinder (c) shown against the total momentum  $K$  along the direction of the cut. Eigenvalues are labelled according to their total spin quantum number using different symbols displayed on the plots. Figure reprinted from Ref. [241].

### 3.1.2. Conventional ordered and gapped states in $d > 1$

*Gapped phases*—. Accessing the ES of quantum interacting systems beyond  $d = 1$  is a challenging task. While entanglement spectroscopy was popularised after the work of Li and Haldane [214] as a smoking gun of topological order for  $d = 2$  non-abelian fractional quantum Hall states (see below in Section 3.2), somehow surprisingly, less is known regarding traditional  $d = 2$  phases of matter, *e.g.* symmetry breaking states or conventional quantum critical points. Indeed, only a few analytical works are available, exploring for example ES for broken continuous symmetry states [96], complex paired superfluids [250], valence-bond solid states [251], or the quantum Ising model [233]. On the numerical side, most of the simulation results have been obtained using diagonalization techniques [252], tensor network approaches [241, 253], or  $d = 2$  DMRG [254, 81, 133].

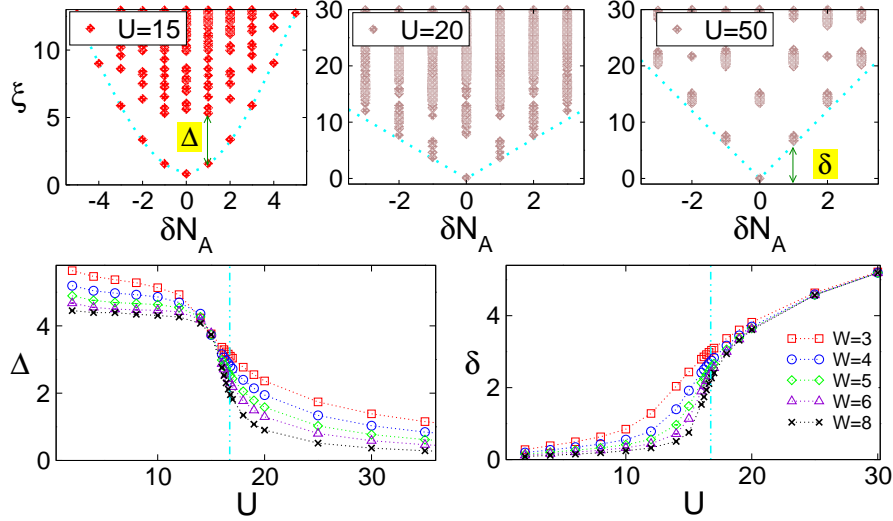


Figure 22: DMRG results for the  $d = 2$  Bose-Hubbard model from Alba *et al.* [81]. Top: ES across the superfluid - Mott insulator transition. Bottom:  $\Delta$  and  $\delta$  (defined in top panels) plotted against the on-site repulsion  $U$  for several values of the boundary length  $W$ . The vertical line denotes the critical repulsion  $U_c \simeq 16.74$ . Reprinted from Ref. [81]

For gapped phases, the structure of the ES reflects the physics at the boundary, similarly to the Heisenberg ladder case [234] discussed above, with a short-range entanglement Hamiltonian following a correspondence between the ES and the edge physics [241, 251]. This is illustrated in Fig. 21 from Ref. [241] where one sees that the AKLT state [255] features the same ES in  $d = 2$  and on a 2-leg ladder.

For the  $d = 2$  Bose-Hubbard model studied by Alba *et al.* [81], in the gapped Mott insulating phase at large on-site repulsion, the ES acquires the boundary structure of a simple tight-binding chain with short-range hopping of the excess particles on top of the insulating state, (see Fig. 22).

*Long-range order*—. The case of long-range ordered states where a continuous symmetry is broken, such as the U(1) for a superfluid [81] or SU(2) for Néel ordered antiferromagnets [133] is more subtle. Indeed, the ES has to reflect the broken symmetry and therefore cannot be a simple edge spectrum of an effective

model with short-range interactions like in the gapped case discussed previously. As suggested by the field theory approach of Metlitski and Grover [96], and observed numerically using DMRG for the superfluid regime of the Bose-Hubbard on the square lattice [81] and the Néel phase of the Heisenberg model on various lattices [133], the ES has to contain both Anderson TOS [121] and oscillators (SW) structures. This is indeed what we can see for the U(1) broken superfluid in Fig. 22 where the TOS yields a quadratic envelope in term of the particle number  $\sim \delta \times (\delta N_A)^2$ , with a "TOS gap"  $\delta$  vanishing with the linear size  $W$  of the subsystem as  $1/W$  (with possible logarithmic corrections [96]). The SW part has a finite gap  $\Delta$  (or possibly slowly vanishing  $\sim 1/\ln W$  [96]) in the ordered regime. As we discuss more below in Section 3.3, when comparing ES to the physical spectrum of a given "entanglement Hamiltonian", one should be careful about the entanglement temperature which renormalizes the ES, here with a factor  $T_{\text{eff}} \sim 1/W$ .

### 3.2. Entanglement spectroscopy of topological order

Quantum states of matter which exhibit topological properties, *e.g.* fractional quantum Hall effect (FQHE) [256], topological insulators [257], chiral or  $\mathbb{Z}_2$  spin liquids [258], AKLT states [255]... have been conjectured by Li and Haldane [214] to display edge excitations in their ground-state ES. This idea has then been extensively pursued for FQHE [259, 260, 261, 262, 263, 264, 265, 266, 267, 268, 269, 270, 271, 272, 273, 274, 188, 275, 276], topological insulators [277, 278, 279, 280, 281, 282, 283, 284], quantum spin liquids [175, 285, 286, 287, 288], valence bond spin states [218, 252, 289, 290, 251, 291], or the toric code [292, 241]. While this field is still relatively young, there has been an impressive number of works since Li and Haldane proposal. Therefore, providing an exhaustive review of such recent developments is clearly out of the scope of the present paper. Below we try to give a short overview, focusing on a few aspects such as the identification of topological order through the ES, the edge-ES correspondence, and the recent advances in topological properties of quantum spin liquids.

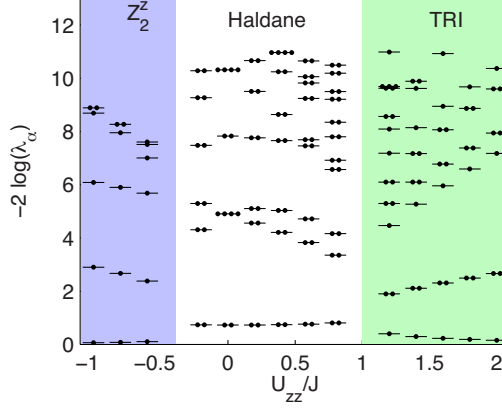


Figure 23: Lower part of the entanglement spectrum of the spin  $s = 1$  chain model Eq. (26). The multiple dots show the degeneracy of the eigenvalues, which is even in the Haldane regime, and odd otherwise. Reprinted from Ref. [293].

### 3.2.1. Identify topological order with entanglement spectra

Before discussing FQHE, one can first illustrate the power of entanglement spectroscopy for characterizing non-trivial states, such as the Haldane phase of spin  $s = 1$  Heisenberg chains with open ends, governed by

$$\mathcal{H} = J \sum_{i=1}^{L-1} \vec{S}_i \cdot \vec{S}_{i+1} + U_{zz} \sum_{i=1}^L (S_i^z)^2 + \dots \quad (26)$$

For  $U_{zz}/J \in [-0.4, 1]$  the ground-state is connected to its parent VBS phase of the AKLT model [255], and is a "symmetry protected topological phase", as also found in Bose-Hubbard [294] or multicomponent fermionic chains [295]. Despite the lack of local order parameter, and the fragility regarding small perturbations of the string (non-local) order and of the edge states, Pollmann and co-workers have shown [293] that provided an appropriate set of symmetries remains preserved, the Haldane phase is stable. The signature of this topological state has to be read in the lower part of the ES, as visible in Fig. 23 where one sees 2 degenerate non-zero eigenvalues, mimicking the edge spectrum of a system with a true physical boundary. Such a stability can be used as an operational definition of the topologically protected Haldane phase [296].

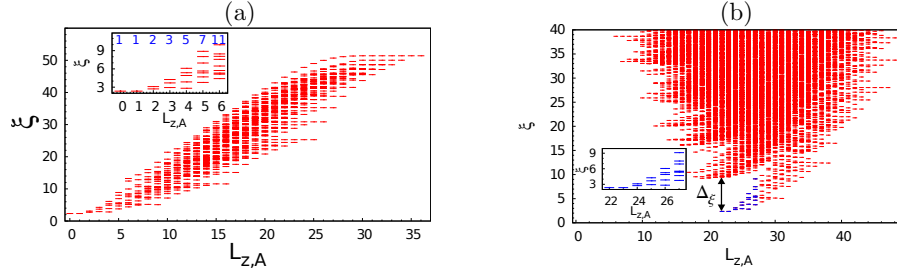


Figure 24: Orbital ES for (a) the Laughlin wave-function at  $\nu = 1/3$  and (b) the Coulomb interaction, both on a sphere geometry. Results from Regnault [297] obtained with 12 fermions (in the sector with 6 particles), keeping 17 orbitals. The inset (a) demonstrates the direct correspondence between the lowest part of the spectrum and the chiral U(1) bosonic edge mode, with the correct counting 1, 1, 2, 3, 5, 7, 11. In (b) the blue levels are the edge modes similar to (a). The entanglement gap  $\Delta_\xi$  separates the universal edge part from the non-universal high eenergy part. Reprinted from [297].

For the FQHE Li and Haldane suggested [214] an orbital bipartition which, while not equivalent, may imitate a real space cut. They conjectured that such an orbital ES should reflect the edge mode. This has effectively been observed in several cases, either for Laughlin wave-functions describing  $\nu = 1/m$  states, the Moore-Read state at  $\nu = 5/2$ , and also beyond model wave-functions through more realistic Hamiltonians including Coulomb interaction. In Fig. 24 we illustrate this with the result obtained by Regnault [297] for the Laughlin model wave-function and the Coulomb case for  $\nu = 1/3$  which both display the correct U(1) edge mode counting. For the more realistic spectrum obtained with Coulomb interactions (panel (b) of Fig. 24), the universal structure, similar to the Laughlin model state, is protected from the non-universal high-energy part by a finite entanglement gap  $\Delta_\xi$ . The universal part is described by CFT [214]. When approaching quantum Hall phase transitions, this entanglement gap has been found to vanish [260, 262, 298].

### 3.2.2. Correspondence between edge and entanglement spectra

A natural question which immediately arises concerns the universal character of the correspondence between the low lying part of the ES and the edge states, as posed by Chandran and co-workers [265] for several FQH states. They found a direct correspondence between mode countings of particle ES, the orbital ES studied by Li and Haldane [214], and bulk quasi-holes using CFT. The latter being equal to the counting of edge modes at physical hard-cut on the sample, they interpret their results as a bulk-edge correspondence [299] for the ES.

Using CFT, a general proof for this correspondence has been proposed by Qi, Katsura and Ludwig [266] for  $d = 2 + 1$  topological states with  $d = 1 + 1$  chiral edges using the cut and glue approach, as illustrated in Fig. 25. Starting by cutting a cylinder in two subsystems A and B which both support gapless chiral edge states, they are then glued together along the edges by switching an interaction between A and B. The cut being considered as a sudden quantum quench, it was proved using boundary CFT that both chiral edge and entanglement Hamiltonians are equivalent. Let us also mention other proofs that have been proposed, also based on CFT [300, 271].

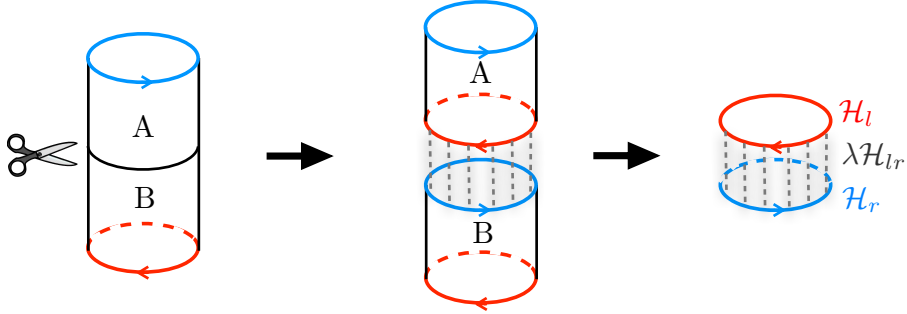


Figure 25: Cut and glue approach [266] applied to a quantum Hall state on a cylinder. The system is cut into A and B, obtaining gapless modes described by chiral Luttinger liquids,  $\mathcal{H}_r$  and  $\mathcal{H}_l$  living on the new edges. We then glue them along the edges by switching on an interaction  $\lambda\mathcal{H}_{lr}$  that couples A and B. The entanglement problem of the quantum Hall state can then be reduced to the problem of entanglement between the two coupled chiral Luttinger liquids [235]. Inspired from Ref. [266].

From a numerical point of view, the tensor networks PEPS formalism [301] gives new insights on this question by directly constructing an "holographic" [302] correspondence between the ES and a boundary Hamiltonian, as initiated by Cirac and co-workers [241, 303] where it was found that for a gapped bulk the ES corresponds to a short-range gapless Hamiltonian [252, 251]. In the case of non-chiral topological phases where there are no protected gapless edge modes, such as the Kitaev toric code model which has  $\mathbb{Z}_2$  topological order, it has been shown [304] that there is no such a correspondence between the ES and edge physics.

### 3.2.3. Chiral spin liquid state

Spin liquids [258] are very good candidates for testing the correspondence between edge modes appearing along a physical cut and the entanglement modes along a virtual edge obtained after bipartition. Quantum spin liquid states have been intensively studied using entanglement spectroscopy tools [173, 175, 285, 286, 287, 288].

Quite recently, the kagomé lattice has again revealed a very rich physics exhibiting chiral phases [305, 306, 285, 286, 287, 288, 307, 308, 288, 309, 310]. Indeed, two types of Heisenberg models have been found to realize the so-called chiral spin liquid state [158, 159], expected to have time-reversal and parity symmetries (spontaneously or explicitly) broken, with a non-zero chiral order. The  $J_1 - J_2 - J_3$  model

$$\mathcal{H} = J_1 \sum_{\langle i,j \rangle} \vec{S}_i \cdot \vec{S}_j + J_2 \sum_{\langle\langle i,j \rangle\rangle} \vec{S}_i \cdot \vec{S}_j + J_3 \sum_{\langle\langle\langle i,j \rangle\rangle\rangle} \vec{S}_i \cdot \vec{S}_j, \quad (27)$$

which preserves both symmetries, studied in Refs. [287, 285, 310], and the  $J - \chi$  model [286, 310], which explicitly break them

$$\mathcal{H} = J \sum_{\langle i,j \rangle} \vec{S}_i \cdot \vec{S}_j + \chi \sum_{i,j,k \in \Delta, \nabla} \vec{S}_i \cdot (\vec{S}_j \times \vec{S}_k). \quad (28)$$

ES, plotted in Fig. 26 for both models, unambiguously show the chiral nature of the edge excitations in momentum space.



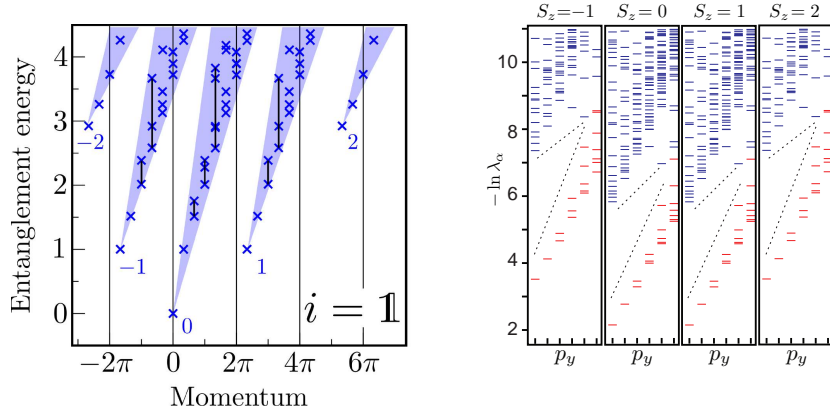


Figure 26: ES of  $s = 1/2$  models on the kagomé lattice Eq. (28) from Ref. [286] (Left) and Eq. (27) from Refs. [287, 285] (Right). Reprinted from Refs. [286, 285].

### 3.3. Entanglement Hamiltonian

The notion of entanglement Hamiltonian  $\mathcal{H}_E$ , simply defined by

$$\rho_A = \exp(-\mathcal{H}_E), \quad (29)$$

has been first discussed in the context of non-interacting systems [128], for which Peschel and Chung [311, 83, 210] have shown that  $\mathcal{H}_E$  has the same free-particle form as the original Hamiltonian. After Li and Haldane work [214] for fractional quantum Hall states, the idea that  $\mathcal{H}_E$  contains some universal properties of the virtual edge induced by the bipartition was vastly popularized for various condensed matter systems [234, 242, 252, 241, 244, 245, 81, 246, 133, 235, 312, 142, 284, 313, 314]. Below we discuss a few representative examples of gapped states, such as spin ladders or  $d = 2$  coupled dimers for which the entanglement Hamiltonian has a short-range nature. We also investigate gapless states where the situation is more involved when correlations get long ranged.

#### 3.3.1. Boundary theories for gapped phases

*Perturbative approach for spin ladders*— After the observation [234, 241] of the correspondence for (gapped) 2-leg spin ladders between the ES and the energy spectrum of a single (gapless) Heisenberg chain (see also Fig. 19), an analytical

perturbative approach was proposed [242, 244, 246] for a real space cut along the rungs (as depicted in the panel (c) of Fig. 19). For a  $s = 1/2$  Heisenberg ladder, governed by the Hamiltonian

$$\mathcal{H} = \sum_i \left( J_2 \vec{S}_{i,1} \cdot \vec{S}_{i,2} + \sum_{\ell=1,2} J_1 \vec{S}_{i,\ell} \cdot \vec{S}_{i+1,\ell} \right), \quad (30)$$

in the strong rung coupling limit  $J_2 \gg J_1$ , the entanglement Hamiltonian derived using 2<sup>nd</sup> order perturbation is a  $s = 1/2$  unfrustrated short-range Heisenberg model<sup>5</sup>

$$\mathcal{H}_E = \frac{2J_1}{J_2} \sum_i \vec{S}_i \cdot \vec{S}_{i+1} + \frac{1}{2} \left( \frac{J_1}{J_2} \right)^2 \sum_i \left( \vec{S}_i \cdot \vec{S}_{i+1} - \vec{S}_i \cdot \vec{S}_{i+2} \right) + O \left( \frac{J_1}{J_2} \right)^3. \quad (31)$$

One can infer the following generic unfrustrated form for the entanglement Hamiltonian, with exponentially decaying exchanges

$$\rho_A = \frac{1}{Z} \exp \left( -\beta_{\text{eff}} \sum_i \sum_r (-1)^{r-1} J_1 e^{-\frac{r-1}{\xi_E}} \vec{S}_i \cdot \vec{S}_{i+r} \right) \quad (32)$$

The effective inverse temperature

$$\beta_{\text{eff}} = \frac{2}{J_2} \left( 1 + \frac{J_1}{4J_2} \right), \quad (33)$$

and  $\xi_E$  is the length scale governing the coupling range. Based on 2<sup>nd</sup> order perturbation [244, 245] we get

$$\xi_E = \frac{1}{\ln(J_2/J_1) + \ln(4 + J_1/J_2)} \propto \frac{1}{\ln(J_2/J_1)}, \quad J_2 \gg J_1, \quad (34)$$

in good agreement with the fact that pair-wise effective interactions at distance  $r$  are generated at  $r^{\text{th}}$ -order perturbation with amplitude  $\sim (J_1/J_2)^r$  [244]. Interestingly this entanglement length  $\xi_E$  is qualitatively different from the true

---

<sup>5</sup>Only pair-wise interactions are considered here, while small multiple  $2p$ -spin interactions are generated at  $p^{\text{th}}$ -order perturbation [241, 244]. For larger spins  $s \geq 1$ , the entanglement Hamiltonian is still well described by a spin- $s$  chain with a nearest-neighbor coupling independent of  $s$ , whereas longer range couplings do depend on  $s$  [245]. For XXZ chains, the  $\mathcal{H}_E$  has a renormalized Ising anisotropy [244, 245], for instance for  $s = 1/2$   $\Delta_{\text{eff}} = \frac{\Delta}{2}(1 + \Delta)$ , which keeps the same value only for free-fermions  $\Delta = 0$  and Heisenberg  $\Delta = 1$  points.

correlation length of the spin ladder  $\xi_{\text{corr}} \sim J_1/J_2$  [315]. While multi-spin (beyond pair-wise) interactions may also play a role [241], the above bilinear Heisenberg chain model Eq. (32) is already a very good approximation for the entanglement Hamiltonian in the rung singlet phase of the Heisenberg ladder, as we demonstrate below using QMC.

*Quantum-thermal mapping*—.  $T = 0$  Rényi entanglement entropies can be exactly identified with thermal entropies at temperature  $\beta = 1$  for the effective model  $\mathcal{H}_E$  defined by Eq. (29). One can also interpret the RDM as a thermal density matrix at inverse temperature  $\beta_{\text{eff}}$  of an effective model whose energy scale is set to  $J_1$  (the energy scale of the underlying Hamiltonian), as in Eq. (32). For a short-range interacting  $s = 1/2$  Heisenberg chain of  $\ell$  sites, CFT predicts [316] for the low temperature regime  $1 \gg T/J_1 \gg 1/\ell$  a thermal entropy  $S_q^{\text{th}}(T) = \frac{c}{3}(1 + \frac{1}{q})\ell T/J_1$ . Critical Luttinger liquids (Section 3.1) display an effective temperature which is vanishing with the subsystem size  $\sim (\ln \ell)/\ell$  [90, 220]. For Heisenberg chains  $T/J_1 = \frac{1}{2} \ln(\ell/a)/\ell$ , thus yielding the Calabrese-Cardy scaling Eq. (5).

For gapped spin ladders the effective temperature is of  $O(1)$ , a regime where there is no analytical expression for  $S_q^{\text{th}}$ . We have therefore performed numerical simulations [135] to compute  $S_q^{\text{th}}(T)$  of a  $s = 1/2$  Heisenberg chain (with nearest-neighbor only) at high temperature using exact diagonalization for  $\ell = 20$  sites, which was then compared to the Rényi-entanglement entropy for  $2 \times 20$  Heisenberg ladders at various Rényi indices and rung couplings  $J_2$ , computed using the improved QMC estimate developed in Ref. [135]. These results are displayed in Fig. 27 for varying rung couplings  $J_2/J_1 = 2, 4, 6, 8, 10$ , where comparing with the simplest nearest-neighbor entanglement Hamiltonian  $\mathcal{H}_E$  ( $\xi_E = 0$ ), we extract the effective inverse temperature for which the two quantities match. If the entanglement Hamiltonian is correct, the effective inverse temperature has to be independent of  $q$ . This is clearly the case if  $J_2/J_1$  becomes large, as visible in the main panel and inset of Fig. 27, where the deviation from Eq. (33) is getting smaller and flatter (as a function of  $q$ ) when  $J_2/J_1$  increases.

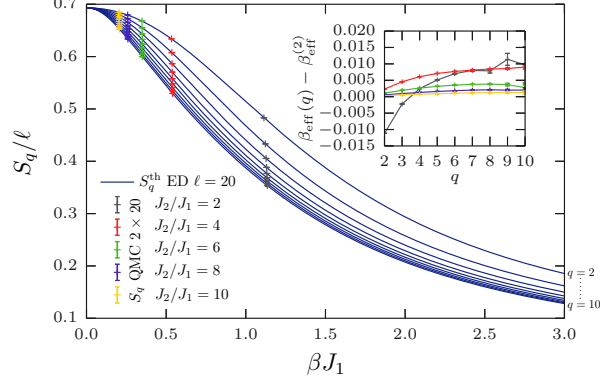


Figure 27: Comparison of the thermal entropies  $S_q^{\text{th}}$  of a  $\ell = 20$  Heisenberg chain with entanglement entropies  $S_q$  of Heisenberg ladders with various rung couplings  $J_2/J_1$  and  $q = 2, \dots, 10$ . Inverse temperatures  $\beta_{\text{eff}}$  at which  $S_q$  matches  $S_q^{\text{th}}$  of the Heisenberg chain is compared to the 2<sup>nd</sup> order result Eq. (33) as a function of  $q$  (inset). Reprinted from [135].

### 3.3.2. Participation spectroscopy

A very powerful tool to further investigate this quantum - thermal mapping is the participation spectroscopy, introduced in [142]. The participation spectrum is defined in a given computational basis  $\{|i\rangle\}$  by the diagonal of the RDM

$$\zeta_i^A = -\ln(\langle i|\rho_A|i\rangle), \quad (35)$$

with  $i = 1, \dots, 2^N$  for a subsystem  $A$  of  $N$  spin 1/2 for example. Using the entanglement Hamiltonian in Eq. (32), the effective participation spectrum

$$\zeta_i^E = \ln Z - \ln(\langle i|\exp(-\beta_{\text{eff}}\mathcal{H}_E)|i\rangle), \quad (36)$$

must fulfil, for all levels  $i$ ,  $\zeta_i^E = \zeta_i^A$ , provided  $\mathcal{H}_E$  is the correct entanglement Hamiltonian and  $\beta_{\text{eff}}$  the effective inverse temperature<sup>6</sup>. Interestingly, participation levels  $\{\zeta_i\}$  are easily measurable with QMC, contrary to the ES, except for the very low lying part which might be accessible<sup>7</sup> in some cases [247, 135, 67].

<sup>6</sup>This condition is necessary but not sufficient.

<sup>7</sup>Note however that the low "energy" part of the ES may not capture universal properties since we are not interested in ground-state but finite temperature properties of the entanglement Hamiltonian.

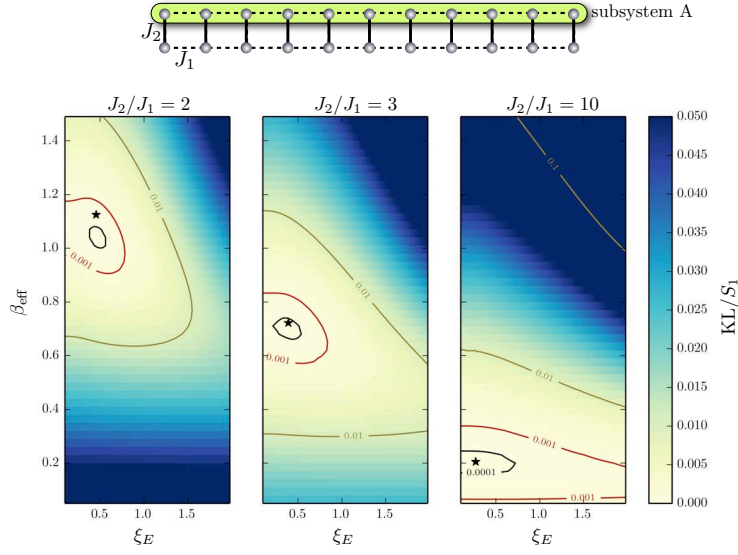


Figure 28: Relative KL divergence  $KL/S_1$  Eq. (37) of subsystem A (see schematic picture) and the effective short-range Hamiltonian Eq. (32) for different inverse temperatures  $\beta_{\text{eff}}$  and entanglement lengths  $\xi_E$ . QMC results for  $2 \times 16$  ladders. The black stars show the location of the second-order perturbative result Eqs. (33)(34).

A quantitative way to compare two spectra relies on the so-called Kullback-Leibler divergence KL [317] which measures the difference between the two probability distributions  $e^{-\zeta^A}$  and  $e^{-\zeta^E}$ . When normalized by the Shannon entropy Eq. (17) at  $q = 1$ , it reads<sup>8</sup>

$$KL/S_1 = \sum_i (\zeta_i^A - \zeta_i^E) e^{-\zeta_i^A} / \sum_i \zeta_i^A e^{-\zeta_i^A}. \quad (37)$$

In Fig. 28 we show a color map of such a KL divergence Eq. (37) comparing the

<sup>8</sup>The KL divergence and its Rényiified version [318]  $I_q = \frac{1}{1-q} \ln \left[ \sum_i e^{-\zeta_i^A} e^{-(q-1)(\zeta_i^A - \zeta_i^E)} \right]$  compare two spectra state by state, including possible degeneracies. Below we display results for  $q = 1$  (KL) which allow to compare the spectra across their entire range, contrary to  $I_{q \gg 1}$  which increases the weight in the low "energy" part. However, it is important to emphasize that we have always checked the stability under variations of  $q$ .

participation spectra of half ladders for various rung couplings  $J_2/J_1$  against the effective short-range Heisenberg chain model Eq. (32) in the parameter space spanned by the effective inverse temperature  $\beta_{\text{eff}}$  and the entanglement length  $\xi_E$ . We clearly see a minimum of the KL divergence with a very small magnitude  $< 10^{-4}$ , in good agreement with the perturbative result Eqs. (33)(34). The KL divergence provides a very precise qualitative tool to test the validity of a given entanglement Hamiltonian.

This approach has also been used for a  $d = 2$  quantum spin model [142], defined by coupled  $s = 1/2$  dimers (Fig. 29)

$$\mathcal{H}_{\text{dim}} = J_1 \sum_{\text{dimers}} \vec{S}_i \cdot \vec{S}_j + J_2 \sum_{\text{links}} \vec{S}_i \cdot \vec{S}_j, \quad (38)$$

with  $J_1, J_2 \geq 0$ . Considering only  $g = J_2/J_1 \leq 1$  ( $g = 1$  being the square lattice Heisenberg antiferromagnet), this model, intensively studied at zero temperature [319, 320, 321, 322, 323, 324], exhibits at  $g_c = 0.52370(1)$  [324] a  $2+1$   $O(3)$  quantum critical point separating a disordered gapped regime for  $g < g_c$  from an antiferromagnetic Néel ordered phase at  $g > g_c$ , with a spontaneous breaking of the  $SU(2)$  symmetry. The participation spectrum of a one-dimensional subsystem (see Fig. 29) in the gapped regime is plotted in Fig. 30 and compared with the one-dimensional effective Hamiltonian Eq. (32). Deep in the gapped regime, the results are very similar to the 2-leg ladder case, with a well-defined minimum in the KL divergences.

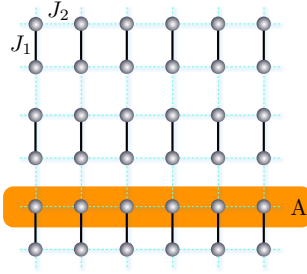


Figure 29: Schematic picture for the square lattice  $s = \frac{1}{2}$  dimerized Heisenberg model Eq. (38). The one-dimensional subsystem A is also schematized.

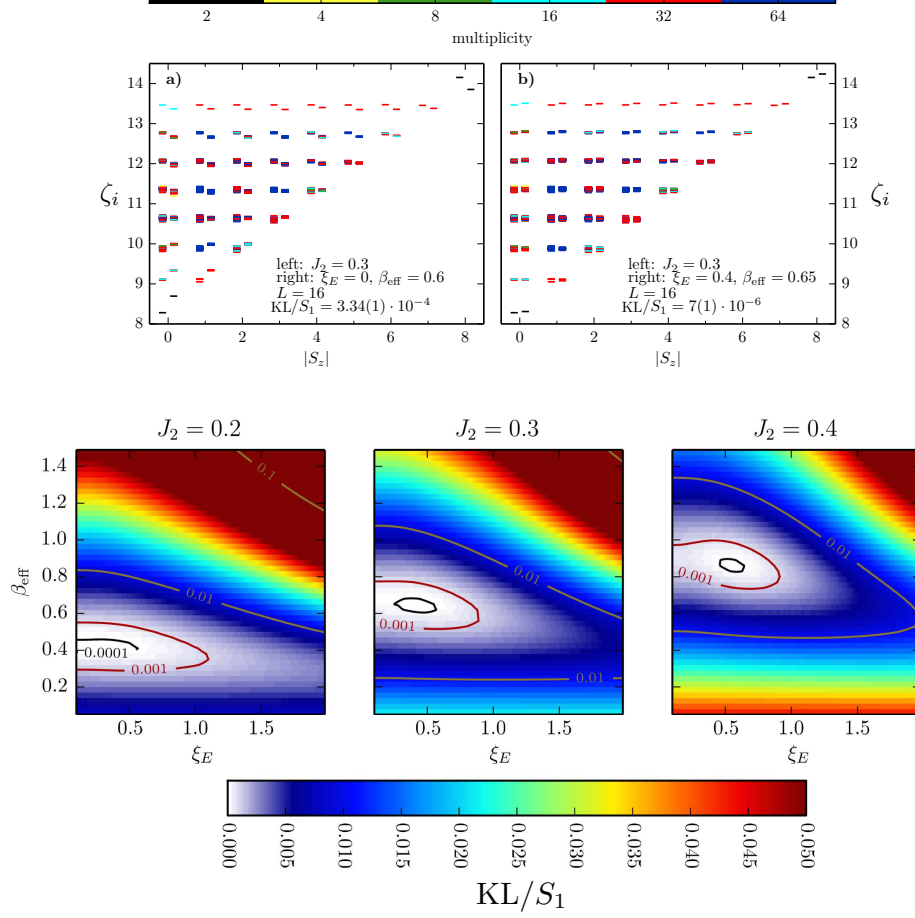


Figure 30: QMC results for the  $16 \times 16$  coupled dimer Hamiltonian Eq. (38). Top: Comparison of participation spectra of the line subsystem for  $J_2/J_1 = 0.3$  with the effective model (32). For each spin  $|S_z|$  sector, two spectra are displayed (left: line subsystem, right: effective model). Panel (a) shows the effective model is the Heisenberg chain with nearest-neighbor only ( $\xi_E = 0$ ) at  $\beta_{\text{eff}} = 0.6$ . Panel (b) shows the improved effective model with  $\xi_E = 0.4$  and  $\beta_{\text{eff}} = 0.65$ . Bottom: Color map of the relative KL divergence  $\text{KL}/S_1$  of the 1d subsystem spectrum and the effective short-range Hamiltonian Eq. (32) for different inverse temperatures  $\beta_{\text{eff}}$  and entanglement lengths  $\xi_E$ . Reprinted from [142].

### 3.3.3. Gapless states

*Quantum critical point*—. When the  $O(3)$  quantum critical point is approached, the entanglement length increases, while the effective temperature slightly de-

creases but remains of order one. As discussed by Cirac *et al.* [241], the short-range nature of the entanglement Hamiltonian qualitatively changes when approaching criticality. Based on the participation spectroscopy analysis [142], the best effective model which captures criticality for the line subsystem is no longer the short-range Hamiltonian Eq. (32) (which cannot display algebraic correlations at finite temperature), but the following unfrustrated power-law decaying model [325, 326, 327]

$$\mathcal{H}_E(\alpha) = J_1 \sum_{i,j} \frac{(-1)^{r_{ij}}}{r_{ij}^\alpha} \vec{S}_i \cdot \vec{S}_j. \quad (39)$$

In Fig. 31 we provide a direct comparison between the short-range model Eq. (32) and the one with power-law interactions Eq. (39) for  $g = 0.5$ , *i.e.* very close to the quantum critical coupling of the  $d = 2$  dimerized Hamiltonian Eq. (38). The latter model clearly displays a much better agreement, with an effective inverse temperature  $\beta_{\text{eff}} J_1 \simeq 1$ , and a power  $\alpha \simeq 2$ .

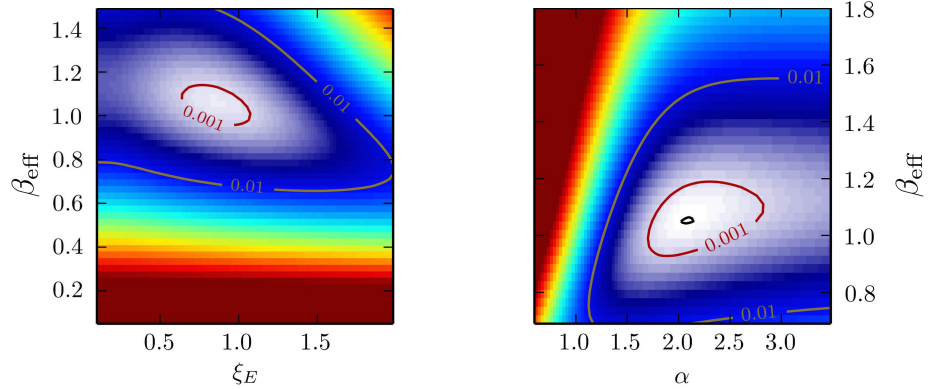


Figure 31: QMC results for the participation spectra of a one-dimensional subsystem in the  $16 \times 16$  coupled dimer Hamiltonian Eq. (38) at  $g = J_2/J_1 = 0.5$ , with the same color code as in Fig. 30. Relative KL divergences  $KL/S_1$  Eq. (37) with the short-range interacting Heisenberg chain model Eq. (32) (left) and the power-law interacting Hamiltonian Eq. (39) (right) for which the minimum is clearly smaller. Reprinted from [142].



*Néel ordered regime*—. Keeping the same one-dimensional setup for subsystem A, one can cross the critical point and explore the Néel ordered side for  $g > g_c$ , as done in Refs. [141, 142]. In this regime, while the power-law model Eq. (39) gives reasonable KL (Fig. 32 top) for parameters  $(\alpha - \beta_{\text{eff}})$  where finite temperature order is expected, a better agreement between participation spectra is found for the model

$$\mathcal{H}_E(\Lambda) = J_1 \sum_{i,j} (-1)^{r_{ij}} \left( \frac{\Lambda}{L} + \frac{1}{r_{ij}^3} \right) \vec{S}_i \cdot \vec{S}_j, \quad (40)$$

as shown in Fig. 32 for three values of  $J_2$  in the Néel regime.

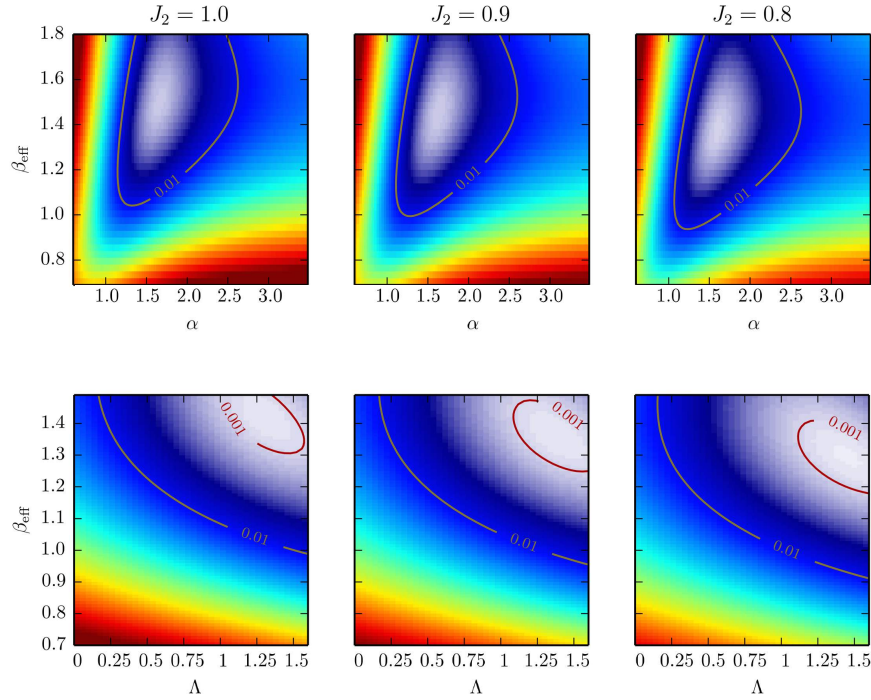


Figure 32: QMC results for the participation spectra of a one-dimensional subsystem in the  $16 \times 16$  Hamiltonian Eq. (38) at  $J_2/J_1 = 0.8, 0.9, 1$  (Néel phase), with the same color code as in Fig. 30. Relative KL divergences  $\text{KL}/S_1$  Eq. (37) with the power-law effective Hamiltonian Eq. (39) (top) and the Lieb-Matis + power-law interacting Hamiltonian Eq. (40) (bottom) for which the minimum is smaller. Reprinted from [142].

Following Refs. [96, 81, 133, 328], we expect the entanglement Hamiltonian to have both TOS and SW structures, as already discussed above for the superfluid regime of the  $d = 2$  Bose-Hubbard model, see Section 3.1.2. In Eq. (40), the  $\Lambda$  term (constant at all distances, with a  $1/L$  normalisation to ensure extensivity) has the Lieb-Mattis [329] form which has TOS but does not sustain relativistic SW excitations, whereas the power-law component  $\sim 1/r^3$  is expected to bring  $\Omega_{\text{sw}} \sim k$  excitations and  $1/r$  decaying spin correlation functions [326].

Entanglement spectroscopy for the Néel state has also been studied using PEPS calculations [313] where it was interpreted using a mapping onto a bosonic  $t - J$  chain with long distance hopping terms.

## 4. Impurity and disorder effects

Disorder and quantum fluctuations have the common tendency to destabilize classical order. Whether intrinsically present in materials, chemically controlled via doping, or explicitly introduced via a random potential (as in ultra-cold atomic systems) or by varying the thickness in superconducting films, randomness can lead to dramatic changes in physical properties of condensed matter systems, as experienced for instance with the Anderson localization [330, 146], the Kondo effect [331, 332], glassy physics [333], etc.

In such a context, entanglement witnesses have provided new tools to investigate various disordered systems as we review below, focusing on three representative examples. In section 4.1, we discuss disordered quantum spin systems which despite some similarities with their clean counterparts, display major differences. Another paradigmatic example of impurity physics is the Kondo effect for which the putative "Kondo screening cloud" can be probed using the concept of impurity entanglement entropy, as we present in Section 4.2. Finally, in Section 4.3 we discuss recent advances in the context on Anderson localization in the presence of interactions, the so-called "many-body localization" from entanglement perspectives, either at and out of equilibrium.

### 4.1. Disordered quantum spin systems

Impurity and disorder in quantum spin systems have been intensively investigated for several decades, in particular in the context of spin-glass physics [334, 335, 333]. For random field and random exchange quantum magnets, the strong disorder decimation method in real space [336, 337, 338] have been used quite intensively, with the celebrated example of the infinite randomness fixed point (IRFP) analytically described by Fisher in a serie of seminal papers for random spin chains [339, 337]. Later these idea have been extended to  $d > 1$  where a numerical approach is inevitable [340, 341, 342].

#### 4.1.1. Entanglement in random spin chains

*Random singlet state for random bonds spin  $s = 1/2$  chains*— Building on the decimation solution of the  $s = 1/2$  random exchange XXZ chain [339] and of the random transverse field Ising chain [337], Refael and Moore [343] have shown that at such an IRFP, the disorder-average von-Neumann entropy follows a similar logarithmic growth with sub-system size  $x$  as in the clean case Eq. (5), but with a smaller prefactor  $c \ln 2$ , where  $c$  is the central charge of the critical clean system ( $c = 1/2$  for Ising and  $c = 1$  for XXZ). This result can be simply understood as a direct consequence of the perturbative structure of the ground-state of the XXZ chain in the limit of strong disorder, the so-called random-singlet state [339] (depicted in Fig. 33) where the probability of finding a singlet of length  $x$  is  $\simeq 1/(3x^2)$  [344]. The quantum Ising case follows immediately using a direct relationship with the XX chain [345] which can be seen as two decoupled quantum Ising chains [346].

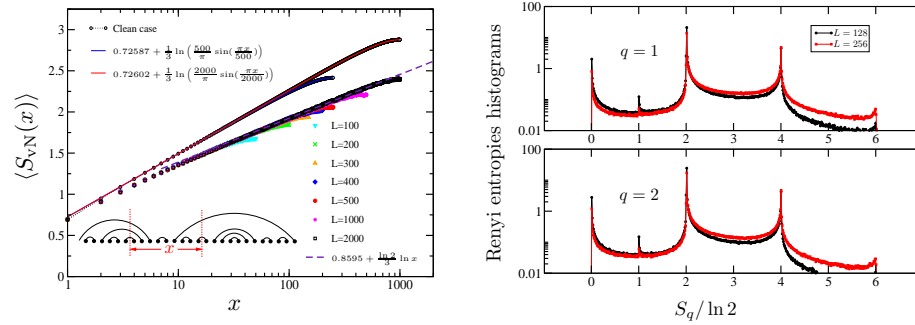


Figure 33: Exact diagonalization results for  $s = 1/2$  XX chains with random bonds. Left (reprinted from [347]): Entanglement entropy of a subsystem of size  $x$  embedded in a closed ring of size  $L$ , shown against  $x$  in a log-linear plot. For clean systems with  $L = 500, 2000$  (open circles),  $S_{\text{vN}}$  is perfectly described by Eq. (5) (red and blue curves). Data for the random case (with a uniform box distribution of couplings  $J \in [0, 1]$ ) have been averaged over  $10^4$  samples for  $L = 500, 1000, 2000$  and  $2 \times 10^4$  samples for  $100 \leq L \leq 400$ . The form  $0.8595 + \frac{\ln 2}{3} \ln x$  (dashed line) fits the data in the regime where finite size effects are absent. Right: Histograms of Rényi entropies  $q = 1, 2$  collected at half-chain over  $\sim 10^6$  independent samples, with  $L = 128, 256$  sites at strong disorder  $P(J) \propto J^{-1+1/D}$  with  $D = 5$ . The peaks, independent on the Rényi parameter, clearly show the random singlet structure.

This surprising analytical prediction was rapidly confirmed numerically [347] using exact diagonalization at the XX point where free-fermion techniques [223] allow to reach quite large chains. These results are shown in Fig. 33 (left panel) where the disorder average von-Neuman entropy displays the expected  $\frac{\ln 2}{3} \ln x$  growth. This was later verified by other groups [344, 348, 349, 350]. The random singlet structure also led to the notion of valence bond entanglement entropy [351, 352, 353, 354, 355] which is asymptotically equivalent to the usual entanglement entropy at the IRFP [351, 355].

For higher order Rényi indices, Fagotti and co-workers [349] have shown that the situation is more subtle. Indeed, depending how the disorder averaging  $\langle \dots \rangle$  is performed, they found a different prefactor for the logarithmic scaling:

$$\langle S_q \rangle = \frac{1}{1-q} \langle \ln \text{Tr} \rho_A^q \rangle = \frac{\ln 2}{3} \ln L + \text{const}(q), \quad (41)$$

while

$$\widetilde{\langle S_q \rangle} = \frac{1}{1-q} \ln \langle \text{Tr} \rho_A^q \rangle = f_q \frac{\ln 2}{3} \ln L + \text{const}'(q), \quad (42)$$

with a non-trivial prefactor  $f_q = \frac{3(\sqrt{5+2^{3-q}}-3)}{2 \ln 2(1-q)} \leq 1$ , vanishing at large  $q$  and recovering  $f_q \rightarrow 1$  when  $q \rightarrow 1$ . This ensemble averaging dependence is the hallmark of infinite randomness physics, as first identified by Fisher for correlations functions in Ref. [337] where typical and average have qualitatively different scalings.

The distribution of  $\text{Tr}(\rho_A^2)$ , shown in the main panel of Fig. 34 for the random singlet state of random XX chains (exact diagonalization results) for increasing system lengths  $L = 16, \dots, 512$ , displays broadening at small values with increasing size, suggesting non-self-averaging entanglement<sup>9</sup>. In the inset of Fig. 34, the log scalings are plotted for  $q = 1, 2$ , showing a very good agreement with the analytical prediction Eq (41) and (42).

---

<sup>9</sup>One may also try to interpret  $\text{Tr}(\rho_A^2)$  as the inverse participation ratio in the Schmidt basis. Using this analogy,  $\widetilde{\langle S_q \rangle}$  would correspond to the average while  $\langle S_q \rangle$  would be the typical value.

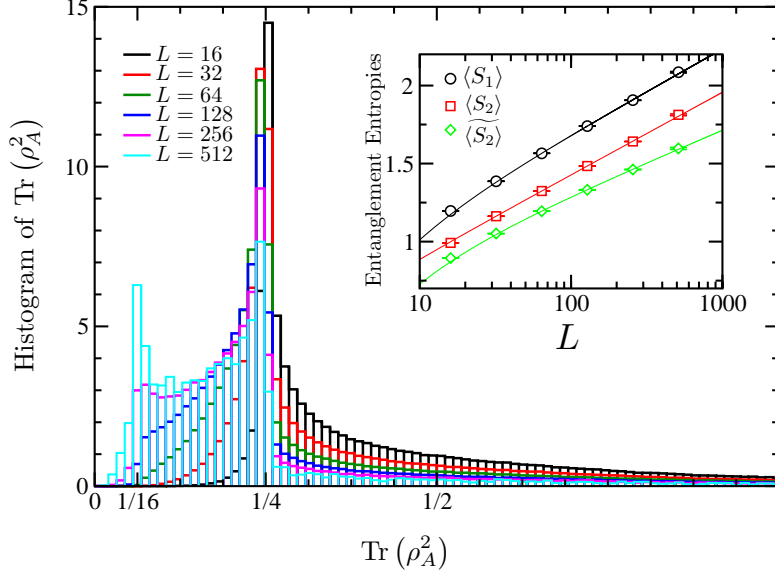


Figure 34: Histogram of  $\text{Tr}(\rho_A^2)$  in the random singlet regime. Exact diagonalization results obtained for random XX chains with  $\sim 10^5$  independent samples, with  $L = 16, \dots, 512$  lattice sites at moderate disorder (full box distribution). Inset: Best fits are  $\langle S_1 \rangle = 0.236(4) \ln x + 0.60(3) - 1.4(4)/x$ ,  $\langle S_2 \rangle = 0.229(2) \ln x + 0.37(1) - 0.15(10)/x$  and  $\langle \widetilde{S}_2 \rangle = 0.180(5) \ln x + 0.47(3) - 1.6(5)/x$ , which compare very well to  $\frac{\ln 2}{3} \simeq 0.231$  and  $f_2 \frac{\ln 2}{3} \simeq 0.177$ .

*Random spin chains with higher spin*—. Infinite randomness fixed points also occur for  $s > 1/2$  chains [356, 357, 358, 359], where Refael and Moore have shown [360] that

$$\langle S_{\text{vN}} \rangle = \frac{\ln(2s+1)}{3} \ln L + \text{constant}. \quad (43)$$

Non-abelian random-singlet states are also expected for disordered chains of Majorana or Fibonacci anyons [361, 362, 363], with a logarithmic von-Neumann entropy whose "effective central charge" pre-factor is given by  $\ln d$ , where  $d$  is the quantum dimension, *e.g.*  $d = \sqrt{2}$  for a Majorana chain, and  $d = (1 + \sqrt{5})/2$  for Fibonacci.

#### 4.1.2. Entanglement, disorder, and RG flows

*Absence of  $c$ -theorem*— Following Zamolodchikov  $c$ -theorem [364] which yields for clean (disorder-free) fixed points a decreasing of entanglement entropy along RG flows, the question whether this also holds in the presence of disorder was addressed after the discovery of decreasing entropies along infinite randomness flows [343, 347, 360]. Two counter examples have shown that this cannot be true for disordered fixed points, as first discussed by Santachiara [365] for generalized quantum Ising chains including the  $N$ -states random Potts chain, and later by Fidkowski and co-workers [362] for disordered chains of Fibonacci anyons. The phase diagram of this disordered golden chain model is sketched in Fig. 35, as also discussed by Refael and Moore in Ref. [366].

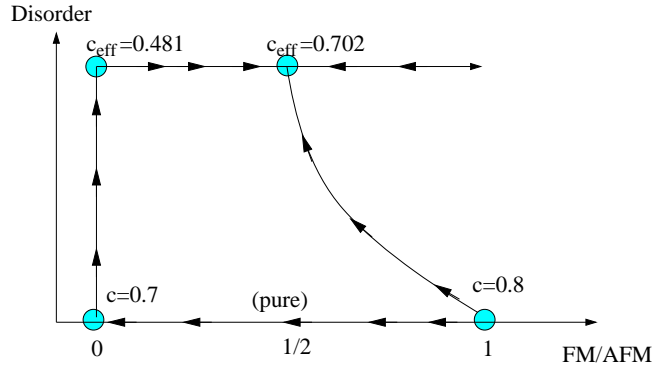


Figure 35: RG flow diagram of the pure and random golden chain with ferromagnetic and antiferromagnetic couplings. Reprinted from [362].

*Engineered disorder*— Interestingly, a volume-law scaling of the entanglement entropy can be achieved for the ground-state of a class of random spin chains where disorder is not random, but engineered, building on the decimation rules such that the probability of finding a singlet at any distance  $x$  is uniform. Designed with very fast decaying couplings, the so-called concentric singlet phase can be constructed [367, 368, 369], with a very strong entanglement entropy proportional to the number of sites inside the subsystem.

Another model where disorder is partly controlled was proposed by Binosi and co-workers [370], through the following disordered quantum Ising chain model

$$\mathcal{H} = - \sum_i J_i (S_i^z S_{i+1}^z + S_i^x), \quad (44)$$

where one sees that the independent random couplings  $J_i$  act on both a site and its adjacent link, such that a perfect (but purely local) correlation is achieved. Using field theory, strong disorder RG, and large scale numerical diagonalization techniques, we have investigated this interesting model in Ref. [371]. For perfect correlation weak disorder is irrelevant, whereas any small breaking of the perfect correlation between field and coupling in Eq. (44) brings the system back to infinite-randomness physics. For larger disorder (and perfect local correlation), there is a line of critical points with unusual properties such as an increase of the entanglement entropy with the disorder strength, as shown in Fig. 36.

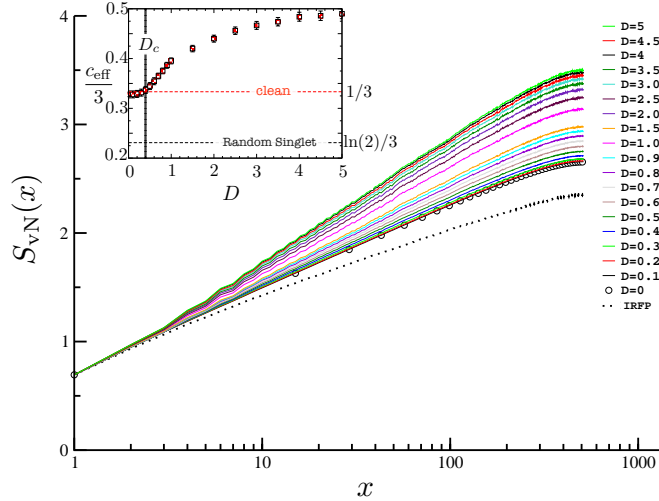


Figure 36: Disorder averaged entanglement (von-Neumann) entropy plotted against subsystem size  $x$  for the critical ground-state of Eq. (44) with correlated disorder for various disorder strengths  $D$  ( $P(J) = J^{-1+1/D}/D$  with chains of 1024 sites averaged over 5 000 disorder realizations). Inset: coefficient of the logarithmic increase of the entanglement entropy plotted against the disorder strength  $D$ . Reprinted from Ref. [371].



This model brings an interesting example where by construction the disordered system is always strictly critical at the local level. This apparent suppression of local randomness protects the clean physics against small disorder, but at strong enough disorder a new physics appears where entanglement increases with the strength of disorder. The XXZ extension of this model was recently studied in Ref. [372], reaching similar conclusions as compared to free fermions.

#### 4.1.3. $d > 1$ Infinite randomness

Infinite randomness physics is not specific to one dimension, as shown for the  $d \geq 2$  disordered quantum Ising model [340, 373, 342, 374], disordered contact process [375], or dissipative systems [376]. However, note that random singlet physics does not describe  $d > 1$  random exchange antiferromagnets [341, 377], where long-range order is surprisingly robust to disorder [377].

Entanglement entropy at the IRFP of the  $d = 2$  random transverse field Ising model on the square lattice has been first studied numerically in [378] where a surprising double logarithmic enhancement of the area law was found  $S \sim L \ln(\ln L)$ , based on strong disorder RG arguments<sup>10</sup>. Later, using larger systems, Yu and co-workers [380] concluded for a pure area law with additive (negative) logarithmic corrections.

Using a greatly improved strong disorder RG algorithm where the  $\mathcal{O}(N^3)$  running time of the naïve algorithm was brought down to  $\mathcal{O}(N \ln N)$  for arbitrary dimension, Kovács and Iglói [373, 342] have studied entanglement of  $d = 2, 3, 4$  disordered quantum Ising models up to  $N \sim 10^6$  spins [382]. This allowed to get a very good control of finite size scaling, as shown in Fig. 37 where the square lattice entropy, plotted as a function of the subsystem size, clearly displays a pure area law as a leading term. Interestingly, corrections to this area law scaling can be precisely computed: in two dimensions, for square

---

<sup>10</sup>Nevertheless, another type of IRFP in higher dimensions occurs in the bond-diluted quantum Ising ferromagnet [379] for which the same authors [378] found (using much larger system sizes) a pure area law contribution at the percolation threshold.

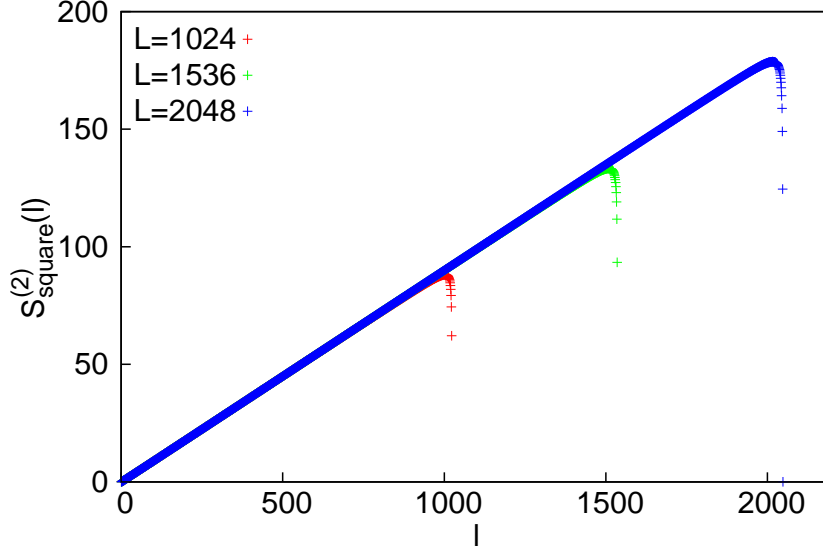


Figure 37: Area law scaling of the von-Neumann entropy of the disordered transverse field Ising model on the square lattice, computed at criticality (infinite disorder fixed point) using SDRG. Reprinted from Ref. [381].

(or slab in higher dimension) subsystems, additive logarithmic corrections are found [382], coming from the 4 corners of a square subsystem, such that

$$S_{\text{vN}} = aL + 4l_1(\pi/2) \ln L + \text{constant} \quad (45)$$

with  $l_1(\pi/2) = -0.029(1)$  obtained for very large clusters, up to  $2048 \times 2048$  (to be compared with  $-0.019(5)$  obtained for smaller systems  $160 \times 160$  by Yu *et al.* [380]). This log correction, arising from  $\pi/2$  corners at a strong disorder fixed point, can be compared to clean critical points contributions studied in Section 2.2.2, and reported in Table 2. More generally, Kovács and Iglói found that additive logarithmic contributions induced by the sharp subsystems boundaries only occur at criticality, as shown in the bottom part of Fig. 38 where the corner part appears to be a universal singular function, describing the log divergence at the critical point with a prefactor whose magnitude and sign depend on the dimension:  $l_1(3d) = 0.012(2)$ , and  $l_1(4d) = -0.006(2)$ .

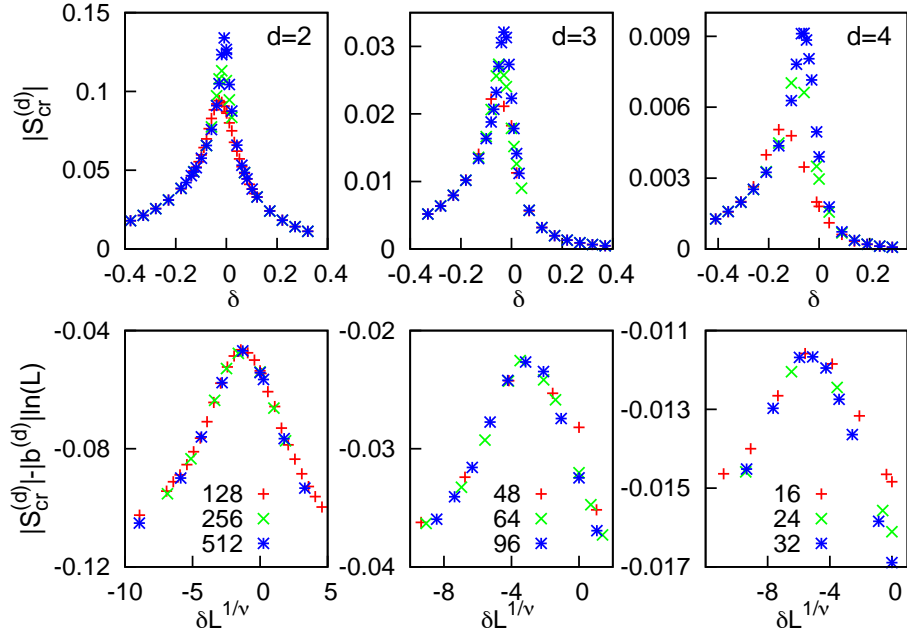


Figure 38: Upper panels: entropy contribution of the corners  $|S_{\text{cr}}^{(d)}|$  in dimension  $d = 2, 3$  and  $4$  for different system sizes as a function of distance to criticality  $\delta$ . Bottom panels: Universal scaling function using  $b^{(2)} = -0.029$ ,  $b^{(3)} = 0.012$ , and  $b^{(4)} = -0.006(2)$ . Reprinted from Ref. [382].

Such universal features of the additive logarithmic corrections to the area law appear to be a promising way to further characterize quantum criticality [111, 114, 113].

## 4.2. Entanglement and Kondo physics

### 4.2.1. Generalities

The resistivity minimum observed in dilute magnetic alloys received a beautiful theoretical explanation by Jun Kondo [331] based on a perturbative calculation which breaks down at low-energy. This is a remarkable condensed matter example of asymptotic freedom [383], with the effective interaction between magnetic impurities and conduction electrons growing when the temperature

decreases. Non-perturbative calculations, based on a scaling approach [384], the renormalization group (RG) [385], Fermi liquid theory [386], Bethe Ansatz [387, 388] provide a very powerful framework to study this non-trivial many-body problem (for a thorough review, see [332]). In particular, the anomalous scattering from magnetic impurities leads to an enhancement of both specific heat and magnetic susceptibility at low temperature, below the Kondo temperature  $T_K$ . The thermal entropy  $S^{\text{Th}}(T)$  is a non-trivial function of  $T$ , reflecting the RG fixed points of the Kondo problem. In the limit of a weak bare Kondo coupling, the impurity contribution  $S_{\text{imp}}^{\text{Th}}(T) \approx \ln 2$  at  $T \gg T_K$  and  $S_{\text{imp}}^{\text{Th}}(T) \rightarrow 0$  at  $T \ll T_K$ . This reflects the fact that the bare coupling of the magnetic impurity to the conduction electrons is very weak so that we obtain essentially the full entropy of a free spin-1/2,  $\ln 2$  at  $T \gg T_K$ . However, as the temperature is lowered the spin becomes "screened" *i.e.* it goes into a singlet state and the impurity entropy is accordingly lost. The asymptotic values of  $S_{\text{imp}}^{\text{Th}}(T)$  at high and low temperatures are characteristic of the RG fixed points of the Kondo Hamiltonian.

However much less is known about real space spatial properties of the Kondo effect, in particular the so-called Kondo screening length  $\xi_K \sim v_F/T_K$  (where  $v_F$  is the Fermi velocity) which is expected to govern spatial correlations at  $T \ll T_K$  [389]. Such a Kondo screening cloud<sup>11</sup>, which can be seen as the region over which a magnetic impurity forms a singlet with a conduction electron, is very hard to experimentally observe in realistic systems because it occurs over quite large distances  $\sim \mu\text{m}$ , and decays as  $1/r^d$  [389], thus making reduced dimensionality better candidates to observe it [391, 392, 393].

#### 4.2.2. Impurity entanglement in the one-channel Kondo problem

Recently, several developments have been made to study how the Kondo length  $\xi_K$  emerges in the entanglement properties of quantum impurity problems [394, 395, 396, 397, 398, 399, 400, 401, 402, 403, 404]. Assuming a direct

---

<sup>11</sup>Probably better described as a "faint fog" [390]

analogy with the thermal impurity entropy which is a scaling function  $f(T/T_K)$ , one might expect the zero temperature impurity entanglement entropy to be also a scaling function  $g(r/\xi_K)$ , where  $r$  is the spatial extension of the subsystem over which entanglement is computed.

The usual Kondo Hamiltonian [405] contains a Heisenberg interaction between a  $s_{\text{imp}} = 1/2$  impurity spin and otherwise non-interacting electrons:

$$\mathcal{H} = \int d^3r \left[ \psi^\dagger (-\nabla^2/2m) \psi + J_K \delta^3(\vec{r}) \psi^\dagger (\vec{\sigma}/2) \psi \cdot \vec{s}_{\text{imp}} \right]. \quad (46)$$

At zero temperature, the impurity spin is screened by the conduction electrons through the formation of a Kondo singlet, expected to take place over a length scale:

$$\xi_K = v_F/T_K \propto e^{1/(\nu J_K)}, \quad (47)$$

where  $\nu$  is the density of states per spin band,  $T_K$  is the Kondo temperature and  $v_F$  the velocity of the fermions. Due to the  $\delta$ -function form of the interaction Eq. (46) can be reduced to a one-dimensional model on a semi-infinite line with the impurity spin at the origin [395]. A further simplification is possible using the spin chain Kondo model [406, 407], depicted in Fig. 39 (a), and governed by the following spin- $\frac{1}{2}$  Heisenberg chain Hamiltonian

$$\mathcal{H} = J_1 \sum_{i=1}^{L-1} \vec{S}_1 \cdot \vec{S}_{i+1} + J_2^c \sum_{i=2}^{L-2} \vec{S}_i \cdot \vec{S}_{i+2} + J'_K \vec{s}_{\text{imp}} \cdot (J_1 \vec{S}_1 + J_2 \vec{S}_2), \quad (48)$$

where the frustrated second neighbor antiferromagnetic coupling is tuned at the critical point  $J_2^c \simeq 0.2412$  [408, 51] where logarithmic corrections vanish<sup>12</sup>.

Numerical simulations on this simplified Kondo model Eq. (48) have been carried out [411, 394, 395, 397], showing that (i) open boundary conditions lead to oscillations of the entanglement entropy, slowly decaying away from the boundaries with an exponent governed by the Luttinger parameter [411];

---

<sup>12</sup>For  $J_2 = 0$  Eq. (48) was shown to be integrable with Bethe Ansatz by Frahm and Zvyagin [409], with also a strong analogy with the Kondo problem but with a modified Kondo temperature  $T_K \sim \exp(-b/\sqrt{J'_K})$ . For  $J_2 > J_2^c$ , the spin chain enters a dimerized phase [410] with a gap and the relation between Eq. (48) and Kondo physics no longer holds.

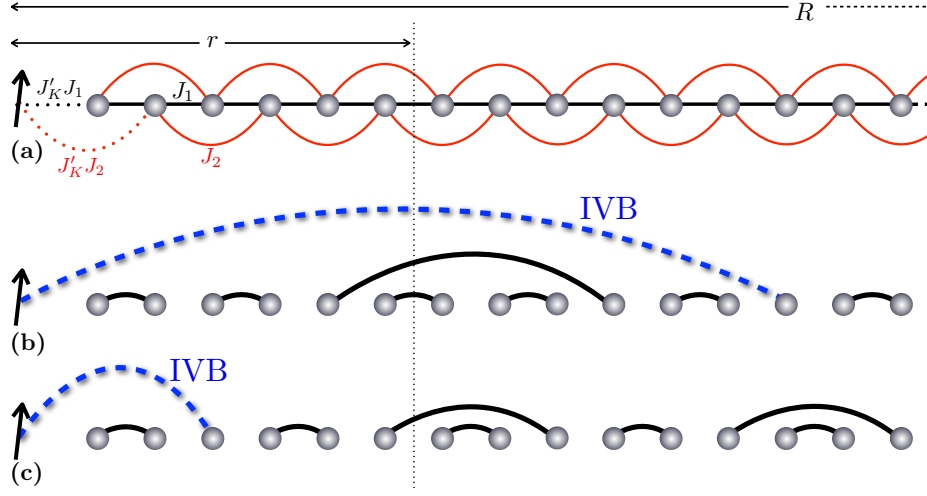


Figure 39: (a) Schematic picture for the open frustrated Heisenberg chain model Eq. (48) coupled to a spin impurity (arrow). (b) and (c) Example of valence bond configurations with the Kondo singlet materialized by the impurity valence bond (IVB) shown (blue dashed bond) for weak (b) and strong (c) coupling regimes. The total chain length is  $R$  and the subsystem has  $r$  sites, including the impurity spin.

and (ii) the impurity contribution to the entanglement entropy appears to be a universal scaling function  $S_{\text{imp}}^{\text{E}}(R, r, J'_K) = g(r/\xi_K, R/\xi_K)$ , where  $r$  ( $R$ ) is the subsystem (full system) size, see Fig. 39, and  $\xi_K(J'_K)$  is the Kondo length.

The simplest quantity to study is the single site impurity entanglement entropy (defined for  $r = 1$ ) which is directly proportional to the impurity magnetization  $\langle s_{\text{imp}}^z \rangle$ . This local observable, studied for the spin-boson model [412, 413, 414] and for the usual Kondo problem [415, 416] was shown to violate scaling in Ref. [395]. Indeed, the Kondo screening mechanism being a non-local many-body quantum effect, scaling properties are expected to occur for many-body correlators, as for instance in the entanglement of a finite size  $r > 1$  region. The impurity contribution to the entanglement entropy was therefore studied [394, 395] in the limit  $1 \ll r \ll R$ , defined by

$$S_{\text{imp}}(R, r, J'_K) = S_{\text{u}}(R, r, J'_K) - S_{\text{u}}(R-1, r-1, 1), \quad (49)$$

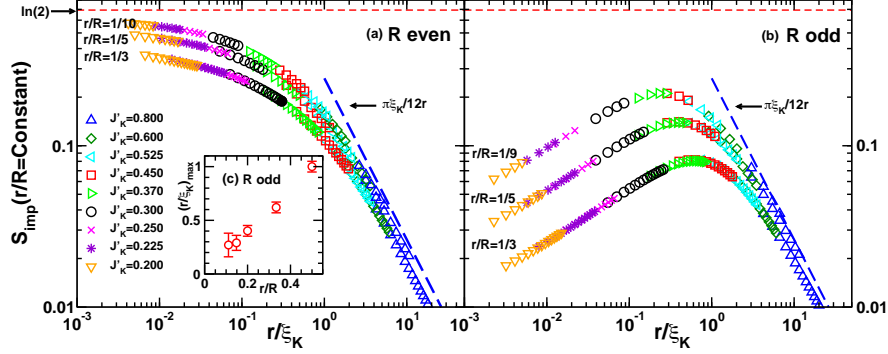


Figure 40: Universal scaling plot of  $S_{\text{imp}}$  at fixed  $r/R$ , (a) for  $R$  even, (b)  $R$  odd. DMRG results for the  $J_1 - J_2$  spin chain Kondo model Eq. (48) for various Kondo couplings  $J'_K$ . Dashed line  $\pi\xi_K/(12r)$  is the Fermi liquid theory prediction. Inset (c): the location of the maximum,  $(r/\xi_K)_{\text{max}}$ , of  $S_{\text{imp}}$  for odd  $R$ , plotted versus  $r/R$ . Reprinted from Ref. [394].

where  $S_u(R, r, J'_K)$  is the uniform part of the entropy for a total system of length  $R$ , a subsystem of length  $r$  and a boundary coupling  $J'_K$ . DMRG simulation results are displayed in Fig. 40 for  $R$  even and odd. In the strong coupling regime  $r/\xi_K \gg 1$ , the local Fermi liquid theory of Nozières [386] predicts  $S_{\text{imp}} = \pi\xi_K/(12r)$ , perfectly captured by the numerical results in Fig. 40. In the opposite limit, when the Kondo cloud is much larger than the subsystem  $r/\xi_K \ll 1$ , DMRG data from Fig. 40 suggest  $\lim_{r/\xi_K \rightarrow 0} \lim_{r/R \rightarrow 0} S_{\text{imp}}(r/\xi_K, r/R) = \ln 2$ , for either parity of  $R$ .

A heuristic picture giving the general features of  $S_{\text{imp}}(r/\xi_K, r/R)$ , for both even and odd  $R$ , sketched in Ref. [394, 395], can be derived from a resonating valence bond view of the ground state, as depicted in Fig. 39 (b,c). We loosely identify  $S_{\text{imp}}$  with  $\ln 2 \times$  the probability of an “impurity valence bond” (IVB) stretching from the impurity site into the region  $> r$  (Fig. 39). The typical length of the IVB is expected to be  $\sim \xi_K$  (for  $\xi_K < R$ ), leading to the monotonic decrease of  $S_{\text{imp}}$  with increasing  $r/\xi_K$ , for  $R$  even, and its vanishing as  $r/\xi_K \rightarrow \infty$ . For  $R$  odd, the ground state contains one unpaired spin. When  $\xi_K \rightarrow \infty$  this unpaired spin is the impurity itself, implying no IVB and hence  $S_{\text{imp}} = 0$ .

As  $\xi_K$  decreases the probability of having an IVB increases, since the unpaired spin becomes more likely to be at another site, due to Kondo screening, but the average length of the IVB, when it is present, decreases. These two effects trade off to give  $S_{\text{imp}}$  a maximum when  $\xi_K \propto R$ , in good agreement with the inset of Fig. 40, at which point the probability of having an IVB becomes  $O(1)$  but the decreasing average size of the IVB starts to significantly reduce the probability of it stretching into the region  $> r$ .

#### 4.2.3. Boundary effects

Conformally invariant boundary fixed points are expected to present a term in the entanglement entropy which corresponds to the zero temperature Affleck-Ludwig impurity entropy  $\ln g$  [417], as pointed out in Ref. [21]. Therefore, in a semi-infinite chain with the subsystem staring at the boundary, Eq. (5) becomes

$$S_q^{\text{OBC}}(r) = \frac{c}{12} \left(1 + \frac{1}{q}\right) \ln r + s_q/2 + \ln g + \dots \quad (50)$$

For the single channel Kondo model  $\ln g = \ln 2$  at the weak coupling fixed point where the impurity is unscreened, and  $\ln g = 0$  at the strong coupling fixed point where it is screened. The thermodynamic impurity entropy decreases monotonically from  $\ln 2$  to 0 with decreasing  $T/T_K$ , in the same way as the impurity entanglement entropy with increasing  $r/\xi_K$ .

The validity of Eq. (50) has been checked numerically for various examples of conformally invariant boundary conditions, for quantum Ising chains [418, 395, 419, 420], a case where there is no boundary induced oscillations, as well as for the two-channel Kondo problem [421]. Conversely, for critical open chain models having a continuous symmetry, slowly decaying oscillations have been reported [411, 422, 423, 424, 425] and interpreted as  $2k_F$ -Friedel oscillations [426], whose decay is governed by the Luttinger parameter [411, 427]. An exact computation for the XX (free-fermions) case was done by Fagotti and Calabrese [427] who derive rigorously the asymptotic behavior for large block sizes on the basis of a recent mathematical theorem for the determinant of Toeplitz plus Hankel matrices. Interestingly, unusual oscillating corrections have been reported for



higher Rényi indices  $q > 1$  for open systems, and also for periodic chains, *i.e.* in the absence of boundary [33, 34, 428].

Despite the good analytical description for free fermions [427], boundary induced oscillations in the von-Neumann entropy still lack for a complete analytical understanding for interacting critical systems. A phenomenological grasp was conjectured, based on DMRG data analysis and a valence bond picture in Ref. [411] where the alternating part in the entropy for critical XXZ chains was found to be directly proportional to the alternating term in the energy density. Indeed, open end breaks translational invariance and a slowly decaying alternating term (at  $2k_F = \pi$  in the absence of external magnetic field) or "dimerization" in the energy density  $E_u(r, R) + (-1)^r E_{\text{stag}}(r, R)$  appears at distance  $r$  for chains of length  $R$ , where for critical chains  $E_{\text{stag}}(r, R) \propto [\frac{2R}{\pi} \sin(\frac{\pi r}{R})]^{-K}$ ,  $K$  being the Luttinger liquid parameter. The oscillating term in the entropy was then found to be intimately related to such energy density oscillations, such that

$$S_{\text{stag}} = -(\pi a^2/2v)E_{\text{stag}}, \quad (51)$$

where  $v$  is the velocity of excitations, and  $a$  the lattice spacing, introduced to make the entanglement entropy a dimensionless quantity. Fig. 41 summarizes these results, obtained in Refs. [411, 396].

It is important to note that boundary induced oscillations are relevant for the DMRG technique which better perform with OBC, and also in the experimental context of cold atoms where such oscillations have been predicted for trapped bosons [429]. Likewise, open ends lead to oscillations in gapped models, such as the  $s = 1$  Heisenberg chain [430], but with an alternating part which decays exponentially fast with the distance from the boundary, confirming the fact that this alternating component is controlled by the spin-spin correlations. Let us finally notice that boundary critical phenomena have also been studied using entanglement renormalization schemes [431, 432].

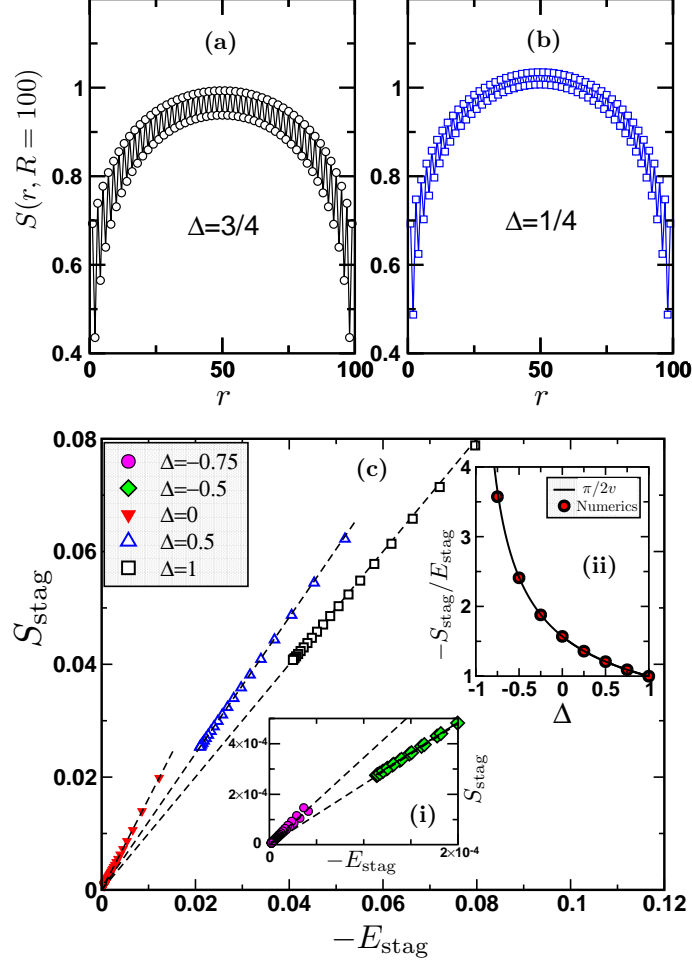


Figure 41: (a) and (b) Von Neuman entropy of XXZ chains of lengths  $R = 100$  with OBC computed with DMRG for various anisotropies  $\Delta$ . One sees the oscillating feature, whose amplitude is reduced when  $\Delta$  decreases. Linear behavior of the staggered part of the entanglement entropy,  $S_{\text{stag}}$  as a function of the staggered energy density,  $-E_{\text{stag}}$ , both computed using DMRG on critical open XXZ chains of size  $200 \leq R \leq 1000$  for various anisotropies  $\Delta$ . Data from free-fermions diagonalization at  $\Delta = 0$  are also shown for  $R = 2000$ . Dashed lines are linear fits of the form Eq. (51). Inset (i) is a zoom close to 0, showing data for  $\Delta = -3/4$  and  $-1/2$ . Inset (ii) shows the proportionality factor against  $\Delta$  extracted from the numerical data (circles), for a larger set of values of  $\Delta$ , which is compared with  $\pi/2v$ . Reprinted from [396] (a,b) and from [411] (c).

#### *4.2.4. Other examples of quantum impurity problems probed by entanglement*

The two-impurity Kondo problem was investigated using two-site entanglement witnesses in Ref. [433], or the more complex many-body Schmidt gap, expected to play the role of an order parameter close to quantum criticality [231], likewise observed for the two-channel Kondo problem [421]. Another example of quantum criticality was studied for the spin-boson model [412] where quantum entanglement of the impurity was studied in great detail [434, 413, 414, 435]. Entanglement entropy was also studied near Kondo-destruction quantum critical points [404].

Local defects in quantum wires, reminiscent of the so-called Kane-Fisher problem [436, 406], have been studied quite intensively using entanglement estimates [437, 438, 439, 60, 440, 402, 57, 441]. Dynamical properties have also been investigated for quantum impurity problems. For instance in quantum Ising chains with local or extended defects, the time evolution of the entanglement entropy, studied by Iglói and co-workers [442], displays a logarithmic growth with a non-universal prefactor which depends on the microscopic details of the defects.

The Kondo cloud dynamics has been probed after a quantum quench in the resonant level model. At long enough time inside the light cone, the Kondo screening cloud relaxes exponentially to the final equilibrium structure, with a relaxation rate given by the emergent energy scale of impurity screening [443]. Finally, universal oscillations in the entanglement levels have also been reported by Bayat and co-workers [444] for the two-impurity Kondo spin chain model after a local quench of the RKKY interaction from RKKY to Kondo regime.

### 4.3. Many-body localization

#### 4.3.1. General properties

The so-called many-body localization phenomenon has attracted a huge interest in recent years, following precursor works [445, 446, 447, 448, 449, 450] which discussed whether Anderson localization [330] can survive interactions. A new paradigm has then emerged for many-body eigenstates of strongly disordered interacting systems which may not obey the "eigenstate thermalization hypothesis" (ETH) [451, 452, 453] and would fail to thermalize [454]. Such a many-body localization (MBL) clearly challenges the very foundations of quantum statistical physics [454, 455] as thermalization in such closed systems cannot occur without external bath (for a recent discussion, see also Ref. [456]). Another interesting property is that MBL may lead to long-range (possibly topological) order, otherwise absent for equilibrated systems [457, 458, 459, 460, 461]. Furthermore, the MBL shares properties with integrable systems, with an extensive number of local integrals of motion [462, 463, 464, 465].

Several numerical studies have recently focused on the MBL phase, and associated phase transitions. Most of the studied models are one-dimensional, mostly for practical reasons: *e.g.* the random field Heisenberg or XXZ chain [466, 467, 468, 469, 470],  $d = 1$  interacting fermions [471, 460, 472] (relevant to the recent experiments [473] on quasi-periodic chains [474]), quantum Ising chains [457, 461, 475], spin-glasses [476], and also translationally-invariant models [477, 478, 479, 480], or driven systems [481]. While exact diagonalization are typically limited to  $\sim 20$  sites [470], larger systems can also be studied using approximate methods such as strong disorder RG techniques, the so-called RSRG-X method [482, 461, 483, 484], or Matrix Product States approaches exploiting the low entanglement property of the MBL regime [485, 486, 487, 488, 489]. However, these techniques are practically limited to strong disorder on the MBL side of the phase diagram where they are well controlled. At weaker disorder, in the ergodic regime, only exact numerical approaches are expected to give quantitatively reliable results.

A canonical example of interacting model which exhibits a MBL transition is the random field Heisenberg  $s = 1/2$  chain<sup>13</sup>, governed by the Hamiltonian

$$\mathcal{H} = \sum_{i=1}^L \left( J \vec{S}_i \cdot \vec{S}_{i+1} - h_i S_i^z \right), \quad (52)$$

where the random field is drawn from a uniform distribution in  $[-h, h]$ . Using a spectral transformation, this model has been studied by exact diagonalization at varying energy densities across the entire spectrum up to  $L = 22$  spins [470] in order to extract the many-body mobility edge shown in Fig. 42.

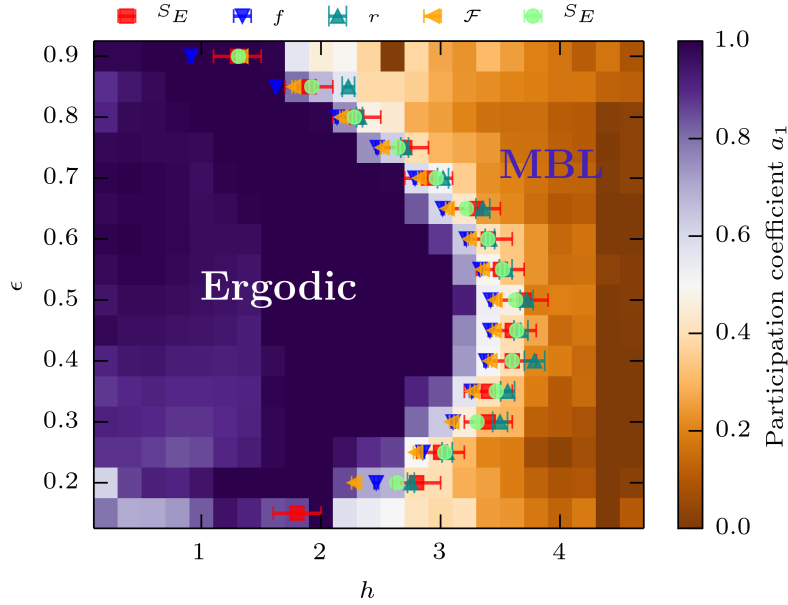


Figure 42: Phase diagram Disorder ( $h$ ) *vs.* Energy density ( $\epsilon$ ) of the random-field Heisenberg chain Eq. (52). The ergodic phase (dark region with a participation entropy coefficient  $a_1 \simeq 1$ ) is separated from the MBL regime (bright region with  $a_1 \ll 1$ ). Various symbols show the energy-resolved MBL transition points extracted from finite size scaling performed over system sizes  $L \in \{14, 15, 16, 17, 18, 19, 20, 22\}$  for different quantities. Reprinted from [470].

<sup>13</sup>Equivalent via a Jordan-Wigner (Matsubara-Matsuda) transformation to interaction spinless fermions (hard-core bosons) in a random potential.

Because the MBL phenomenon leads to the absence of thermalization, we do not expect any sort of thermodynamic signatures of a localization/delocalization transition in finite temperature observables. Instead, the transition has to be studied either at infinite temperature, *i.e.* with all eigenstates equally weighted [471, 467], or by targeting eigenstates at finite energy density above the ground-state [475, 470], which is better justified for systems having a many-body mobility edge at finite energy density  $\epsilon$  (Fig. 42). Another possibility to study such a dynamical transition is to make a global quench from a high-energy unentangled product state [468, 462].

Numerical studies of the many-body eigenstates provide a very precise and quantitative way to characterize the localized/delocalized nature of the system. For example, a popular way to differentiate extended and localized phases relies on the spectral statistics from random matrix theory [490]. As exploited in several works [447, 448, 471, 467, 491, 476, 470], the ergodic regime harbors a statistical distribution of level spacings which follows Wigner’s surmise of the Gaussian orthogonal ensemble (GOE), while a Poisson distribution is expected for localized states. At the transition, it is not clear whether there is a continuous family of critical theories [476] or semi-Poisson statistics [492, 493, 494].

	Delocalized	Transition	MBL
Spectral statistics	GOE	?	Poisson
Entanglement entropy $S^E(L)$	volume-law	volume-law <sup>14</sup>	area law
Entanglement variance $\sigma_E^2(L)$	vanishes	diverges	finite
Entanglement dynamics $S^E(t)$	$t^{1/z}$	$\ln t$	$\ln t$

Table 3: Various properties of ergodic and MBL phases, as well as at the transition.

The level statistics properties are summarized in Table 3, together with entanglement features across the different regimes. Below we discuss in detail how entangled are the eigenstates in both delocalized and MBL regimes, as well

<sup>14</sup>See discussions in Refs. [495, 496, 493].

as at the transition between the two regimes. We first focus on eigenstates at equilibrium for which a clear transition from a volume to an area law scaling of the entropy is observed. Then, the non-equilibrium situation is examined through quantum quenches, starting from high-energy untangled states.

#### 4.3.2. Area vs. volume law for highly excited states

Thermalization in isolated quantum systems implies that the system itself acts as its own heat bath [497]. This is the case for the so-called ergodic regime (adjacent of the MBL phase, see Fig. 42) where ETH [451, 452] is expected to hold. In this delocalized phase, the RDM of a high energy eigenstate can be viewed as a thermal density matrix at high temperature. Therefore, the entanglement entropy of such a highly excited eigenstate is very close to the thermodynamic entropy of the subsystem at high temperature, thus exhibiting a volume-law scaling. Such delocalized eigenstates can therefore be described as pure random states [498]. Volume-law entanglement at high temperature has been verified for disorder-free quantum spin chains [395, 499, 500, 501], as well as for the ergodic regime of weakly disordered chains [460, 475, 470].

*Many-body localization*—. On the other hand, contrary to the thermal phase, the MBL regime does not obey ETH [467] and the eigenstates sustain a much smaller (area law) entanglement, qualitatively closer to the entanglement entropy of a ground-state [13]. Such qualitatively distinct properties have been clearly shown numerically in various exact diagonalization studies [460, 475, 470]. In Fig. 43 (a-b) exact diagonalization results of model Eq. (52) are shown for the disorder-average von-Neumann entropy of half-chains for eigenstates lying in the middle of the many-body spectrum ( $\epsilon = 0.5$  in Fig. 42) as a function of size  $L$  and disorder strength  $h$ . The transition from volume to sub-volume scaling is clearly visible, as provided by the scaling plot in panel (b). Numerical data are compatible with a volume-law entanglement entropy at criticality [495], and with a strict area law scaling for the MBL regime (dashed line in panel (b))

of Fig. 43)<sup>15</sup>. Breakdown of the area law at the delocalization transition was recently exploited in a numerical linked cluster expansion study [503] to locate the MBL transition<sup>16</sup>.

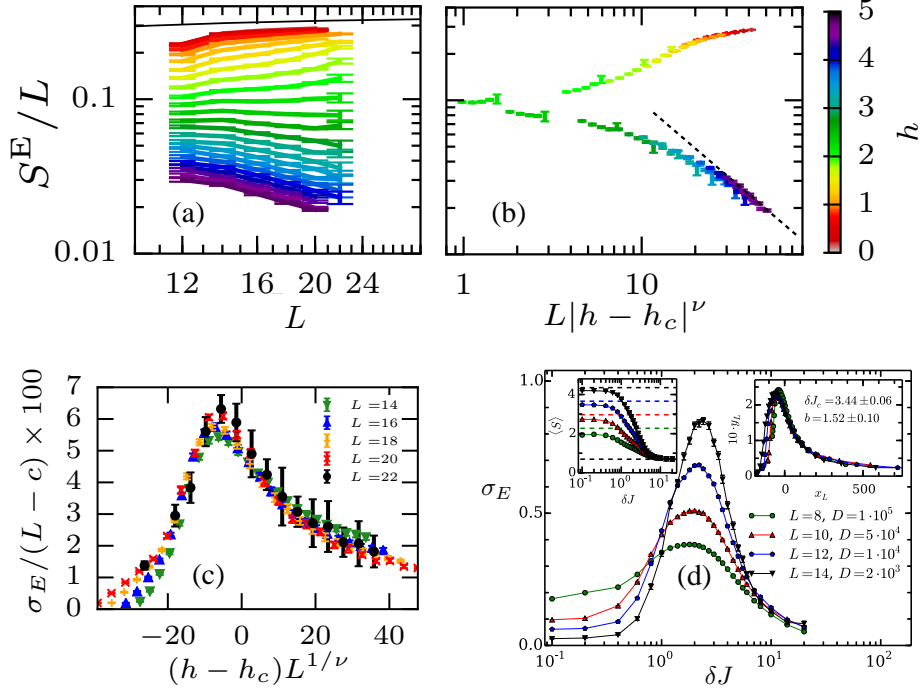


Figure 43: Exact diagonalization results for the disorder-average entanglement (von-Neumann) entropy at half-chain for (a-c) the random field Heisenberg chain model Eq. (52) at a fixed energy density  $\epsilon = 0.8$  with  $L = 12, \dots, 22$  [470], and (d) on a disordered quantum Ising chain computed at a fixed energy density in the middle of the many-body spectrum, with  $L = 8, \dots, 14$  [475]. (a) There is a clear transition from a volume-law at small disorder  $h$  to a sub-volume law at  $h > h_c \sim 2.3$ , compatible from the scaling plot (b) with a strict area law (dashed line). (c-d) Singular behavior of the standard deviation  $\sigma_E$  of the entropy at the transition. Reprinted from [470] (a-c) and from [475] (d).

<sup>15</sup>In the MBL regime, Bauer and Nayak [460] reported a weak logarithmic violation of the area law for the maximum entropy, obtained from the (sample-dependent) optimal bipartition. A logarithmic violation was also found using matrix product states [502].

<sup>16</sup>This study concluded for a critical boundary  $h_c(\epsilon)$  larger than the one of Fig. 42 from [470].



Another very interesting point concerns the entropy histograms, as discussed in Refs. [460, 475, 470, 504], for which a qualitative change is observed across the different regimes. The evolution of the standard deviation  $\sigma_E$  with increasing system length  $L$  provides a quantitative tool, plotted in Fig. 43 (c-d). While in the delocalized regime  $\sigma_E(L) \rightarrow 0$  (in agreement with Ref. [505]), it remains constant in the localized phase, and diverges with  $L$  at the transition. This is likely a signature of an absence of self-averaging for the entropy, and a possible signature of infinite randomness physics at criticality [506].

A quite surprising feature concerns the structure of the ES, as explored by Yang and co-workers [507] for high-energy levels in both ETH and MBL regimes. In the delocalized phase, they found a "two-component" structure of the entanglement levels, with a universal part corresponding to genuine random states [498], and a non-universal (model-dependent) part. Interestingly, the universal part lies in the "high-energy" sector of the ES, in contrast with usual expectations (see Section 3). The universal fraction decreases when the MBL transition is approached and vanishes in the MBL regime. This observed effect for high-energy eigenstates clearly contrasts with ground-states of either pure [214, 215] or disordered systems [508] for which the universal part (if it exists [233]) is rather expected in the "low-energy" part. However, it is not excluded that such a two-component structure will vanish in the thermodynamic limit.

*Random bonds*—.  $SU(2)_k$  anyonic chains [509] with random bonds [361, 362, 363] have also been studied in their high-energy regime [484], using RSRG-X techniques [482]. The well-known Ising ( $k = 2$ ), Potts ( $k = 4$ ), and Heisenberg ( $k = \infty$ ) cases are included in this family of models. In contrast with the random field case Eq. (52), Vasseur and co-workers [484] have found for random  $SU(2)_k$  chains a set of infinite randomness fixed points that are the infinite-temperature analogs of Damle-Huse fixed points [359]. The entanglement entropy of high-energy eigenstates, sketched in Fig. 44, displays a crossover from a volume-law scaling  $\sim L$  at small lengths  $L \ll k$  to the asymptotic regime  $\sim \ln L$

for  $L \gg \xi_k^{(2)} \sim \exp(k^3/4\pi^2)$ . This logarithmic asymptotic behavior is also confirmed for the quantum Ising case  $k = 2$  by Huang and Moore in Ref. [483]. Consequences for the Heisenberg case are interesting since we expect volume-law entropy and self-thermalization only in this  $k \rightarrow \infty$  limit. Note also that for random-bonds XXZ chains, the strong disorder MBL regime is of spin-glass type with a strict area law entropy, as found in [510].

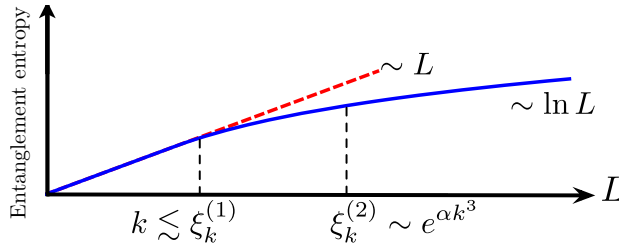


Figure 44: Entanglement entropy at high energy for random bonds  $SU(2)_k$  chains. Reprinted from [484].

#### 4.3.3. Entanglement growth after global quantum quenches

The spreading in time of entanglement after a quantum quench is a topic which has attracted a huge amount of work, in the wake of nonequilibrium dynamics in isolated interacting quantum systems [511]. For integrable systems, it was originally shown [512, 513] that the block entropy grows linearly with time  $S(t) \sim t$  after a sudden global quench<sup>17</sup>, using both analytical (CFT) and numerical (exact diagonalization and time-dependent DMRG). This was also confirmed for non-integrable systems [516] where the ballistic growth of  $S(t)$  contrasts with energy transport which is diffusive.

Intuitively, due to the finite velocity of excitations we expect a finite velocity of propagation of information in quantum systems with local interac-

<sup>17</sup>There is a qualitative difference between global and local quenches [514]. While the former displays ballistic spreading of entanglement, the later exhibits a much slower logarithmic growth [515].

tions, resulting in a Lieb-Robinson bound for entanglement spreading [517, 518]:  $S(t) \leq v_{\text{LR}} t$ . Quite remarkably, Burrell and Osborne have shown that for disordered XY spin chains [519], the effective light cone grows much slower  $\sim \ln t$ , thus yielding an entanglement spreading at most growing logarithmically with time, at least for non-interacting disordered fermionic chains.

We now discuss in details these properties of entanglement spreading in disordered interacting quantum systems after a global quench, starting at  $t = 0$  from a high-energy untangled product state  $|\Psi(0)\rangle$ , and letting the system evolve under the unitary evolution  $\exp(-iHt)|\Psi(0)\rangle$ .

*Logarithmic scaling in quantum glass phases and in the MBL regime*—. One of the first numerical observation of a slow logarithmic growth of entanglement entropy after a global quench in disordered systems was achieved by De Chiara and co-workers [513] for XX spin chains with random bonds,<sup>18</sup> following a quench from the simple (high-energy) Néel state  $|\uparrow\downarrow\uparrow\downarrow \dots\rangle$ . A very slow spreading of entanglement  $S(t) \sim \ln(\ln t)$  was also observed for the disordered transverse field Ising chain [520], with a saturation value at long time  $\sim \ln L$ . However, when interactions are turned on, Vosk and Altman have shown using a dynamical RG approach [462] for random bonds XXZ (in the easy-plane regime) that starting from the Néel state, the entanglement entropy would increase much faster with time:  $S(t) \sim (\ln t)^{2/\phi}$  where  $\phi = (1 + \sqrt{5})/2$  is the golden mean. Moreover, Vasseur and co-workers [484] have also shown that for a large class of random bonds systems, a modified logarithmic growth  $S(t) \sim (\ln t)^{1/\psi_k}$  is expected [461, 484], with an exponent  $\psi_k < 1$  which depends on the nature of the quantum critical glass phase. For the general class of  $\text{SU}(2)_k$  quantum critical anyonic glasses [361, 362, 363, 484], the non-trivial tunnelling exponent for excited states  $\psi_k$  has also been computed by Vasseur and co-workers [484]. For the Heisenberg  $\text{SU}(2)$  point,  $\psi_{k \rightarrow \infty} \rightarrow 0$ , yielding a faster growth for  $S(t)$ .

---

<sup>18</sup>And no random field, thus preserving the particle-hole symmetry of the Hamiltonian for which we do not expect Anderson localization.

It is interesting to remark that interactions lead to an entanglement growth which exceeds the upper bound  $\propto \ln t$  proved for disordered free-fermions [519]. Moreover, the large time asymptotic value is a volume-law  $S_{t \rightarrow \infty} \sim L$ , albeit with a small (non-thermal) prefactor, and which may also depend on the initial state [521], as well as on disorder strength. Nevertheless, the SU(2) Heisenberg case is special since RG breaks down [462, 484, 522] and ETH may still hold.

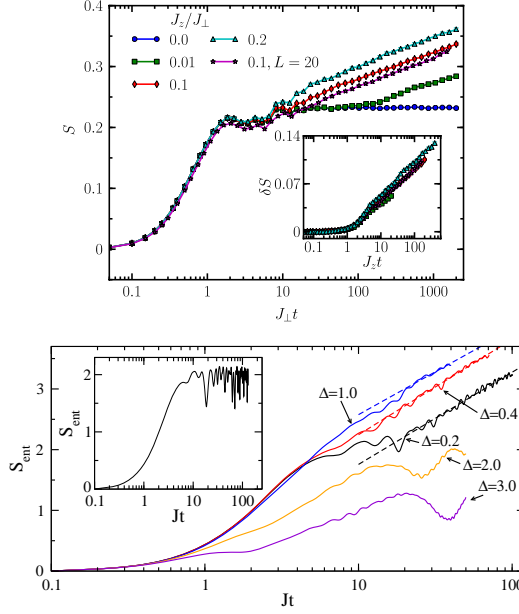


Figure 45: Entanglement entropy growth from an unentangled product state for different interaction strengths  $J_z$  or  $\Delta$  of the XXZ  $s = 1/2$  chain for very strongly disordered random fields, in the MBL regime. Reprinted from [468] (Top) and from [523] (Bottom).

The situation also changes drastically (as compared to non-interacting) for random fields or random potentials [466, 468, 524, 462, 523]. This is illustrated in Fig. 46 where we see that only infinitesimal interactions yield an unbounded growth of entanglement entropy [468] in the random field XXZ chain, in great contrast with free fermions for which the entropy quickly saturate to a strict area law. Interactions induce dephasing [524, 463] and give rise to a classical picture based on the so-called "l-bits" representation for the MBL regime [454]. Distant

spins are weakly coupled  $V(\ell) \sim \exp(-\ell/\xi)$  and therefore get slowly entangled, after a long time  $\ln t \sim \ell$ , leading to a very slow entanglement growth

$$S_{\text{MBL}}(t) \propto \ln t, \quad (53)$$

up to saturation to a *volume-law*<sup>19</sup>. The above scaling has a prefactor which is controlled by both the initial state before the quench and the localization length in the MBL phase [521]. This dephasing is triggered by the interactions, as confirmed for long-range interacting models [525] where the entanglement growth is faster, algebraic in time with an exponent controlled by the power-law interaction<sup>20</sup>. Below, we summarize in Table 4 the different behaviors of entanglement entropy growth after a global quench from a non-entangled initial product state in the strongly disordered regime of various models. At the MBL-ETH transition, while the l-bits picture breaks down, logarithmic spreading is still expected as a consequence of the infinite randomness nature of this critical point with a tunneling exponent  $\psi = 1$  [506].

Interaction	Model	EE growth	$t = \infty$
No	Random field/potential (AL)	bounded	area law
	Transverse field Ising or Random bonds/hopping	$\ln(\ln t)$	$\propto \ln L$
Yes	Random field/potential (MBL)	$\ln t$	$\propto L$
	Random bonds XXZ	$\ln^{2/\phi} t$	$\propto L$
	Random bond $\text{SU}(2)_k$	$\ln^{1/\psi_k} t$	$\propto L$

Table 4: Entanglement entropy growth after a quench from a high-energy unentangled state for different one-dimensional quantum spin/particles models, either interacting or not, in their strong disorder regime. The size  $L$  scaling of the infinite time saturation limit is also given.

<sup>19</sup>This does not mean an equilibrated thermal state though.

<sup>20</sup>This is relevant for dipolar cold gases, good candidates for observing MBL [526, 527, 528].

*Sub-ballistic entanglement growth in the delocalized regime*—. Upon decreasing the disorder strength, the (dynamical) transition from the MBL phase to the ETH regime displays sharp signatures in the entanglement growth properties, changing from a slow logarithmic spreading to a ballistic growth expected in the absence of disorder [512, 513, 516]. Asking whether ballistic spreading holds in the entire delocalized ETH regime, numerical [529, 530, 531, 532, 533] and analytical [506, 534, 535] works have revealed the existence of an intermediate delocalized regime where the dynamical response is anomalously slow. Sometimes dubbed "sub-diffusive", this regime is expected close to criticality in one dimension where the entanglement spreading may be blocked by bottlenecks made of rare critical segments of length  $\lambda$ . In such "Griffiths" [536] regions, the entanglement spreading is drastically slowed, and occurs on time scales  $\ln t \sim \lambda$ . For a system of length  $L$ , the longest of such rare regions typically scales  $\lambda^* \sim \xi \ln(L/\xi)$  [506, 534],  $\xi$  being a characteristic length diverging at the transition. Therefore the waiting time for entanglement spreading is dominated by  $\tau^* \sim L^{\xi/a}$ , yielding

$$S(t) \sim t^{1/z}, \quad (54)$$

with a dynamical exponent  $z \sim \xi$  diverging when the ETH-MBL transition is approached, in agreement with infinite randomness ( $z = \infty$ ) and a logarithmic growth at the transition.

This sub-ballistic entanglement spreading was verified numerically [532] using a Krylov space method allowing to perform exact diagonalization calculations for random-field Heisenberg chains Eq. (52) up to  $L = 28$  sites. Results [532] are displayed in Fig. 46 where the slow algebraic growth of the von-Neuman entropy after a sudden quench from an initial non-entangled basis state is clearly visible<sup>21</sup>. The dynamical exponent  $z$  is extracted as a function of the disorder strength  $h$  of the random longitudinal field, and plotted in Fig. 46 (e).

---

<sup>21</sup>In order to respect the energy-resolved character of this ETH-MBL transition discussed above (see Fig. 42 for the mobility edge extracted in [470]), the quenched states are chosen to be in the middle of the spectrum.

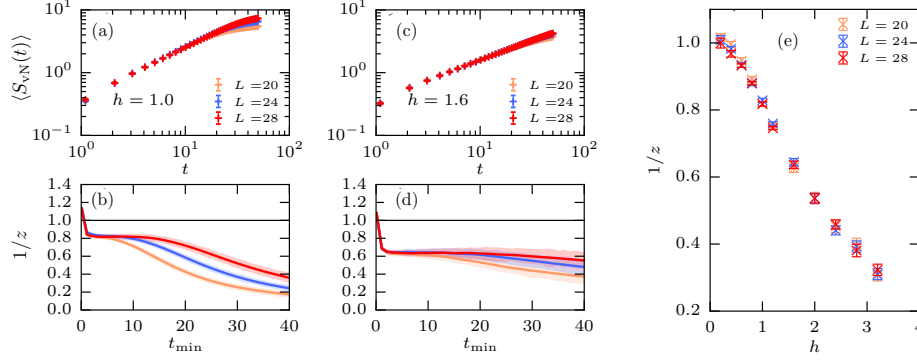


Figure 46: (a) and (c): Disorder averaged time evolution of the entanglement entropy  $\langle S_{\text{vN}}(t) \rangle$  in open random-field Heisenberg chains for different system sizes and two values of disorder. (b) and (d): Logarithmic derivative of the disorder averaged time evolution of  $\langle S_{\text{vN}}(t) \rangle$ , obtained by power-law fits over 8 points in time, starting from  $t_{\text{min}}$ . The formation of plateaus corresponds to the power-law regime, with growing extent with  $L$ . The plateaus determine the range of the power-law regime, over which the exponent  $1/z$  is extracted, displayed as a function of disorder in panel (e). Reprinted from [532]).

The anomalous sub-ballistic regime for the entanglement entropy inside the ETH phase is found to persist in an extended parameter region, seemingly down to very small  $h$ . At first sight, this seems hard to reconcile with the fact that a sub-diffusive regime is attached to rare Griffiths regions [506, 534, 529], thus only expected close to the MBL transition. One should remember however that in the quench protocol, inhomogeneity is also present in the initial product state where energy density fluctuate locally leading to anomalously "hot" and "cold" regions. The presence of a mobility edge [470] in the random-field Heisenberg model Eq. (52) may be responsible for such a large extension for the anomalous dynamical regime observed in Ref. [532] using such a global quench protocol.

#### 4.3.4. Open questions

An important open issue concerns experimentally relevant realizations of MBL. While very new, it appears to become a flourishing field with a growing number of striking proposals, coming either from traditional condensed matter systems [537] or from quantum gas labs [473, 538, 539]. The measurement

of entanglement growth in cold atom setups is in principle possible (see next section) using newly developed techniques [540]. For systems of trapped ionic chains with controlled disorder, the growth of quantum Fisher information [541] (giving a lower bound on the entanglement) has been measured [538].

Logarithmic entanglement spreading is expected to be the smoking gun of MBL, but one should ask whether the sub-ballistic growth found in most of the delocalized regime [532] is a generic feature in the presence of disorder, or is it model-dependent? A natural question follows regarding a possible transition between a ballistic and a sub-ballistic regime for entanglement spreading inside the delocalized regime.

Another important open issue touches the question of the nature of the localized - delocalized transition and the possible ergodicity breaking at the transition, as well as in its vicinity [495, 542, 493].

Finally, let us also mention the interesting and strongly debated question of MBL in disorder-free systems [477, 543, 544, 478, 545, 480, 479, 546, 547].



## 5. Towards entanglement measurement

Experimental detection of entanglement is a vast topic [548] for which many different setups have been explored [549, 550, 551, 552, 553, 554, 555, 556, 557, 558, 559, 560, 561]. Among them, bulk solid-state systems, where correlations and quantum entanglement usually go hand in hand [562], are potentially interesting systems to measure and exploit entanglement. Strongly correlated phases and quantum dynamics can be interpreted as a signature of quantum entanglement, as for instance discussed for the dipolar spin glass  $\text{LiHo}_x\text{Y}_{1-x}\text{F}_4$  [551], spin-1/2 antiferromagnets  $\text{CN}[\text{Cu}(\text{NO}_3)_2 \cdot 2.5\text{D}_2\text{O}]$  [563, 564, 565] or  $[\text{Cu}(\text{DCOO})_2 \cdot 4\text{D}_2\text{O}]$  [566], supramolecular antiferromagnetic rings (Purple- $\text{Cr}_7\text{Ni}$ ) [567], Kondo screening in atomic chains [568], and more generally in neutron scattering experiments [569, 570]. Similar signatures are also expected for optical lattice experiments [571].

Long-distance entanglement between solid-state qubits is also a major issue for quantum communication schemes [5, 572]. In this context, spin networks have been proposed to be promising setups to realize a quantum data bus [573, 574, 575, 576, 577]. Interestingly, the spin-ladder compound  $\text{Sr}_{14}\text{Cu}_{24}\text{O}_{41}$  (see Fig. 47) [578] appears to be a good candidate for long-range entanglement between unpaired spins which gets entangled at low temperature, coupled by an effective coupling  $J_{\text{eff}}$  across  $\ell = 220 - 250 \text{ \AA}$  [579], as sketched in Fig. 47.

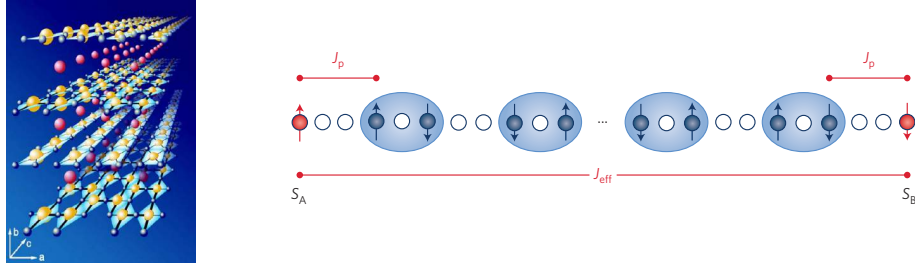


Figure 47: Left: three-dimensional representation of the spin-ladder material  $\text{Sr}_{14}\text{Cu}_{24}\text{O}_{41}$ . Right: one-dimensional structure made of spin-dimer chains with isolated spins (red) coupled over long distance  $\ell \simeq 220 - 250 \text{ \AA}$  through the effective coupling  $J_{\text{eff}}$ . Reprinted from [579]

Nevertheless, in most of these works the low-temperature entanglement is seen through few-body correlations that are measured using standard solid-state physics probe, such as heat capacity, susceptibility, neutron scattering. It is however much more difficult to access many-body entanglement estimates, like the entanglement entropy for instance. In the rest of this section we discuss the few proposals that have been recently discussed, either using noise and fluctuations in solid-state and mesoscopic systems, or in cold atom experiments.

### 5.1. *Quantum noise and bipartite fluctuations*

Fluctuations of globally conserved quantities, such as the number of particles for U(1) symmetric itinerant systems, or the total magnetization for O(2) magnets, are key measurable quantities which can reflect the amount of entanglement present in a subsystem. First discussed in the context of mesoscopic systems [580, 581, 582, 583, 584, 585], the link between entanglement entropy and bipartite fluctuations has been explored later by several authors [44, 45, 46, 47, 48, 104, 49, 51, 50, 52, 54, 55, 57, 586].

Below we first describe free fermions where there is an exact correspondence between cumulants and entanglement entropies [45, 48, 49]. Then we discuss interacting systems in one dimension, and beyond. While there is a quantitative link for Luttinger liquids between bipartite fluctuations and entanglement entropy [47, 49, 220], this is no longer true for interacting two-dimensional systems [104], although quantum critical points can be detected using fluctuations [51]. We finally address the key issue of experimental detection for nano- or meso-electronic devices such as quantum point contacts and also for more traditional solid-state bulk systems such as quantum magnets.

#### 5.1.1. *Bipartite fluctuation as an entanglement meter*

*Free fermions*—. For systems that can be mapped to non-interacting fermions, the entanglement entropy can be accessed experimentally through the full counting statistics of a conserved U(1) charge, such as the particle number  $N$  for instance when studying the charge transfer across mesoscopic conductors [587,

58, 588, 589]. The idea of using quantum noise as an entanglement meter, first proposed by Klich and Levitov [45], was further explored by Song and co-workers [48, 49] who derived exact expressions Eq. (57) for the von-Neuman and the Rényi entropies in terms of cumulants  $C_n$ . The second cumulant  $C_2$ , also called the fluctuations is defined by

$$\mathcal{F} = \langle (N_A - \langle N_A \rangle)^2 \rangle \quad (55)$$

where  $\langle N_A \rangle$  is the ground-state expectation value of the particle number in a subsystem  $A$ . Higher order cumulants, defined by

$$C_n = (-i\partial_\lambda)^n \ln \chi(\lambda)|_{\lambda=0}, \quad (56)$$

where the generating function  $\chi(\lambda) = \langle \exp(i\lambda N_A) \rangle$ , enter in the following expansions [48, 49], only involving even cumulant  $C_{2p}$ :

$$S_{\text{vN}} = \lim_{R \rightarrow \infty} \sum_{p=1}^{R/2} \alpha_{2p}(R) C_{2p}, \quad (57)$$

and

$$S_{q>1} = \lim_{R \rightarrow \infty} \sum_{p=1}^{qR/2} \beta_{2p}(q, R) C_{2p}, \quad (58)$$

with  $\beta_{2p}(q, R) = \frac{1}{1-q} \sum_{r=1}^R \sum_{m=0}^r \sum_{s=2p}^{qr} (-1)^{r+s+qr+qm} \times \frac{1}{r} \binom{R}{r} \binom{r}{m} \binom{qm}{qr-s} \frac{\mathcal{S}_1(s, 2p)}{(s-1)!}$ ,  $\alpha_{2p}(R) = 2 \sum_{k=2p-1}^R \frac{\mathcal{S}_1(k, 2p-1)}{k!k}$ , and where  $\mathcal{S}_1(s, 2p)$  are the unsigned Stirling numbers of the first kind. In the case of gaussian fluctuations, only the variance  $C_2$  is non-zero, which considerably simplifies the expressions, yielding

$$S_q = \frac{\pi^2}{6} \left( 1 + \frac{1}{q} \right) C_2. \quad (59)$$

*Interacting systems: Luttinger liquids*—. For one-dimensional critical (zero-temperature) Luttinger liquids, taking a subsystem of length  $\ell$ , its RDM can be described as the thermal density matrix of an open Luttinger liquid with the same velocity  $u$  and Luttinger parameter  $K$  [221, 220] at an effective low temperature  $T_{\text{ent}} = u \ln(\ell/\ell_0)/(\pi\ell)$ , where  $\ell_0$  is an order one length scale. Ignoring irrelevant corrections, a Luttinger liquid is equivalent to a free boson model

whose partition function at inverse temperature  $\beta$  is exactly known [406]:

$$Z(\ell, \beta) = \zeta(\ell, \beta) \sum_{m=-\ell/2}^{\ell/2} \exp\left(-\beta \frac{\pi u}{2K\ell} m^2\right), \quad (60)$$

where  $\zeta(\ell, \beta) = \prod_{n=1}^{\infty} [2 \sinh(\frac{u\pi}{4\ell T} n)]^{-1}$ , and  $m = -\ell/2, \dots, \ell/2$  are the conserved charges (here the magnetization of a spin-1/2 chain, see [406]). From this expression, we immediately see that the normalized weights  $p_m$  of the  $S^z = \pm m$  sectors have a Gaussian distribution with a variance  $C_2(\ell, T) = (K\ell T)/(u\pi)$ . Therefore using the quantum/thermal correspondence [220], the leading scaling of zero-temperature bipartite fluctuations in a subsystem of length  $\ell$  is given by

$$C_2(\ell) = \frac{K}{\pi^2} \ln(\ell/\ell_0), \quad (61)$$

while the Rényi entropy  $S_q^{\text{th}}(\beta) = \frac{q\beta}{1-q} [F(\beta) - F(q\beta)] = \frac{\pi}{6u} \left(1 + \frac{1}{q}\right) \ell/\beta$  gives for the general relation between entanglement entropies and bipartite fluctuations:

$$S_q(\ell) = \frac{\pi^2}{6K} \left(1 + \frac{1}{q}\right) C_2(\ell) + O(1), \quad (62)$$

in agreement with previous works [47].

The logarithmic scaling Eq. (61) of the bipartite fluctuations  $C_2(\ell)$  can be checked for using DMRG or QMC simulations [47, 49]. Here we show QMC results in the ground-state of spin-1/2 XXZ chains in the antiferromagnetic critical regime for  $C_2$  of half-chains  $\ell = L/2$  in Fig. 48 for various anisotropies  $\Delta$  and sizes  $L = 16, 32, 64, 128, 256$ . In the entire antiferromagnetic critical regime  $\Delta \in [0, 1]$  the scaling of  $C_2$  is logarithmic, while it tends to saturate once  $\Delta > 1$ , as clearly visible in the left panel of Fig. 48. A logarithmic fit of the QMC data to the form  $C_2 = K_{\text{eff}}/\pi^2 \ln L + \text{constant}$  yields estimates for the Luttinger parameters plotted in the right part of Fig. 48, in very good agreement with the exact expression known from Bethe ansatz Eq. (22).

It is fair to say that the second cumulant is a quite simple observable to measure within QMC or DMRG simulations. It therefore provides a very interesting quantity to access the Luttinger liquid parameter  $K$  when it is unknown. Conversely, if the value of  $K$  at a quantum critical point  $g_c$  is known but the

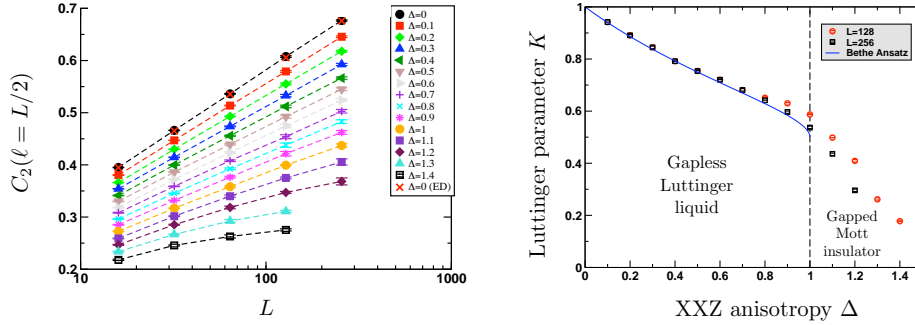


Figure 48: Left: QMC results for the fluctuations  $C_2(\ell = L/2)$  plotted against the total system size  $L$  for periodic chains of lengths  $L = 16, 32, 64, 128, 256$ . Different symbols are for different values of the XXZ anisotropy. For the XX point  $\Delta = 0$ , QMC data (black circles) are also compared to exact diagonalization (free-fermions) results (red crosses). Logarithmic scaling is observed in the critical regime  $\Delta \leq 1$  whereas for  $\Delta > 1$   $C_2$  tends to saturate at large  $L$ . Inset: schematic picture for the periodic ring where subsystem A is taken with  $x = L/2$  sites. Right: Prefactor  $K_{\text{eff}}$  of the logarithmic scaling Eq. (61) extracted by fitting QMC data for  $L \in [2^{p-1}, 2^p]$  with  $L = 128$  ( $p = 7$ ) and  $L = 256$  ( $p = 8$ ). The blue line shows the exact Bethe Ansatz result for  $K(\Delta)$  Eq. (22).

precise value of  $g_c$  is not, we will see below that measuring the second cumulant  $C_2$  provides a very efficient way to estimate the critical coupling.

### 5.1.2. Bipartite fluctuations to detect quantum criticality

*One dimension: Luttinger liquids—* Following the previous discussion, we show how efficient the use of Eq. (61) is to locate 1D quantum critical points with a high accuracy.

(i) *Frustrated spin chain:* The first model we study is the frustrated spin-1/2  $J_1 - J_2$  chain, governed by the Hamiltonian

$$\mathcal{H}_{J_1-J_2} = \sum_i (J_1 \mathbf{S}_i \cdot \mathbf{S}_{i+1} + J_2 \mathbf{S}_i \cdot \mathbf{S}_{i+2}) , \quad (63)$$

where we define  $\lambda = J_2/J_1 \geq 0$ . For  $\lambda \leq \lambda_c$ , this model has power-law critical correlations and a logarithmic scaling of entanglement entropy Eq. (5), while at  $\lambda_c \simeq 0.2412$  a Berezinsky-Kosterlitz-Thouless (BKT) transition into a dimerized phase occurs [410, 590, 408] where the entropy obeys a strict area law (see

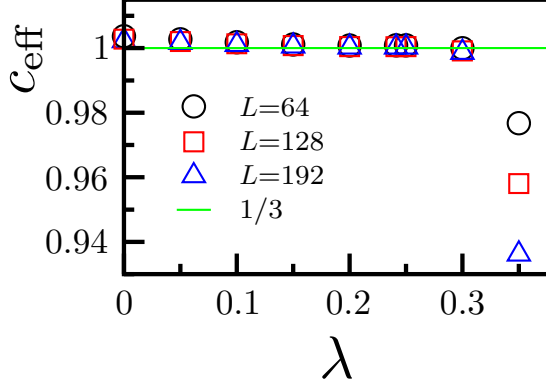


Figure 49: Coefficient of a logarithmic fit for the von Neumann entanglement entropy as a function of the second neighbor coupling  $J_2$ . DMRG results for  $L = 64, 128, 192$  sites. Reprinted from [591].

Fig. 2). A precise estimate of  $\lambda_c$  using entanglement entropy turns out to be very difficult, as explored by Alet and co-workers in [591]. This is illustrated in Fig. 49 where the effective (size-dependent) central charge, estimated from DMRG data for various system sizes, is plotted against the frustrated coupling  $\lambda$ . The crossing of the data to the value  $c_{\text{eff}} = 1$ , expected to occur at  $\lambda_c$  where irrelevant logarithmic corrections vanish [406] is very difficult to detect, and in practice less precise as compared to spin-spin correlation function [408].

The effect of marginal corrections is much more pronounced in the bipartite fluctuations of the magnetization which involve the uniform part of the spin correlations inside subsystem  $A$

$$C_2 = \sum_{i,j \in A} [\langle S_i^z S_j^z \rangle - \langle S_i^z \rangle \langle S_j^z \rangle]. \quad (64)$$

where additive logarithmic corrections are well-known [592]. Fitting DMRG data to the form Eq. (61), one can extract an effective (size-dependent) Luttinger parameter as a function of  $\lambda$ . This is plotted in the left panel of Fig. 50 where one clearly sees the vanishing of the marginal corrections leading to  $K_c = 0.5$  at  $\lambda_c = 0.2412(3)$ , in perfect agreement with the best estimate  $\lambda_c = 0.241167(5)$  [408].

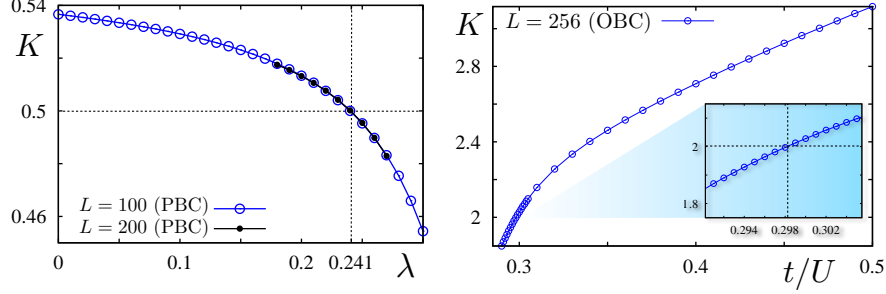


Figure 50: Left: Effective Luttinger parameter  $K$  of the  $J_1 - J_2$  chain extracted via (61) and plotted against the frustration parameter  $\lambda$ . DMRG data for  $L = 100$  (open circles) and  $L = 200$  (black dots) for periodic chains. Right: Same for the Bose-Hubbard chain at filling unity plotted against  $t/U$  for  $L = 256$  and open boundary conditions. Inset: zoom close to the transition. Reprinted from [51].

(ii) *Bose-Hubbard chain at unit filling*: Another very interesting example is provided by the one-dimensional Bose-Hubbard model (for a review, see [593]) with one particle per site, governed by the following Hamiltonian

$$\mathcal{H} = -t \sum_{\langle ij \rangle} b_i^\dagger b_j + \frac{U}{2} \sum_i n_i (n_i - 1) - \sum_i \mu n_i, \quad (65)$$

where  $t$  is the hopping amplitude,  $U$  the on-site repulsion, and  $\mu$  the chemical potential chosen such that  $\langle n_i \rangle = 1$  in the ground-state. For unit filling, the quantum phase transition from a superfluid to a Mott insulator is of BKT type [594]. The exponent governing the algebraic decay of the Green's function  $\langle b_r^\dagger b_0 \rangle \propto r^{-1/2K}$  in the superfluid phase  $K \geq 2$  jumps at the transition from  $K_c = 2$  to 0 in the Mott insulator [216]. The precise determination of the critical ratio  $(t/U)_c$  turns out to be very difficult using finite size numerics, as summarized in Table 5 and Fig. 51. As discussed in details in [51], bipartite fluctuations of the particle number provide a very simple and efficient tool to detect the transition with a very high accuracy, as shown in panel right of Fig. 50. The Luttinger parameter  $K$  is extracted from fitting  $C_2$  to Eq. (61) for various sizes  $L = 64, 128$ , and 256 (the latter is shown in Fig. 50). By performing finite size

scaling we obtain a very precise estimate  $\lambda_c = 0.2989(2)$ , in good agreement with the most reliable estimates (see Table 5 and Fig. 51). Note that the bipartite fluctuations allow to estimate the critical point with a very high accuracy, the numerical cost being quite low.

Year	Reference	Technique	Observable	Estimate
1991	Krauth [595]	Bethe Ansatz		0.2887
1992	Batrouni <i>et al.</i> [596]	QMC	Stiffness	0.21(1)
1994	Elesin <i>et al.</i> [597]	ED	Gap	0.275(5)
1996	Kashurnikov <i>et al.</i> [598]	QMC	Gap	0.300(5)
1999	Elstner <i>et al.</i> [599]	Strong coupling	Gap	0.26(1)
2000	Kühner <i>et al.</i> [600]	DMRG	Correlations	0.297(10)
2008	Zakrzewski <i>et al.</i> [601]	TEBD	Correlations	0.2975(5)
2008	Laüchli <i>et al.</i> [424]	DMRG	Entanglement	0.298(5)
2008	Roux <i>et al.</i> [602]	DMRG	Gap	0.303(9)
2011	Ejima <i>et al.</i> [603]	DMRG	Correlations	0.305(1)
2011	Danshita <i>et al.</i> [604]	TEBD	Excitations	0.319(1)
2012	Rachel <i>et al.</i> [51]	DMRG	Fluctuations	0.2989(2)
2015	Gerster <i>et al.</i> [605]	Tensor network	Stiffness	0.299(2)

Table 5: Various estimates for the critical coupling of the one-dimensional Bose-Hubbard model Eq. (65) at unit filling. These estimates are also plotted *vs.* year in Fig. 51. One should emphasize on the most accurate result (second last line) obtained using bipartite fluctuations [51].

*Beyond one dimension—.* One can also study quantum critical points in higher dimension, as done in [51] for two-dimensional coupled  $s = 1/2$  Heisenberg ladders (see Fig. 52), described by the following Hamiltonian

$$\mathcal{H} = \sum_{\text{ladd.}} \mathbf{S}_i \cdot \mathbf{S}_j + \sum_{\text{inter-ladd.}} \lambda \mathbf{S}_i \cdot \mathbf{S}_j. \quad (66)$$



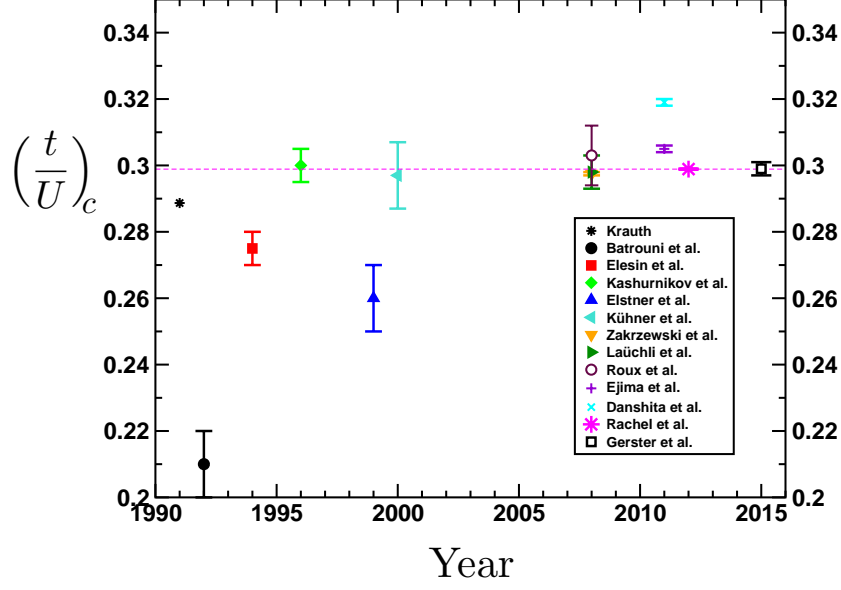


Figure 51: Various critical point estimates of the Superfluid - Mott Insulator transition in the one-dimensional Bose-Hubbard model at unit filling. The plotted values in function of time refers to those of Table 5.

This model displays two gapped rung-singlet phases if the inter-ladder coupling  $\lambda_c^1 > \lambda > \lambda_c^2$  with  $\lambda_c^1 = 0.31407(5)$  [320] and  $\lambda_c^2 = 1.9096(2)$  [323], and a gapless Néel ordered phase in between, as shown in Fig. 52 (a).  $T = 0$  fluctuations of the total magnetization in a sub-system  $\mathcal{A}$  of size  $L/2 \times L$ , embedded in a periodic square lattice  $L \times L$  are shown in Fig. 52 (b-c), with square lattices size up to  $L \times L = 10^4$ , for the isotropic square lattice  $\lambda = 1$  (Néel) and for weakly coupled ladders with  $\lambda = 0.1$  (gapped rung singlet I). In contrast with the entanglement (or Rényi) entropy which displays a strict area law both phases, the second cumulant follows different scalings [48]:

$$\mathcal{F}(\ell) \sim \begin{cases} \alpha \ell \ln \ell + \beta \ell + \gamma & (\text{Gapless Néel}) \\ \beta' \ell + \gamma' & (\text{Gapped Rung Singlet}). \end{cases} \quad (67)$$

Therefore,  $\mathcal{F}/\ell$  plotted for different sizes displays a crossing point at  $\lambda_c$ , as observed in panel (c) of Fig. 52. The spin stiffness  $\rho_s$ , also known to be a useful

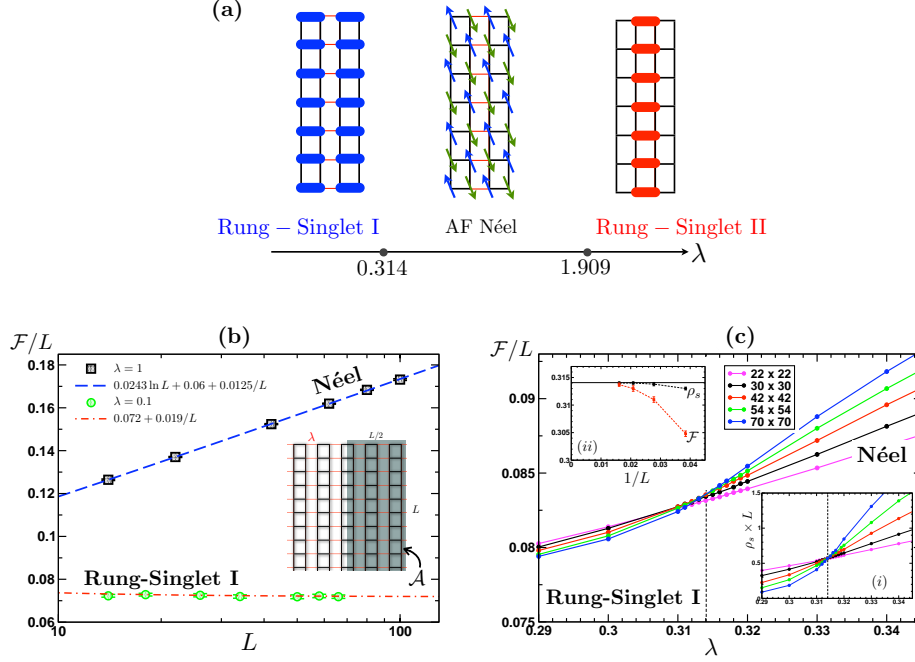


Figure 52: QMC results for  $T = 0$  fluctuations  $\mathcal{F}$  of the total magnetization in a region  $\mathcal{A}$  for 2D coupled spin- $\frac{1}{2}$  ladders [Eq. (66)], depicted in the inset of (a). Panel (b):  $\mathcal{F}/L$  increases logarithmically with  $L$  in the Néel regime (black squares  $\lambda = 1$ ) whereas it saturates to a constant in the gapped state (green circles  $\lambda = 0.1$ ). Panel (c):  $\mathcal{F}/L$ , plotted *vs.*  $\lambda$  for various system sizes, displays a crossing point at  $\lambda_c$ . Insets: (i) crossing of the stiffness  $\rho_s \times L$  at  $\lambda_c$  for the same sizes; (ii)  $1/L$  convergence of the crossing point for  $\mathcal{F}$  (red squares) and  $\rho_s$  (black circles) to the critical value (horizontal black line)  $\lambda_c = 0.31407$  [320]. Reprinted from [51].

quantity to locate quantum criticality, is shown in the right inset (ii) of Fig. 52 (c) where a similar crossing is observed for  $\rho_s \times L^{d+z-2}$ , with  $z = 1$  and  $d = 2$ . As usual for such a technique, a drift of the crossing point is observed with  $L$ , as visible in the left inset (i) of Fig. 52 (b). Already known for a few other models [321, 323], the crossing points obtained from the stiffness converge very rapidly with  $1/L$  to the bulk value  $\lambda_c$ , whereas we found a slower convergence for the estimates obtained from  $\mathcal{F}/L$ . Despite such effect (which may not be

generic but model dependent), this simple example clearly shows that  $\mathcal{F}$  is a very useful quantity to locate a quantum critical point between ordered and disordered phases for  $d > 1$ .

### 5.1.3. Experimental proposal

*Quantum point contact*—. A quantum point contact is a beam splitter with tunable transmission and reflection that serves as a "door" between electron reservoirs [45, 104], as depicted in Fig. 53. Time fluctuations of the current measured at this quantum point contact are exactly the bipartite fluctuations when replacing the temporal window  $t$  by the spatial extent  $x$ . Due to space-time duality, such a replacement is always allowed for conformally invariant systems [48], even when they are interacting. Quantum point contacts with free-electron reservoirs offer the opportunity to directly measure entanglement entropy. The first few cumulants, in particular  $C_2$ , have already been successfully measured [606, 607, 608].

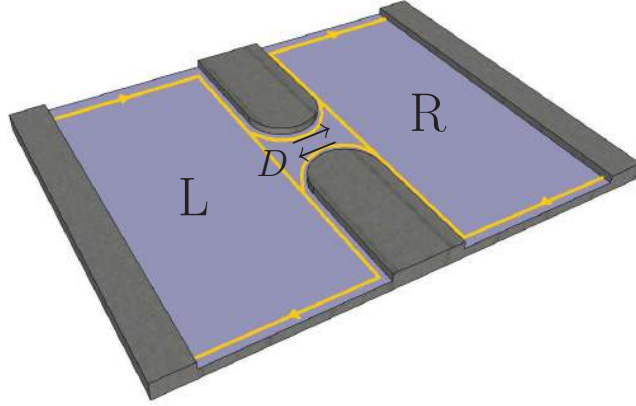


Figure 53: Quantum point contact with chiral edge states (yellow lines) along the edges of a two-dimensional electron gas in a perpendicular magnetic field. The sample is divided into a left (L) and a right (R) region by a split gate acting as a quantum point contact. Electrons in the two in-coming edge states are transmitted with probability  $D$  or reflected with probability  $1 - D$ . Reprinted from [49].

*Quantum antiferromagnets*—. Bipartite fluctuations can also be measured in  $O(2)$  symmetric quantum magnets, where the  $z$ -component of spin  $S^z$  being the conserved charge, playing the role of particle number in mesoscopic and cold atom systems. The second cumulant of a subsystem  $A$

$$\mathcal{F}_A = \sum_{i,j \in A} [\langle S_i^z S_j^z \rangle - \langle S_i^z \rangle \langle S_j^z \rangle]. \quad (68)$$

can be understood as the Curie constant of the partial susceptibility, defined by  $\mathcal{F}_A = T \times \left( \frac{d\langle S_A^z \rangle}{dh_A} \right)_{h_A \rightarrow 0}$  where  $h_A$  is a small uniform external magnetic field applied to region  $A$  *only*. As proposed in [48, 49], such a setup can be realized by applying the magnetic field over the entire sample while region  $B$  (the rest of the system) is protected by superconducting Meissner screens. Sketched in Fig. 54, such screens would eliminate the external field as well as the magnetic response outside region  $A$ . By varying the size of  $A$  and extrapolating to very low temperature, the scaling of  $\mathcal{F}_A$  could be measured.

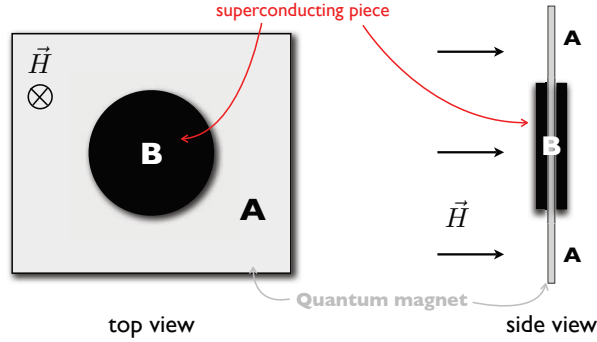


Figure 54: Experimental setup proposed to extract the second cumulant (bipartite fluctuation)  $\mathcal{F}_A$  of the magnetization within a subsystem  $A$ . The superconducting device (black disk) is placed on top of the quantum antiferromagnet (on region  $B$ ) so that the Meissner effect will cancel the external field  $h_B = 0$  in the antiferromagnet whereas  $h_A = H$ . This Meissner screen is also placed on the other side such that only the  $A$  contribution of the field-induced magnetization is measured. Reprinted from [49]

## 5.2. Entanglement detection and measure in cold atom experiments

Quantum information processing using cold atoms trapped in optical lattices has been intensively discussed by many authors [609, 610, 611, 612, 613, 614]. Recently, theoretical proposals to directly extract entanglement witnesses, such as the Rényi entropies, have been debated in the context of artificial matter loaded in optical lattices. Below, we discuss the few theoretical proposal that have been suggested in the context of ultra-cold atoms, and present the very first experimental achievements.

### 5.2.1. Theoretical proposals using SWAP-based protocols

Using previous ideas based on copying a quantum system  $q$  times [615], and applying a SWAP operation [616, 131], Abanin and Demler [617] proposed a general method to measure  $q$ -Rényi entropies for integer  $q \geq 2$ . The idea is based on the SWAP protocol, illustrated in Fig. 55 for  $q = 2$  copies of a one-dimensional system partitionned in two parts  $A_{1,2}$  and  $B_{1,2}$ , controlled by a two-level system which plays the role of a quantum switch. Writting the ground-states  $|\text{GS}\rangle = \left(\sum_i \lambda_i |\phi_i^{A1}\rangle \otimes |\phi_i^{B1}\rangle\right) \otimes \left(\sum_j \lambda_j |\phi_j^{A2}\rangle \otimes |\phi_j^{B2}\rangle\right)$  and  $|\text{GS}'\rangle = \left(\sum_i \lambda_i |\phi_i^{A1}\rangle \otimes |\phi_i^{B2}\rangle\right) \otimes \left(\sum_j \lambda_j |\phi_j^{A2}\rangle \otimes |\phi_j^{B1}\rangle\right)$  of the two configurations (a) and (b) in Fig. 55, the second Rényi entropy is given by the overlap

$$\langle \text{GS} | \text{GS}' \rangle = \sum_i \lambda_i^4 = \exp(-S_2). \quad (69)$$

In order to evaluate this overlap, a weak tunneling is introduced between the two states of the quantum switch, leading to an hybridization of the two ground-states:  $|\text{GS}\rangle \otimes |\uparrow\rangle$  and  $|\text{GS}'\rangle \otimes |\downarrow\rangle$ . Studying Rabi oscillations of the quantum switch between the two ground-states gives a direct access to the above overlap Eq. (69) which is directly proportional to the Rabi frequency.

In the same time, Daley and co-workers [618] proposed a slightly different but related theoretical setup where entanglement growth is tracked during a quench dynamics of two identical copies of a boson chain whose mutual coupling is reduced. After tunneling has occurred, a measurement of the SWAP operator is achieved by measuring the parity number,

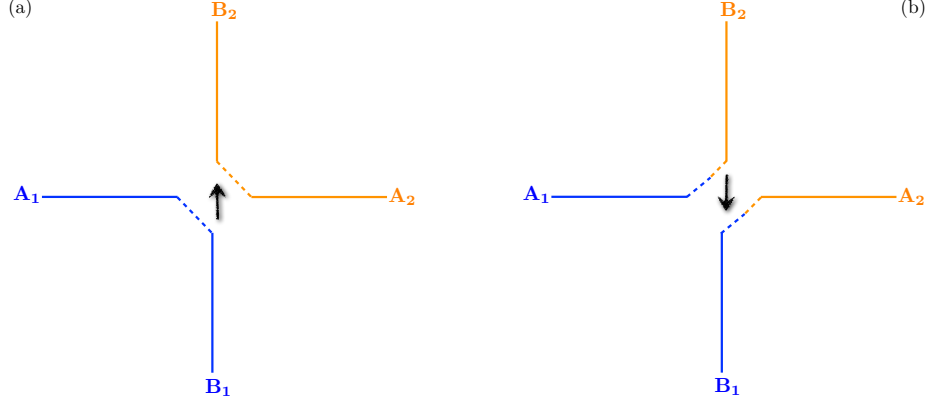


Figure 55: Proposal for measuring the  $q = 2$  Rényi entropy, inspired from Abanin and Demler [617]. Two identical copies are split in pairs of half-chains arranged in a cross geometry. A quantum switch (two-level system  $\uparrow$  or  $\downarrow$  at the center) controls the way in which the half-chains are connected by selectively allowing tunneling to one of the neighbors. The ground-states overlap Eq. (69) of the two configurations is directly proportional to the  $q = 2$  Rényi entropy, and can be measured by studying Rabi oscillations of the quantum switch.

### 5.2.2. First measurements

Based on some earlier theoretical proposals [619, 620], Islam *et al.* [540] realized the first measurement of the second Rényi entropy by making interference between two copies of a 4-site Bose-Hubbard chain in an optical lattice. Building on the quantum gas microscope technique [621, 622], the second moment of the RDM (the purity) is accessed without resorting to quantum tomography [623]. Using a 50% - 50% beam splitter the purity is directly estimated by measuring the average particle number parity. The measured second Rényi entropy is shown across the superfluid - insulator transition in Fig. 56.

Using a different protocol, essentially based on particle number fluctuations [624], Fukuhara and co-workers [625] have measured two-site entanglement between the spins of ultra-cold atoms loaded in an optical lattice. Starting with a localized spin-flip excitation, the time evolution of the concurrence between distant spins has been recorded through the measure of transverse spin correlations.

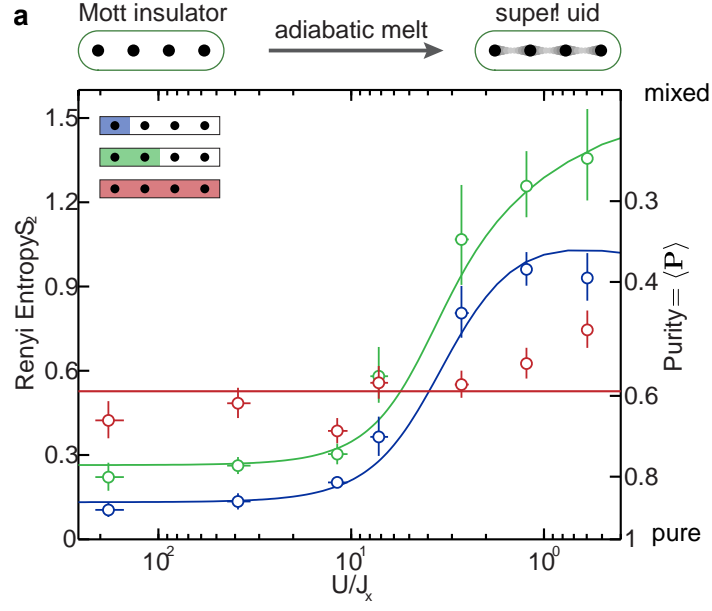


Figure 56: Ground-state entanglement entropy and purity measured on a 4-site Bose-Hubbard chain across the Mott insulator to superfluid transition for different sub-systems (different colors). Circles are data and solid lines are exact diagonalization results. Reprinted from [540].

## 6. Conclusion

### 6.1. Summary

In this review we have tried to give a general, while non-exhaustive, survey of the flourishing recent activity in the field of quantum entanglement in condensed matter physics, focusing on bipartite entanglement for clean and disordered systems.

Let us briefly summarize the main results we have reviewed. The ground-state of most correlated quantum systems exhibits an area law entanglement entropy, at most logarithmically enhanced for Luttinger, Fermi or Bose liquids. While the area law prefactor is expected to display a cusp singularity at quantum critical points, universality is encoded in sub-dominant terms, such as additive constants or corner contributions. Symmetry breakings or topological order can be clearly identified through such sub-leading corrections beyond area law in generalized Rényi entanglement entropies. Regarding entanglement spectroscopy, we have seen that entanglement levels can contain more information than the entropies, and the "low-energy" part carries some universality for 1+1 conformal field theory, gapped states, broken symmetry phases, topological order. Quantum disordered systems such as random spin models, quantum (Kondo) impurity problems, or many-body localized systems all display fascinating entanglement properties. The most recent example being the many-body localization problem where highly excited states exhibit a dynamical transition between ergodic and non-ergodic regimes with qualitatively different entanglement properties, as well as anomalous entanglement spreading following a global quantum quench. On the experimental side, bipartite fluctuations in mesoscopic and solid state systems represent a promising tool to measure entanglement, as well as recent realizations in ultra-cold atom experiments.

### 6.2. Open questions

Let us give some directions towards a few open questions. The recently debated universality of entanglement spectra remains a largely open issue, leading to the question of the conditions under which an entanglement spectrum is



universal. A particularly interesting aspect is the spatial variation of the entanglement temperature, decaying away from the (real-space) cut for area law ground states.

Another key point concerns the computational aspects of entanglement in strongly correlated systems, in particular for highly entangled states for which going beyond brute force exact diagonalization (restricted to small systems) is a central issue, in particular to understand ergodicity breaking in interacting disordered systems at high energy. Systems with long-range couplings, relevant to cold atom experiments, are also very challenging to numerical simulations since ground-state entanglement is no longer bounded to an area law.

Several aspects remain to be understood for  $d \geq 2$  systems, in particular for non-Fermi liquid states where the logarithmic enhancement of the area law appears to be related but distinct from the free-fermion result. Shape dependence is also a very interesting topic where for instance in  $d = 2$  corner contributions carry a universal additive logarithmic correction in the entropy for conformal field theories. However, is universality in such corner terms also present at disordered quantum critical points?

Finally, the idea of a quantum revolution promoted by X.-G. Wen [626] where there is unification between matter and quantum information is a very attractive one, but whether or not the standard model does emerge from long-ranged entangled qubits remains certainly an open issue.

## Acknowledgments

It is a great pleasure to warmly thank all my collaborators in works devoted to entanglement in condensed matter systems during the past decade: Ian Affleck, Fabien Alet, Sylvain Capponi, Ming-Shyang Chang, Christian Flindt, José Hoyos, Israel Klich, Karyn Le Hur, David Luitz, Matthieu Mambrini, Eduardo Miranda, Alexandru Petrescu, Xavier Plat, Stephan Rachel, Nicolas Regnault, Zoran Ristivojevitich, Francis Song, Erik Sørensen, André Vieira, Thomas Vojta.

This work was supported by the Agence Nationale de la Recherche under programs ANR-11-IS04-005-0 and ANR-14-CE32-0018-02.

## 7. Bibliography

### References

- [1] A. Einstein, B. Podolsky, and N. Rosen, [Phys. Rev. \*\*47\*\*, 777 \(1935\)](#).
- [2] E. Schrödinger, [Naturwissenschaften \*\*23\*\*, 807 \(1935\)](#).
- [3] J. S. BELL, [Rev. Mod. Phys. \*\*38\*\*, 447 \(1966\)](#).
- [4] A. Aspect, J. Dalibard, and G. Roger, [Phys. Rev. Lett. \*\*49\*\*, 1804 \(1982\)](#).
- [5] C. H. Bennett, G. Brassard, C. Crépeau, R. Jozsa, A. Peres, and W. K. Wootters, [Phys. Rev. Lett. \*\*70\*\*, 1895 \(1993\)](#).
- [6] D. Bouwmeester, J.-W. Pan, K. Mattle, M. Eibl, H. Weinfurter, and A. Zeilinger, [Nature \*\*390\*\*, 575 \(1997\)](#).
- [7] P. Shor, [SIAM J. Comput. \*\*26\*\*, 1484 \(1997\)](#).
- [8] W. K. Wootters, [Phys. Rev. Lett. \*\*80\*\*, 2245 \(1998\)](#).
- [9] N. Gisin, G. Ribordy, W. Tittel, and H. Zbinden, [Rev. Mod. Phys. \*\*74\*\*, 145 \(2002\)](#).
- [10] S. Ryu and T. Takayanagi, [Phys. Rev. Lett. \*\*96\*\*, 181602 \(2006\)](#).
- [11] L. Amico, R. Fazio, A. Osterloh, and V. Vedral, [Rev. Mod. Phys. \*\*80\*\*, 517 \(2008\)](#).
- [12] R. Horodecki, P. Horodecki, M. Horodecki, and K. Horodecki, [Rev. Mod. Phys. \*\*81\*\*, 865 \(2009\)](#).
- [13] J. Eisert, M. Cramer, and M. B. Plenio, [Rev. Mod. Phys. \*\*82\*\*, 277 \(2010\)](#).
- [14] I. M. Georgescu, S. Ashhab, and F. Nori, [Rev. Mod. Phys. \*\*86\*\*, 153 \(2014\)](#).
- [15] L. Aolita, F. d. Melo, and L. Davidovich, [Rep. Prog. Phys. \*\*78\*\*, 042001 \(2015\)](#).

- [16] M. A. Nielsen and I. L. Chuang, *Quantum computation and quantum information* (2000).
- [17] J. Preskill, [Journal of Modern Optics](#) **47**, 127 (2000).
- [18] A. Osterloh, L. Amico, G. Falci, and R. Fazio, [Nature](#) **416**, 608 (2002).
- [19] T. J. Osborne and M. A. Nielsen, [Phys. Rev. A](#) **66**, 032110 (2002).
- [20] G. Vidal, J. I. Latorre, E. Rico, and A. Kitaev, [Phys. Rev. Lett.](#) **90**, 227902 (2003).
- [21] P. Calabrese and J. Cardy, [J. Stat. Mech.](#) **2004**, P06002 (2004).
- [22] U. Schollwöck, [Annals of Physics](#) **326**, 96 (2011).
- [23] L. Bombelli, R. K. Koul, J. Lee, and R. D. Sorkin, [Phys. Rev. D](#) **34**, 373 (1986).
- [24] M. Srednicki, [Phys. Rev. Lett.](#) **71**, 666 (1993).
- [25] C. Callan and F. Wilczek, [Physics Letters B](#) **333**, 55 (1994).
- [26] C. Holzhey, F. Larsen, and F. Wilczek, [Nuclear Physics B](#) **424**, 443 (1994).
- [27] S. Hawking, J. Maldacena, and A. Strominger, [J. High Energy Phys.](#) **05**, 001 (2001).
- [28] M. B. Hastings, [J. Stat. Mech.](#) **2007**, P08024 (2007).
- [29] P. Jordan and E. Wigner, [Z. Physik](#) **47**, 631 (1928).
- [30] J. L. Black and V. J. Emery, [Phys. Rev. B](#) **23**, 429 (1981).
- [31] F. G. S. L. Brandão and M. Horodecki, [Nat Phys](#) **9**, 721 (2013).
- [32] B.-Q. Jin and V. E. Korepin, [Journal of Statistical Physics](#) **116**, 79 (2004).
- [33] P. Calabrese, M. Campostrini, F. Essler, and B. Nienhuis, [Phys. Rev. Lett.](#) **104**, 095701 (2010).

- [34] J. Cardy and P. Calabrese, [J. Stat. Mech.](#) **2010**, P04023 (2010).
- [35] M. M. Wolf, [Phys. Rev. Lett.](#) **96**, 010404 (2006).
- [36] D. Gioev and I. Klich, [Phys. Rev. Lett.](#) **96**, 100503 (2006).
- [37] W. Li, L. Ding, R. Yu, T. Roscilde, and S. Haas, [Phys. Rev. B](#) **74**, 073103 (2006).
- [38] T. Barthel, M.-C. Chung, and U. Schollwöck, [Phys. Rev. A](#) **74**, 022329 (2006).
- [39] R. Helling, H. Leschke, and W. Spitzer, [Int Math Res Notices](#) **2011**, 1451 (2011).
- [40] B. Swingle, [Phys. Rev. Lett.](#) **105**, 050502 (2010).
- [41] H. Leschke, A. V. Sobolev, and W. Spitzer, [Phys. Rev. Lett.](#) **112**, 160403 (2014).
- [42] B. Swingle, [Phys. Rev. B](#) **86**, 035116 (2012).
- [43] W. Ding, A. Seidel, and K. Yang, [Phys. Rev. X](#) **2**, 011012 (2012).
- [44] I. Klich, G. Refael, and A. Silva, [Phys. Rev. A](#) **74**, 032306 (2006).
- [45] I. Klich and L. Levitov, [Phys. Rev. Lett.](#) **102**, 100502 (2009).
- [46] B. Hsu, E. Grosfeld, and E. Fradkin, [Phys. Rev. B](#) **80**, 235412 (2009).
- [47] H. F. Song, S. Rachel, and K. Le Hur, [Phys. Rev. B](#) **82**, 012405 (2010).
- [48] H. F. Song, N. Laflorencie, S. Rachel, and K. Le Hur, [Phys. Rev. B](#) **83**, 224410 (2011).
- [49] H. F. Song, S. Rachel, C. Flindt, I. Klich, N. Laflorencie, and K. Le Hur, [Phys. Rev. B](#) **85**, 035409 (2012).
- [50] P. Calabrese, M. Mintchev, and E. Vicari, [EPL](#) **98**, 20003 (2012).

- [51] S. Rachel, N. Laflorencie, H. F. Song, and K. Le Hur, [Phys. Rev. Lett. \*\*108\*\*, 116401 \(2012\)](#).
- [52] R. Süsstrunk and D. A. Ivanov, [EPL \*\*100\*\*, 60009 \(2012\)](#).
- [53] B. Swingle, [Phys. Rev. B \*\*86\*\*, 045109 \(2012\)](#).
- [54] E. Vicari, [Phys. Rev. A \*\*85\*\*, 062104 \(2012\)](#).
- [55] V. Eisler, [Phys. Rev. Lett. \*\*111\*\*, 080402 \(2013\)](#).
- [56] I. Klich, [J. Stat. Mech. \*\*2014\*\*, P11006 \(2014\)](#).
- [57] A. Petrescu, H. F. Song, S. Rachel, Z. Ristivojevic, C. Flindt, N. Laflorencie, I. Klich, N. Regnault, and K. L. Hur, [J. Stat. Mech. \*\*2014\*\*, P10005 \(2014\)](#).
- [58] Y. M. Blanter and M. Büttiker, [Physics Reports \*\*336\*\*, 1 \(2000\)](#).
- [59] P. Calabrese, M. Mintchev, and E. Vicari, [Phys. Rev. Lett. \*\*107\*\*, 020601 \(2011\)](#).
- [60] P. Calabrese, M. Mintchev, and E. Vicari, [EPL \*\*97\*\*, 20009 \(2012\)](#).
- [61] V. Eisler and Z. Rácz, [Phys. Rev. Lett. \*\*110\*\*, 060602 \(2013\)](#).
- [62] R. Marino, S. N. Majumdar, G. Schehr, and P. Vivo, [Phys. Rev. Lett. \*\*112\*\*, 254101 \(2014\)](#).
- [63] P. Calabrese, P. Le Doussal, and S. N. Majumdar, [Phys. Rev. A \*\*91\*\*, 012303 \(2015\)](#).
- [64] Y. Zhang, T. Grover, and A. Vishwanath, [Phys. Rev. Lett. \*\*107\*\*, 067202 \(2011\)](#).
- [65] J. McMinis and N. M. Tubman, [Phys. Rev. B \*\*87\*\*, 081108 \(2013\)](#).
- [66] T. Grover, Y. Zhang, and A. Vishwanath, [New J. Phys. \*\*15\*\*, 025002 \(2013\)](#).

- [67] F. F. Assaad, T. C. Lang, and F. Parisen Toldin, [Phys. Rev. B \*\*89\*\*, 125121 \(2014\)](#).
- [68] P. Broecker and S. Trebst, [J. Stat. Mech. \*\*2014\*\*, P08015 \(2014\)](#).
- [69] L. Wang and M. Troyer, [Phys. Rev. Lett. \*\*113\*\*, 110401 \(2014\)](#).
- [70] F. F. Assaad, [Phys. Rev. B \*\*91\*\*, 125146 \(2015\)](#).
- [71] B. Swingle and T. Senthil, [Phys. Rev. B \*\*87\*\*, 045123 \(2013\)](#).
- [72] B. I. Halperin, P. A. Lee, and N. Read, [Phys. Rev. B \*\*47\*\*, 7312 \(1993\)](#).
- [73] J. Shao, E.-A. Kim, F. D. M. Haldane, and E. H. Rezayi, [Phys. Rev. Lett. \*\*114\*\*, 206402 \(2015\)](#).
- [74] A. Paramekanti, L. Balents, and M. P. A. Fisher, [Phys. Rev. B \*\*66\*\*, 054526 \(2002\)](#).
- [75] H.-H. Lai, K. Yang, and N. E. Bonesteel, [Phys. Rev. Lett. \*\*111\*\*, 210402 \(2013\)](#).
- [76] H.-H. Lai and K. Yang, [arXiv:1510.03428 \(2015\)](#).
- [77] L. Pastur and V. Slavin, [Phys. Rev. Lett. \*\*113\*\*, 150404 \(2014\)](#).
- [78] A. C. Potter, [arXiv:1408.1094 \(2014\)](#).
- [79] M. Pouranvari, Y. Zhang, and K. Yang, [Advances in Condensed Matter Physics \*\*2015\*\*, 397630 \(2015\)](#).
- [80] W. Ding and K. Yang, [Phys. Rev. A \*\*80\*\*, 012329 \(2009\)](#).
- [81] V. Alba, M. Haque, and A. M. Läuchli, [Phys. Rev. Lett. \*\*110\*\*, 260403 \(2013\)](#).
- [82] M. B. Plenio, J. Eisert, J. Dreißig, and M. Cramer, [Phys. Rev. Lett. \*\*94\*\*, 060503 \(2005\)](#).
- [83] M.-C. Chung and I. Peschel, [Phys. Rev. B \*\*62\*\*, 4191 \(2000\)](#).

- [84] M. A. Metlitski, C. A. Fuertes, and S. Sachdev, [Phys. Rev. B \*\*80\*\*, 115122 \(2009\)](#).
- [85] H. Casini and M. Huerta, [Phys. Rev. D \*\*85\*\*, 125016 \(2012\)](#).
- [86] A. Kallin, K. Hyatt, R. Singh, and R. Melko, [Phys. Rev. Lett. \*\*110\*\*, 135702 \(2013\)](#).
- [87] J. Helmes and S. Wessel, [Phys. Rev. B \*\*89\*\*, 245120 \(2014\)](#).
- [88] I. Frérot and T. Roscilde, [arXiv:1512.00805 \(2015\)](#).
- [89] E. Fradkin and J. E. Moore, [Phys. Rev. Lett. \*\*97\*\*, 050404 \(2006\)](#).
- [90] V. E. Korepin, [Phys. Rev. Lett. \*\*92\*\*, 096402 \(2004\)](#).
- [91] B. Hsu, M. Mulligan, E. Fradkin, and E.-A. Kim, [Phys. Rev. B \*\*79\*\*, 115421 \(2009\)](#).
- [92] J.-M. Stéphan, S. Furukawa, G. Misguich, and V. Pasquier, [Phys. Rev. B \*\*80\*\*, 184421 \(2009\)](#).
- [93] H. Casini and M. Huerta, [J. Phys. A: Math. Theor. \*\*42\*\*, 504007 \(2009\)](#).
- [94] L. Tagliacozzo, G. Evenbly, and G. Vidal, [Phys. Rev. B \*\*80\*\*, 235127 \(2009\)](#).
- [95] J.-M. Stéphan, G. Misguich, and V. Pasquier, [Phys. Rev. B \*\*84\*\*, 195128 \(2011\)](#).
- [96] M. A. Metlitski and T. Grover, [arXiv:1112.5166 \(2011\)](#).
- [97] H. Ju, A. B. Kallin, P. Fendley, M. B. Hastings, and R. G. Melko, [Phys. Rev. B \*\*85\*\*, 165121 \(2012\)](#).
- [98] J.-M. Stéphan, H. Ju, P. Fendley, and R. G. Melko, [New J. Phys. \*\*15\*\*, 015004 \(2013\)](#).
- [99] S. Inglis and R. G. Melko, [New J. Phys. \*\*15\*\*, 073048 \(2013\)](#).



- [100] A. B. Kallin, E. M. Stoudenmire, P. Fendley, R. R. P. Singh, and R. G. Melko, *J. Stat. Mech.* **2014**, P06009 (2014).
- [101] E. M. Stoudenmire, P. Gustainis, R. Johal, S. Wessel, and R. G. Melko, *Phys. Rev. B* **90**, 235106 (2014).
- [102] X. Chen, G. Y. Cho, T. Faulkner, and E. Fradkin, *J. Stat. Mech.* **2015**, P02010 (2015).
- [103] C. Akers, O. Ben-Ami, V. Rosenhaus, M. Smolkin, and S. Yankielowicz, *arXiv:1512.00791* (2015).
- [104] H. F. Song, C. Flindt, S. Rachel, I. Klich, and K. Le Hur, *Phys. Rev. B* **83**, 161408 (2011).
- [105] A. Kitaev and J. Preskill, *Phys. Rev. Lett.* **96**, 110404 (2006).
- [106] M. Levin and X.-G. Wen, *Phys. Rev. Lett.* **96**, 110405 (2006).
- [107] T. Devakul and R. R. P. Singh, *Phys. Rev. B* **90**, 054415 (2014).
- [108] S. Furukawa and G. Misguich, *Phys. Rev. B* **75**, 214407 (2007).
- [109] H. Casini and M. Huerta, *Nuclear Physics B* **764**, 183 (2007).
- [110] B. Swingle, *arXiv:1010.4038* (2010).
- [111] P. Bueno, R. C. Myers, and W. Witczak-Krempa, *Phys. Rev. Lett.* **115**, 021602 (2015).
- [112] N. Laflorencie, D. J. Luitz, and F. Alet, *Phys. Rev. B* **92**, 115126 (2015).
- [113] P. Bueno and R. C. Myers, *J. High Energy Phys.* **8**, 1 (2015).
- [114] P. Bueno, R. C. Myers, and W. Witczak-Krempa, *J. High Energy Phys.* **09**, 1 (2015).
- [115] S. Sahoo, E. M. Stoudenmire, J.-M. Stéphan, T. Devakul, R. R. P. Singh, and R. G. Melko, *arXiv:1509.00468* (2015).

- [116] T. Nishioka, S. Ryu, and T. Takayanagi, *J. Phys. A: Math. Theor.* **42**, 504008 (2009).
- [117] R. R. P. Singh, R. G. Melko, and J. Oitmaa, *Phys. Rev. B* **86**, 075106 (2012).
- [118] J. Helmes and S. Wessel, *Phys. Rev. B* **92**, 125120 (2015).
- [119] F. Kos, D. Poland, and D. Simmons-Duffin, *J. High Energ. Phys.* **6**, 1 (2014).
- [120] A. B. Kallin, M. B. Hastings, R. G. Melko, and R. R. P. Singh, *Phys. Rev. B* **84**, 165134 (2011).
- [121] P. W. Anderson, *Phys. Rev.* **86**, 694 (1952).
- [122] C. Lhuillier, *arXiv:cond-mat/0502464* (2005).
- [123] D. J. Luitz, X. Plat, F. Alet, and N. Laflorencie, *Phys. Rev. B* **91**, 155145 (2015).
- [124] P. Chandra and B. Doucot, *Phys. Rev. B* **38**, 9335 (1988).
- [125] E. Manousakis, *Rev. Mod. Phys.* **63**, 1 (1991).
- [126] M. Takahashi, *Phys. Rev. B* **40**, 2494 (1989).
- [127] J. E. Hirsch and S. Tang, *Phys. Rev. B* **40**, 4769 (1989).
- [128] I. Peschel and V. Eisler, *J. Phys. A: Math. Theor.* **42**, 504003 (2009).
- [129] I. Frérot and T. Roscilde, *Phys. Rev. B* **92**, 115129 (2015).
- [130] B. Kulchytskyy, C. M. Herdman, S. Inglis, and R. G. Melko, *Phys. Rev. B* **92**, 115146 (2015).
- [131] M. Hastings, I. González, A. Kallin, and R. Melko, *Phys. Rev. Lett.* **104**, 157201 (2010).
- [132] H.-C. Jiang, H. Yao, and L. Balents, *Phys. Rev. B* **86**, 024424 (2012).

- [133] F. Kolley, S. Depenbrock, I. P. McCulloch, U. Schollwöck, and V. Alba, [Phys. Rev. B \*\*88\*\*, 144426 \(2013\)](#).
- [134] S. Humeniuk and T. Roscilde, [Phys. Rev. B \*\*86\*\*, 235116 \(2012\)](#).
- [135] D. J. Luitz, X. Plat, N. Laflorencie, and F. Alet, [Phys. Rev. B \*\*90\*\*, 125105 \(2014\)](#).
- [136] J.-M. Stéphan, [Phys. Rev. B \*\*90\*\*, 045424 \(2014\)](#).
- [137] M. P. Zaletel, J. H. Bardarson, and J. E. Moore, [Phys. Rev. Lett. \*\*107\*\*, 020402 \(2011\)](#).
- [138] Y. Y. Atas and E. Bogomolny, [Phys. Rev. E \*\*86\*\*, 021104 \(2012\)](#).
- [139] F. C. Alcaraz and M. A. Rajabpour, [Phys. Rev. Lett. \*\*111\*\*, 017201 \(2013\)](#).
- [140] D. J. Luitz, F. Alet, and N. Laflorencie, [Phys. Rev. Lett. \*\*112\*\*, 057203 \(2014\)](#).
- [141] D. J. Luitz, F. Alet, and N. Laflorencie, [Phys. Rev. B \*\*89\*\*, 165106 \(2014\)](#).
- [142] D. J. Luitz, N. Laflorencie, and F. Alet, [J. Stat. Mech. \*\*2014\*\*, P08007 \(2014\)](#).
- [143] F. C. Alcaraz and M. A. Rajabpour, [Phys. Rev. B \*\*90\*\*, 075132 \(2014\)](#).
- [144] C. Monthus, [J. Stat. Mech. \*\*2015\*\*, P04007 \(2015\)](#).
- [145] F. C. Alcaraz and M. A. Rajabpour, [Phys. Rev. B \*\*91\*\*, 155122 \(2015\)](#).
- [146] F. Evers and A. D. Mirlin, [Rev. Mod. Phys. \*\*80\*\*, 1355 \(2008\)](#).
- [147] G. Misguich, V. Pasquier, and M. Ishikawa, unpublished (2015).
- [148] K. S. D. Beach, F. Alet, M. Mambrini, and S. Capponi, [Phys. Rev. B \*\*80\*\*, 184401 \(2009\)](#).
- [149] T. A. Tóth, A. M. Läuchli, F. Mila, and K. Penc, [Phys. Rev. Lett. \*\*105\*\*, 265301 \(2010\)](#).

- [150] A. Smerald, H. T. Ueda, and N. Shannon, [Phys. Rev. B \*\*91\*\*, 174402 \(2015\)](#).
- [151] X. G. Wen, [Phys. Rev. B \*\*44\*\*, 2664 \(1991\)](#).
- [152] C. Nayak, S. H. Simon, A. Stern, M. Freedman, and S. Das Sarma, [Rev. Mod. Phys. \*\*80\*\*, 1083 \(2008\)](#).
- [153] X.-G. Wen, [arXiv:1506.05768 \(2015\)](#).
- [154] X. G. Wen, [Int. J. Mod. Phys. B \*\*04\*\*, 239 \(1990\)](#).
- [155] X. Chen, Z.-C. Gu, and X.-G. Wen, [Phys. Rev. B \*\*82\*\*, 155138 \(2010\)](#).
- [156] A. Hamma, R. Ionicioiu, and P. Zanardi, [Physics Letters A \*\*337\*\*, 22 \(2005\)](#).
- [157] A. Kitaev, [Annals of Physics \*\*321\*\*, 2 \(2006\)](#).
- [158] V. Kalmeyer and R. B. Laughlin, [Phys. Rev. Lett. \*\*59\*\*, 2095 \(1987\)](#).
- [159] X. G. Wen, F. Wilczek, and A. Zee, [Phys. Rev. B \*\*39\*\*, 11413 \(1989\)](#).
- [160] R. B. Laughlin, [Phys. Rev. Lett. \*\*50\*\*, 1395 \(1983\)](#).
- [161] G. Moore and N. Read, [Nuclear Physics B \*\*360\*\*, 362 \(1991\)](#).
- [162] J.-M. Stéphan, G. Misguich, and V. Pasquier, [J. Stat. Mech. \*\*2012\*\*, P02003 \(2012\)](#).
- [163] E. Ardonne, P. Fendley, and E. Fradkin, [Annals of Physics \*\*310\*\*, 493 \(2004\)](#).
- [164] R. Moessner and S. L. Sondhi, [Phys. Rev. Lett. \*\*86\*\*, 1881 \(2001\)](#).
- [165] D. S. Rokhsar and S. A. Kivelson, [Phys. Rev. Lett. \*\*61\*\*, 2376 \(1988\)](#).
- [166] S. Depenbrock, I. P. McCulloch, and U. Schollwöck, [Phys. Rev. Lett. \*\*109\*\*, 067201 \(2012\)](#).

- [167] Y. Zhang, T. Grover, and A. Vishwanath, [Phys. Rev. B \*\*84\*\*, 075128 \(2011\)](#).
- [168] S. V. Isakov, M. B. Hastings, and R. G. Melko, [Nat Phys \*\*7\*\*, 772 \(2011\)](#).
- [169] J. Wildeboer, A. Seidel, and R. G. Melko, [arXiv:1510.07682 \(2015\)](#).
- [170] A. M. Läuchli, E. J. Bergholtz, and M. Haque, [New J. Phys. \*\*12\*\*, 075004 \(2010\)](#).
- [171] H.-C. Jiang, Z. Wang, and L. Balents, [Nat Phys \*\*8\*\*, 902 \(2012\)](#).
- [172] Y. Zhang, T. Grover, A. Turner, M. Oshikawa, and A. Vishwanath, [Phys. Rev. B \*\*85\*\*, 235151 \(2012\)](#).
- [173] D. Poilblanc, N. Schuch, D. Pérez-García, and J. I. Cirac, [Phys. Rev. B \*\*86\*\*, 014404 \(2012\)](#).
- [174] L. Cincio and G. Vidal, [Phys. Rev. Lett. \*\*110\*\*, 067208 \(2013\)](#).
- [175] D. Poilblanc and N. Schuch, [Phys. Rev. B \*\*87\*\*, 140407 \(2013\)](#).
- [176] H.-C. Jiang, R. R. P. Singh, and L. Balents, [Phys. Rev. Lett. \*\*111\*\*, 107205 \(2013\)](#).
- [177] Y.-M. Lu, Y. Ran, and P. A. Lee, [Phys. Rev. B \*\*83\*\*, 224413 \(2011\)](#).
- [178] Y. Iqbal, F. Becca, S. Sorella, and D. Poilblanc, [Phys. Rev. B \*\*87\*\*, 060405 \(2013\)](#).
- [179] R. R. P. Singh and D. A. Huse, [Phys. Rev. B \*\*76\*\*, 180407 \(2007\)](#).
- [180] S. Yan, D. A. Huse, and S. R. White, [Science \*\*332\*\*, 1173 \(2011\)](#).
- [181] S.-S. Gong, W. Zhu, L. Balents, and D. N. Sheng, [Phys. Rev. B \*\*91\*\*, 075112 \(2015\)](#).
- [182] F. Kolley, S. Depenbrock, I. P. McCulloch, U. Schollwöck, and V. Alba, [Phys. Rev. B \*\*91\*\*, 104418 \(2015\)](#).
- [183] S. Iblisdir, J. I. Latorre, and R. Orús, [Phys. Rev. Lett. \*\*98\*\*, 060402 \(2007\)](#).

- [184] M. Haque, O. Zozulya, and K. Schoutens, [Phys. Rev. Lett. \*\*98\*\*, 060401 \(2007\)](#).
- [185] O. S. Zozulya, M. Haque, K. Schoutens, and E. H. Rezayi, [Phys. Rev. B \*\*76\*\*, 125310 \(2007\)](#).
- [186] J. Wildeboer and N. E. Bonesteel, [arXiv:1510.08817 \(2015\)](#).
- [187] N. Read and E. Rezayi, [Phys. Rev. B \*\*59\*\*, 8084 \(1999\)](#).
- [188] R. S. K. Mong, M. P. Zaletel, F. Pollmann, and Z. Papić, [arXiv:1505.02843 \(2015\)](#).
- [189] W. Zhu, S. S. Gong, F. D. M. Haldane, and D. N. Sheng, [Phys. Rev. Lett. \*\*115\*\*, 126805 \(2015\)](#).
- [190] Z. Liu, A. Vaezi, K. Lee, and E.-A. Kim, [arXiv:1502.05391 \(2015\)](#).
- [191] S. Nishimoto, N. Shibata, and C. Hotta, [Nat Commun \*\*4\*\* \(2013\)](#).
- [192] S. Capponi, O. Derzhko, A. Honecker, A. M. Läuchli, and J. Richter, [Phys. Rev. B \*\*88\*\*, 144416 \(2013\)](#).
- [193] T. Picot, M. Ziegler, R. Orus, and D. Poilblanc, [arXiv:1508.07189 \(2015\)](#).
- [194] K. Roychowdhury, S. Bhattacharjee, and F. Pollmann, [Phys. Rev. B \*\*92\*\*, 075141 \(2015\)](#).
- [195] A. E. B. Nielsen, G. Sierra, and J. I. Cirac, [Nat Commun \*\*4\*\* \(2013\)](#).
- [196] H. Bombin and M. A. Martin-Delgado, [Phys. Rev. Lett. \*\*97\*\*, 180501 \(2006\)](#).
- [197] S. S. Jahromi and A. Langari, [arXiv:1512.00756 \(2015\)](#).
- [198] T. Grover, A. M. Turner, and A. Vishwanath, [Phys. Rev. B \*\*84\*\*, 195120 \(2011\)](#).
- [199] I. Kimchi, J. G. Analytis, and A. Vishwanath, [Phys. Rev. B \*\*90\*\*, 205126 \(2014\)](#).

- [200] M. Pretko and T. Senthil, [arXiv:1510.03863](#) (2015).
- [201] C. Castelnovo and C. Chamon, [Phys. Rev. B](#) **76**, 174416 (2007).
- [202] C. Castelnovo and C. Chamon, [Phys. Rev. B](#) **76**, 184442 (2007).
- [203] J. Helmes, J.-M. Stéphan, and S. Trebst, [Phys. Rev. B](#) **92**, 125144 (2015).
- [204] S. R. White, [Phys. Rev. Lett.](#) **69**, 2863 (1992).
- [205] U. Schollwöck, [Rev. Mod. Phys.](#) **77**, 259 (2005).
- [206] S. Liang and H. Pang, [Phys. Rev. B](#) **49**, 9214 (1994).
- [207] T. Nishino, [J. Phys. Soc. Jpn.](#) **64**, 3598 (1995).
- [208] S. R. White and D. J. Scalapino, [Phys. Rev. Lett.](#) **80**, 1272 (1998).
- [209] I. Peschel, M. Kaulke, and Ö. Legeza, [Ann. Phys.](#) **8**, 153 (1999).
- [210] M.-C. Chung and I. Peschel, [Phys. Rev. B](#) **64**, 064412 (2001).
- [211] S.-A. Cheong and C. L. Henley, [Phys. Rev. B](#) **69**, 075111 (2004).
- [212] S.-A. Cheong and C. L. Henley, [Phys. Rev. B](#) **69**, 075112 (2004).
- [213] V. Eisler, Ö. Legeza, and Z. Rácz, [J. Stat. Mech.](#) **2006**, P11013 (2006).
- [214] H. Li and F. D. M. Haldane, [Phys. Rev. Lett.](#) **101**, 010504 (2008).
- [215] P. Calabrese and A. Lefevre, [Phys. Rev. A](#) **78**, 032329 (2008).
- [216] T. Giamarchi, *Quantum Physics in One Dimension* (2003).
- [217] F. C. Alcaraz, M. N. Barber, M. T. Batchelor, R. J. Baxter, and G. R. W. Quispel, [J. Phys. A: Math. Gen.](#) **20**, 6397 (1987).
- [218] F. Pollmann and J. E. Moore, [New J. Phys.](#) **12**, 025006 (2010).
- [219] V. Alba, M. Haque, and A. M. Läuchli, [J. Stat. Mech.](#) **2012**, P08011 (2012).

- [220] N. Laflorencie and S. Rachel, *J. Stat. Mech.* **2014**, P11013 (2014).
- [221] A. M. Läuchli, [arXiv:1303.0741](#) (2013).
- [222] X. Deng and L. Santos, *Phys. Rev. B* **84**, 085138 (2011).
- [223] I. Peschel, *J. Stat. Mech.* **2004**, P06004 (2004).
- [224] V. Alba, M. Haque, and A. M. Läuchli, *Phys. Rev. Lett.* **108**, 227201 (2012).
- [225] G. Wong, I. Klich, L. A. P. Zayas, and D. Vaman, *J. High Energ. Phys.* **12**, 1 (2013).
- [226] B. Swingle and J. McGreevy, [arXiv:1505.07106](#) (2015).
- [227] R. Thomale, D. P. Arovas, and B. A. Bernevig, *Phys. Rev. Lett.* **105**, 116805 (2010).
- [228] G. De Chiara, L. Lepori, M. Lewenstein, and A. Sanpera, *Phys. Rev. Lett.* **109**, 237208 (2012).
- [229] L. Lepori, G. De Chiara, and A. Sanpera, *Phys. Rev. B* **87**, 235107 (2013).
- [230] S. M. Giampaolo, S. Montangero, F. Dell’Anno, S. De Siena, and F. Illuminati, *Phys. Rev. B* **88**, 125142 (2013).
- [231] A. Bayat, H. Johannesson, S. Bose, and P. Sodano, *Nat Commun* **5** (2014).
- [232] R. Lundgren, J. Blair, M. Greiter, A. Läuchli, G. A. Fiete, and R. Thomale, *Phys. Rev. Lett.* **113**, 256404 (2014).
- [233] A. Chandran, V. Khemani, and S. L. Sondhi, *Phys. Rev. Lett.* **113**, 060501 (2014).
- [234] D. Poilblanc, *Phys. Rev. Lett.* **105**, 077202 (2010).
- [235] R. Lundgren, Y. Fuji, S. Furukawa, and M. Oshikawa, *Phys. Rev. B* **88**, 245137 (2013).



- [236] E. Dagotto and T. M. Rice, [Science](#) **271**, 618 (1996).
- [237] P. Abbamonte, G. Blumberg, A. Rusydi, A. Gozar, P. G. Evans, T. Siegrist, L. Venema, H. Eisaki, E. D. Isaacs, and G. A. Sawatzky, [Nature](#) **431**, 1078 (2004).
- [238] M. Klanjšek, H. Mayaffre, C. Berthier, M. Horvatić, B. Chiari, O. Pivovarsana, P. Bouillot, C. Kollath, E. Orignac, R. Citro, and T. Giamarchi, [Phys. Rev. Lett.](#) **101**, 137207 (2008).
- [239] C. Rüegg, K. Kiefer, B. Thielemann, D. F. McMorrow, V. Zapf, B. Normand, M. B. Zvonarev, P. Bouillot, C. Kollath, T. Giamarchi, S. Capponi, D. Poilblanc, D. Biner, and K. W. Krämer, [Phys. Rev. Lett.](#) **101**, 247202 (2008).
- [240] J. des Cloizeaux and J. J. Pearson, [Phys. Rev.](#) **128**, 2131 (1962).
- [241] J. I. Cirac, D. Poilblanc, N. Schuch, and F. Verstraete, [Phys. Rev. B](#) **83**, 245134 (2011).
- [242] I. Peschel and M.-C. Chung, [EPL](#) **96**, 50006 (2011).
- [243] S. Furukawa and Y. B. Kim, [Phys. Rev. B](#) **83**, 085112 (2011).
- [244] A. M. Läuchli and J. Schliemann, [Phys. Rev. B](#) **85**, 054403 (2012).
- [245] J. Schliemann and A. M. Läuchli, [J. Stat. Mech.](#) **2012**, P11021 (2012).
- [246] X. Chen and E. Fradkin, [J. Stat. Mech.](#) **2013**, P08013 (2013).
- [247] C.-M. Chung, L. Bonnes, P. Chen, and A. M. Läuchli, [Phys. Rev. B](#) **89**, 195147 (2014).
- [248] J. Eisert and M. Cramer, [Phys. Rev. A](#) **72**, 042112 (2005).
- [249] I. Peschel and J. Zhao, [J. Stat. Mech.](#) **2005**, P11002 (2005).
- [250] J. Dubail and N. Read, [Phys. Rev. Lett.](#) **107**, 157001 (2011).

- [251] R. A. Santos, [Phys. Rev. B \*\*87\*\*, 035141 \(2013\)](#).
- [252] J. Lou, S. Tanaka, H. Katsura, and N. Kawashima, [Phys. Rev. B \*\*84\*\*, 245128 \(2011\)](#).
- [253] I. Pižorn, F. Verstraete, and R. M. Konik, [Phys. Rev. B \*\*88\*\*, 195102 \(2013\)](#).
- [254] A. J. A. James and R. M. Konik, [Phys. Rev. B \*\*87\*\*, 241103 \(2013\)](#).
- [255] I. Affleck, T. Kennedy, E. H. Lieb, and H. Tasaki, [Phys. Rev. Lett. \*\*59\*\*, 799 \(1987\)](#).
- [256] D. C. Tsui, H. L. Stormer, and A. C. Gossard, [Phys. Rev. Lett. \*\*48\*\*, 1559 \(1982\)](#).
- [257] M. Z. Hasan and C. L. Kane, [Rev. Mod. Phys. \*\*82\*\*, 3045 \(2010\)](#).
- [258] L. Balents, [Nature \*\*464\*\*, 199 \(2010\)](#).
- [259] N. Regnault, B. A. Bernevig, and F. D. M. Haldane, [Phys. Rev. Lett. \*\*103\*\*, 016801 \(2009\)](#).
- [260] O. S. Zozulya, M. Haque, and N. Regnault, [Phys. Rev. B \*\*79\*\*, 045409 \(2009\)](#).
- [261] A. M. Läuchli, E. J. Bergholtz, J. Suorsa, and M. Haque, [Phys. Rev. Lett. \*\*104\*\*, 156404 \(2010\)](#).
- [262] R. Thomale, A. Sterdyniak, N. Regnault, and B. A. Bernevig, [Phys. Rev. Lett. \*\*104\*\*, 180502 \(2010\)](#).
- [263] J. Schliemann, [Phys. Rev. B \*\*83\*\*, 115322 \(2011\)](#).
- [264] M. Hermanns, A. Chandran, N. Regnault, and B. A. Bernevig, [Phys. Rev. B \*\*84\*\*, 121309 \(2011\)](#).
- [265] A. Chandran, M. Hermanns, N. Regnault, and B. A. Bernevig, [Phys. Rev. B \*\*84\*\*, 205136 \(2011\)](#).

- [266] X.-L. Qi, H. Katsura, and A. W. W. Ludwig, [Phys. Rev. Lett. \*\*108\*\*, 196402 \(2012\)](#).
- [267] Z. Liu, E. J. Bergholtz, H. Fan, and A. M. Läuchli, [Phys. Rev. B \*\*85\*\*, 045119 \(2012\)](#).
- [268] A. Sterdyniak, A. Chandran, N. Regnault, B. A. Bernevig, and P. Bonderson, [Phys. Rev. B \*\*85\*\*, 125308 \(2012\)](#).
- [269] J. Dubail, N. Read, and E. H. Rezayi, [Phys. Rev. B \*\*85\*\*, 115321 \(2012\)](#).
- [270] I. D. Rodríguez, S. H. Simon, and J. K. Slingerland, [Phys. Rev. Lett. \*\*108\*\*, 256806 \(2012\)](#).
- [271] J. Dubail, N. Read, and E. H. Rezayi, [Phys. Rev. B \*\*86\*\*, 245310 \(2012\)](#).
- [272] Z. Liu and E. J. Bergholtz, [Phys. Rev. B \*\*87\*\*, 035306 \(2013\)](#).
- [273] M. P. Zaletel, R. S. K. Mong, and F. Pollmann, [Phys. Rev. Lett. \*\*110\*\*, 236801 \(2013\)](#).
- [274] T. H. Hsieh and L. Fu, [Phys. Rev. Lett. \*\*113\*\*, 106801 \(2014\)](#).
- [275] Y.-C. He, S. Bhattacharjee, R. Moessner, and F. Pollmann, [arXiv:1506.01645 \(2015\)](#).
- [276] N. Regnault, [arXiv:1510.07670 \(2015\)](#).
- [277] A. M. Turner, Y. Zhang, and A. Vishwanath, [Phys. Rev. B \*\*82\*\*, 241102 \(2010\)](#).
- [278] L. Fidkowski, [Phys. Rev. Lett. \*\*104\*\*, 130502 \(2010\)](#).
- [279] L. Fidkowski and A. Kitaev, [Phys. Rev. B \*\*83\*\*, 075103 \(2011\)](#).
- [280] A. Alexandradinata, T. L. Hughes, and B. A. Bernevig, [Phys. Rev. B \*\*84\*\*, 195103 \(2011\)](#).
- [281] N. Regnault and B. A. Bernevig, [Phys. Rev. X \*\*1\*\*, 021014 \(2011\)](#).

- [282] A. M. Turner, F. Pollmann, and E. Berg, [Phys. Rev. B \*\*83\*\*, 075102 \(2011\)](#).
- [283] C. Fang, M. J. Gilbert, and B. A. Bernevig, [Phys. Rev. B \*\*87\*\*, 035119 \(2013\)](#).
- [284] M. Hermanns, Y. Salimi, M. Haque, and L. Fritz, [J. Stat. Mech. \*\*2014\*\*, P10030 \(2014\)](#).
- [285] Y.-C. He, D. N. Sheng, and Y. Chen, [Phys. Rev. Lett. \*\*112\*\*, 137202 \(2014\)](#).
- [286] B. Bauer, L. Cincio, B. P. Keller, M. Dolfi, G. Vidal, S. Trebst, and A. W. W. Ludwig, [Nat Commun \*\*5\*\* \(2014\)](#).
- [287] S.-S. Gong, W. Zhu, and D. N. Sheng, [Sci. Rep. \*\*4\*\* \(2014\)](#).
- [288] D. Poilblanc, J. I. Cirac, and N. Schuch, [Phys. Rev. B \*\*91\*\*, 224431 \(2015\)](#).
- [289] R. A. Santos, F. N. C. Paraan, V. E. Korepin, and A. Klümper, [EPL \*\*98\*\*, 37005 \(2012\)](#).
- [290] C.-Y. Huang and F.-L. Lin, [Phys. Rev. B \*\*84\*\*, 125110 \(2011\)](#).
- [291] R. A. Santos, C.-M. Jian, and R. Lundgren, [arXiv:1511.01489 \(2015\)](#).
- [292] H. Yao and X.-L. Qi, [Phys. Rev. Lett. \*\*105\*\*, 080501 \(2010\)](#).
- [293] F. Pollmann, A. M. Turner, E. Berg, and M. Oshikawa, [Phys. Rev. B \*\*81\*\*, 064439 \(2010\)](#).
- [294] E. G. Dalla Torre, E. Berg, and E. Altman, [Phys. Rev. Lett. \*\*97\*\*, 260401 \(2006\)](#).
- [295] H. Nonne, P. Lecheminant, S. Capponi, G. Roux, and E. Boulat, [Phys. Rev. B \*\*81\*\*, 020408 \(2010\)](#).
- [296] F. Pollmann, E. Berg, A. M. Turner, and M. Oshikawa, [Phys. Rev. B \*\*85\*\*, 075125 \(2012\)](#).
- [297] N. Regnault, “[Entanglement Spectroscopy and its application to the fractional quantum Hall phases,](#)” (2013).

- [298] Z. Liu, H.-L. Guo, V. Vedral, and H. Fan, [Phys. Rev. A \*\*83\*\*, 013620 \(2011\)](#).
- [299] B. I. Halperin, [Phys. Rev. B \*\*25\*\*, 2185 \(1982\)](#).
- [300] B. Swingle and T. Senthil, [Phys. Rev. B \*\*86\*\*, 045117 \(2012\)](#).
- [301] R. Orús, [Annals of Physics \*\*349\*\*, 117 \(2014\)](#).
- [302] R. Bousso, [Rev. Mod. Phys. \*\*74\*\*, 825 \(2002\)](#).
- [303] N. Schuch, D. Poilblanc, J. I. Cirac, and D. Pérez-García, [Phys. Rev. Lett. \*\*111\*\*, 090501 \(2013\)](#).
- [304] W. W. Ho, L. Cincio, H. Moradi, D. Gaiotto, and G. Vidal, [Phys. Rev. B \*\*91\*\*, 125119 \(2015\)](#).
- [305] L. Messio, B. Bernu, and C. Lhuillier, [Phys. Rev. Lett. \*\*108\*\*, 207204 \(2012\)](#).
- [306] L. Messio, C. Lhuillier, and G. Misguich, [Phys. Rev. B \*\*87\*\*, 125127 \(2013\)](#).
- [307] L. Cincio, G. Vidal, and B. Bauer, [arXiv:1506.03351 \(2015\)](#).
- [308] S. Yang, T. B. Wahl, H.-H. Tu, N. Schuch, and J. I. Cirac, [Phys. Rev. Lett. \*\*114\*\*, 106803 \(2015\)](#).
- [309] S. Bieri, L. Messio, B. Bernu, and C. Lhuillier, [Phys. Rev. B \*\*92\*\*, 060407 \(2015\)](#).
- [310] A. Wietek, A. Sterdyniak, and A. M. Läuchli, [Phys. Rev. B \*\*92\*\*, 125122 \(2015\)](#).
- [311] I. Peschel and M.-C. Chung, [J. Phys. A: Math. Gen. \*\*32\*\*, 8419 \(1999\)](#).
- [312] J. Schliemann, [J. Stat. Mech. \*\*2014\*\*, P09011 \(2014\)](#).
- [313] D. Poilblanc, [J. Stat. Mech. \*\*2014\*\*, P10026 \(2014\)](#).
- [314] I. Klich, D. Vaman, and G. Wong, [arXiv:1501.00482 \(2015\)](#).

- [315] M. Greven, R. J. Birgeneau, and U. J. Wiese, [Phys. Rev. Lett. \*\*77\*\*, 1865 \(1996\)](#).
- [316] I. Affleck, [Phys. Rev. Lett. \*\*56\*\*, 746 \(1986\)](#).
- [317] S. Kullback and R. A. Leibler, [Ann. Math. Statist. \*\*22\*\* \(1951\)](#).
- [318] Rényi, A., [Proceedings of the Fourth Berkeley Symposium on Mathematical Statistics and Probability: Contributions to the Theory of Statistics \*\*1\*\*, 547 \(1961\)](#).
- [319] M. Troyer, M. Imada, and K. Ueda, [J. Phys. Soc. Jpn. \*\*66\*\*, 2957 \(1997\)](#).
- [320] M. Matsumoto, C. Yasuda, S. Todo, and H. Takayama, [Phys. Rev. B \*\*65\*\*, 014407 \(2001\)](#).
- [321] L. Wang, K. S. D. Beach, and A. W. Sandvik, [Phys. Rev. B \*\*73\*\*, 014431 \(2006\)](#).
- [322] A. F. Albuquerque, M. Troyer, and J. Oitmaa, [Phys. Rev. B \*\*78\*\*, 132402 \(2008\)](#).
- [323] S. Wenzel and W. Janke, [Phys. Rev. B \*\*79\*\*, 014410 \(2009\)](#).
- [324] A. W. Sandvik, [AIP Conference Proceedings \*\*1297\*\*, 135 \(2010\)](#).
- [325] E. Yusuf, A. Joshi, and K. Yang, [Phys. Rev. B \*\*69\*\*, 144412 \(2004\)](#).
- [326] N. Laflorencie, I. Affleck, and M. Berciu, [J. Stat. Mech. \*\*2005\*\*, P12001 \(2005\)](#).
- [327] K. S. D. Beach, [arXiv:0707.0297 \(2007\)](#).
- [328] L. Rademaker, [arXiv:1507.04402 \(2015\)](#).
- [329] E. Lieb and D. Mattis, [Journal of Mathematical Physics \*\*3\*\*, 749 \(1962\)](#).
- [330] P. W. Anderson, [Phys. Rev. \*\*109\*\*, 1492 \(1958\)](#).
- [331] J. Kondo, [Prog. Theor. Phys. \*\*32\*\*, 37 \(1964\)](#).

- [332] A. C. Hewson, *The Kondo Problem to Heavy Fermions* (Cambridge University Press, Cambridge, UK, 1993).
- [333] K. Binder and A. P. Young, *Rev. Mod. Phys.* **58**, 801 (1986).
- [334] S. F. Edwards and P. W. Anderson, *J. Phys. F: Met. Phys.* **5**, 965 (1975).
- [335] S. Kirkpatrick and D. Sherrington, *Phys. Rev. B* **17**, 4384 (1978).
- [336] S.-k. Ma, C. Dasgupta, and C.-k. Hu, *Phys. Rev. Lett.* **43**, 1434 (1979).
- [337] D. S. Fisher, *Phys. Rev. B* **51**, 6411 (1995).
- [338] F. Igloi and C. Monthus, *Physics Reports* **412** (2005).
- [339] D. S. Fisher, *Phys. Rev. B* **50**, 3799 (1994).
- [340] O. Motrunich, S.-C. Mau, D. A. Huse, and D. S. Fisher, *Phys. Rev. B* **61**, 1160 (2000).
- [341] Y.-C. Lin, R. Mélin, H. Rieger, and F. Igloi, *Phys. Rev. B* **68**, 024424 (2003).
- [342] I. A. Kovács and F. Igloi, *Phys. Rev. B* **83**, 174207 (2011).
- [343] G. Refael and J. E. Moore, *Phys. Rev. Lett.* **93**, 260602 (2004).
- [344] J. A. Hoyos, A. P. Vieira, N. Laflorencie, and E. Miranda, *Phys. Rev. B* **76**, 174425 (2007).
- [345] F. Igloi and R. Juhász, *EPL* **81**, 57003 (2008).
- [346] L. Turban, *Physics letters. A* **104**, 435 (1984).
- [347] N. Laflorencie, *Phys. Rev. B* **72**, 140408 (2005).
- [348] F. Igloi and Y.-C. Lin, *J. Stat. Mech.* **2008**, P06004 (2008).
- [349] M. Fagotti, P. Calabrese, and J. E. Moore, *Phys. Rev. B* **83**, 045110 (2011).

- [350] M. Pouranvari and K. Yang, [Phys. Rev. B \*\*88\*\*, 075123 \(2013\)](#).
- [351] F. Alet, S. Capponi, N. Laflorencie, and M. Mambrini, [Phys. Rev. Lett. \*\*99\*\*, 117204 \(2007\)](#).
- [352] R. W. Chhajlany, P. Tomczak, and A. Wójcik, [Phys. Rev. Lett. \*\*99\*\*, 167204 \(2007\)](#).
- [353] M. Mambrini, [Phys. Rev. B \*\*77\*\*, 134430 \(2008\)](#).
- [354] J. L. Jacobsen and H. Saleur, [Phys. Rev. Lett. \*\*100\*\*, 087205 \(2008\)](#).
- [355] H. Tran and N. E. Bonesteel, [Phys. Rev. B \*\*84\*\*, 144420 \(2011\)](#).
- [356] R. A. Hyman and K. Yang, [Phys. Rev. Lett. \*\*78\*\*, 1783 \(1997\)](#).
- [357] C. Monthus, O. Golinelli, and T. Jolicœur, [Phys. Rev. B \*\*58\*\*, 805 \(1998\)](#).
- [358] G. Refael, S. Kehrein, and D. S. Fisher, [Phys. Rev. B \*\*66\*\*, 060402 \(2002\)](#).
- [359] K. Damle and D. A. Huse, [Phys. Rev. Lett. \*\*89\*\*, 277203 \(2002\)](#).
- [360] G. Refael and J. E. Moore, [Phys. Rev. B \*\*76\*\*, 024419 \(2007\)](#).
- [361] N. E. Bonesteel and K. Yang, [Phys. Rev. Lett. \*\*99\*\*, 140405 \(2007\)](#).
- [362] L. Fidkowski, G. Refael, N. E. Bonesteel, and J. E. Moore, [Phys. Rev. B \*\*78\*\*, 224204 \(2008\)](#).
- [363] L. Fidkowski, H.-H. Lin, P. Titum, and G. Refael, [Phys. Rev. B \*\*79\*\*, 155120 \(2009\)](#).
- [364] A. B. Zomolodchikov, [Soviet Journal of Experimental and Theoretical Physics Letters \*\*43\*\*, 730 \(1986\)](#).
- [365] R. Santachiara, [J. Stat. Mech. \*\*2006\*\*, L06002 \(2006\)](#).
- [366] G. Refael and J. E. Moore, [J. Phys. A: Math. Theor. \*\*42\*\*, 504010 \(2009\)](#).
- [367] G. Vitagliano, A. Riera, and J. I. Latorre, [New J. Phys. \*\*12\*\*, 113049 \(2010\)](#).



- [368] G. Ramírez, J. Rodríguez-Laguna, and G. Sierra, [J. Stat. Mech.](#) **2014**, P10004 (2014).
- [369] G. Ramírez, J. Rodríguez-Laguna, and G. Sierra, [J. Stat. Mech.](#) **2015**, P06002 (2015).
- [370] D. Binosi, G. De Chiara, S. Montangero, and A. Recati, [Phys. Rev. B](#) **76**, 140405 (2007).
- [371] J. A. Hoyos, N. Laflorencie, A. P. Vieira, and T. Vojta, [EPL](#) **93**, 30004 (2011).
- [372] J. C. Getelina, F. C. Alcaraz, and J. A. Hoyos, [arXiv:1511.00618](#) (2015).
- [373] I. A. Kovács and F. Iglói, [Phys. Rev. B](#) **82**, 054437 (2010).
- [374] C. Monthus and T. Garel, [J. Stat. Mech.](#) **2012**, P01008 (2012).
- [375] T. Vojta, A. Farquhar, and J. Mast, [Phys. Rev. E](#) **79**, 011111 (2009).
- [376] T. Vojta, C. Kotabage, and J. A. Hoyos, [Phys. Rev. B](#) **79**, 024401 (2009).
- [377] N. Laflorencie, S. Wessel, A. Läuchli, and H. Rieger, [Phys. Rev. B](#) **73**, 060403 (2006).
- [378] Y.-C. Lin, F. Iglói, and H. Rieger, [Phys. Rev. Lett.](#) **99**, 147202 (2007).
- [379] T. Senthil and S. Sachdev, [Phys. Rev. Lett.](#) **77**, 5292 (1996).
- [380] R. Yu, H. Saleur, and S. Haas, [Phys. Rev. B](#) **77**, 140402 (2008).
- [381] I. Kovács, *Infinitely Disordered Critical Behavior in Higher Dimensional Quantum Systems*, [Ph.D. thesis](#), Eötvös Loránd University (2012).
- [382] I. A. Kovács and F. Iglói, [EPL](#) **97**, 67009 (2012).
- [383] D. J. Gross, [Nuclear Physics B - Proceedings Supplements](#) **74**, 426 (1999).
- [384] P. W. Anderson, [J. Phys. C: Solid State Phys.](#) **3**, 2436 (1970).

- [385] K. G. Wilson, [Rev. Mod. Phys. \*\*47\*\*, 773 \(1975\)](#).
- [386] P. Nozières, [J Low Temp Phys \*\*17\*\*, 31 \(1974\)](#).
- [387] N. Andrei, [Phys. Rev. Lett. \*\*45\*\*, 379 \(1980\)](#).
- [388] P. B. Wiegmann, [J. Phys. C: Solid State Phys. \*\*14\*\*, 1463 \(1981\)](#).
- [389] I. Affleck, [arXiv:0911.2209 \(2009\)](#).
- [390] G. Bergmann, [Phys. Rev. B \*\*77\*\*, 104401 \(2008\)](#).
- [391] I. Affleck and P. Simon, [Phys. Rev. Lett. \*\*86\*\*, 2854 \(2001\)](#).
- [392] E. S. Sørensen and I. Affleck, [Phys. Rev. Lett. \*\*94\*\*, 086601 \(2005\)](#).
- [393] R. G. Pereira, N. Laflorencie, I. Affleck, and B. I. Halperin, [Phys. Rev. B \*\*77\*\*, 125327 \(2008\)](#).
- [394] E. S. Sørensen, M.-S. Chang, N. Laflorencie, and I. Affleck, [J. Stat. Mech. \*\*2007\*\*, L01001 \(2007\)](#).
- [395] E. S. Sørensen, M.-S. Chang, N. Laflorencie, and I. Affleck, [J. Stat. Mech. \*\*2007\*\*, P08003 \(2007\)](#).
- [396] I. Affleck, N. Laflorencie, and E. S. Sørensen, [J. Phys. A: Math. Theor. \*\*42\*\*, 504009 \(2009\)](#).
- [397] P. Sodano, A. Bayat, and S. Bose, [Phys. Rev. B \*\*81\*\*, 100412 \(2010\)](#).
- [398] E. Eriksson and H. Johannesson, [Phys. Rev. B \*\*84\*\*, 041107 \(2011\)](#).
- [399] A. Deschner and E. S. Sørensen, [J. Stat. Mech. \*\*2011\*\*, P10023 \(2011\)](#).
- [400] A. Bayat, S. Bose, P. Sodano, and H. Johannesson, [Phys. Rev. Lett. \*\*109\*\*, 066403 \(2012\)](#).
- [401] H. Saleur, P. Schmitteckert, and R. Vasseur, [Phys. Rev. B \*\*88\*\*, 085413 \(2013\)](#).

- [402] R. Vasseur, J. L. Jacobsen, and H. Saleur, [Phys. Rev. Lett. \*\*112\*\*, 106601 \(2014\)](#).
- [403] S.-S. B. Lee, J. Park, and H.-S. Sim, [Phys. Rev. Lett. \*\*114\*\*, 057203 \(2015\)](#).
- [404] J. H. Pixley, T. Chowdhury, M. T. Miecnikowski, J. Stephens, C. Wagner, and K. Ingersent, [Phys. Rev. B \*\*91\*\*, 245122 \(2015\)](#).
- [405] N. Andrei, K. Furuya, and J. H. Lowenstein, [Rev. Mod. Phys. \*\*55\*\*, 331 \(1983\)](#).
- [406] S. Eggert and I. Affleck, [Phys. Rev. B \*\*46\*\*, 10866 \(1992\)](#).
- [407] N. Laflorencie, E. S. Sørensen, and I. Affleck, [J. Stat. Mech. \*\*2008\*\*, P02007 \(2008\)](#).
- [408] S. Eggert, [Phys. Rev. B \*\*54\*\*, R9612 \(1996\)](#).
- [409] H. Frahm and A. A. Zvyagin, [J. Phys.: Condens. Matter \*\*9\*\*, 9939 \(1997\)](#).
- [410] F. D. M. Haldane, [Phys. Rev. B \*\*25\*\*, 4925 \(1982\)](#).
- [411] N. Laflorencie, E. S. Sørensen, M.-S. Chang, and I. Affleck, [Phys. Rev. Lett. \*\*96\*\*, 100603 \(2006\)](#).
- [412] A. J. Leggett, S. Chakravarty, A. T. Dorsey, M. P. A. Fisher, A. Garg, and W. Zwerger, [Rev. Mod. Phys. \*\*59\*\*, 1 \(1987\)](#).
- [413] A. Kopp and K. L. Hur, [Phys. Rev. Lett. \*\*98\*\*, 220401 \(2007\)](#).
- [414] K. Le Hur, P. Doucet-Beaupré, and W. Hofstetter, [Phys. Rev. Lett. \*\*99\*\*, 126801 \(2007\)](#).
- [415] E. S. Sørensen and I. Affleck, [Phys. Rev. B \*\*53\*\*, 9153 \(1996\)](#).
- [416] V. Barzykin and I. Affleck, [Phys. Rev. Lett. \*\*76\*\*, 4959 \(1996\)](#).
- [417] I. Affleck and A. W. W. Ludwig, [Phys. Rev. Lett. \*\*67\*\*, 161 \(1991\)](#).

- [418] H.-Q. Zhou, T. Barthel, J. O. Fjærestad, and U. Schollwöck, [Phys. Rev. A \*\*74\*\*, 050305 \(2006\)](#).
- [419] L. Taddia, J. C. Xavier, F. C. Alcaraz, and G. Sierra, [Phys. Rev. B \*\*88\*\*, 075112 \(2013\)](#).
- [420] L. Taddia, [arXiv:1309.4003 \(2013\)](#).
- [421] B. Alkurtass, A. Bayat, I. Affleck, S. Bose, H. Johannesson, P. Sodano, E. S. Sørensen, and K. L. Hur, [arXiv:1509.02949 \(2015\)](#).
- [422] Ö. Legeza, J. Sólyom, L. Tincani, and R. M. Noack, [Phys. Rev. Lett. \*\*99\*\*, 087203 \(2007\)](#).
- [423] E. Szirmai, Ö. Legeza, and J. Sólyom, [Phys. Rev. B \*\*77\*\*, 045106 \(2008\)](#).
- [424] A. M. Läuchli and C. Kollath, [J. Stat. Mech. \*\*2008\*\*, P05018 \(2008\)](#).
- [425] G. Roux, S. Capponi, P. Lecheminant, and P. Azaria, [Eur. Phys. J. B \*\*68\*\*, 293 \(2008\)](#).
- [426] J. Friedel, [Nuovo Cim \*\*7\*\*, 287 \(2007\)](#).
- [427] M. Fagotti and P. Calabrese, [J. Stat. Mech. \*\*2011\*\*, P01017 \(2011\)](#).
- [428] P. Calabrese and F. H. L. Essler, [J. Stat. Mech. \*\*2010\*\*, P08029 \(2010\)](#).
- [429] M. Campostrini and E. Vicari, [Phys. Rev. A \*\*81\*\*, 063614 \(2010\)](#).
- [430] H. Fan, V. Korepin, V. Roychowdhury, C. Hadley, and S. Bose, [Phys. Rev. B \*\*76\*\*, 014428 \(2007\)](#).
- [431] G. Evenbly, R. N. C. Pfeifer, V. Picó, S. Iblisdir, L. Tagliacozzo, I. P. McCulloch, and G. Vidal, [Phys. Rev. B \*\*82\*\*, 161107 \(2010\)](#).
- [432] P. Silvi, V. Giovannetti, P. Calabrese, G. E. Santoro, and R. Fazio, [J. Stat. Mech. \*\*2010\*\*, L03001 \(2010\)](#).
- [433] S. Y. Cho and R. H. McKenzie, [Phys. Rev. A \*\*73\*\*, 012109 \(2006\)](#).

- [434] T. A. Costi and R. H. McKenzie, [Phys. Rev. A \*\*68\*\*, 034301 \(2003\)](#).
- [435] K. L. Hur, [Annals of Physics \*\*323\*\*, 2208 \(2008\)](#).
- [436] C. L. Kane and M. P. A. Fisher, [Phys. Rev. Lett. \*\*68\*\*, 1220 \(1992\)](#).
- [437] I. Peschel, [J. Phys. A: Math. Gen. \*\*38\*\*, 4327 \(2005\)](#).
- [438] J. Zhao, I. Peschel, and X. Wang, [Phys. Rev. B \*\*73\*\*, 024417 \(2006\)](#).
- [439] T. J. G. Apollaro and F. Plastina, [Phys. Rev. A \*\*74\*\*, 062316 \(2006\)](#).
- [440] L. Freton, E. Boulat, and H. Saleur, [Nuclear Physics B \*\*874\*\*, 279 \(2013\)](#).
- [441] M. Pouranvari, K. Yang, and A. Seidel, [Phys. Rev. B \*\*91\*\*, 075115 \(2015\)](#).
- [442] F. Iglói, Z. Szatmári, and Y.-C. Lin, [Phys. Rev. B \*\*80\*\*, 024405 \(2009\)](#).
- [443] S. Ghosh, P. Ribeiro, and M. Haque, [J. Stat. Mech. \*\*2015\*\*, P08002 \(2015\)](#).
- [444] A. Bayat, S. Bose, H. Johannesson, and P. Sodano, [Phys. Rev. B \*\*92\*\*, 155141 \(2015\)](#).
- [445] L. Fleishman and P. W. Anderson, [Phys. Rev. B \*\*21\*\*, 2366 \(1980\)](#).
- [446] B. L. Altshuler, Y. Gefen, A. Kamenev, and L. S. Levitov, [Phys. Rev. Lett. \*\*78\*\*, 2803 \(1997\)](#).
- [447] P. Jacquod and D. L. Shepelyansky, [Phys. Rev. Lett. \*\*79\*\*, 1837 \(1997\)](#).
- [448] B. Georgeot and D. L. Shepelyansky, [Phys. Rev. Lett. \*\*81\*\*, 5129 \(1998\)](#).
- [449] I. V. Gornyi, A. D. Mirlin, and D. G. Polyakov, [Phys. Rev. Lett. \*\*95\*\*, 206603 \(2005\)](#).
- [450] D. M. Basko, I. L. Aleiner, and B. L. Altshuler, [Annals of Physics \*\*321\*\*, 1126 \(2006\)](#).
- [451] J. M. Deutsch, [Phys. Rev. A \*\*43\*\*, 2046 \(1991\)](#).
- [452] M. Srednicki, [Phys. Rev. E \*\*50\*\*, 888 \(1994\)](#).

- [453] M. Rigol, V. Dunjko, and M. Olshanii, [Nature](#) **452**, 854 (2008).
- [454] R. Nandkishore and D. A. Huse, [Annual Review of Condensed Matter Physics](#) **6**, 15 (2015).
- [455] E. Altman and R. Vosk, [Annual Review of Condensed Matter Physics](#) **6**, 383 (2015).
- [456] R. Nandkishore, S. Gopalakrishnan, and D. A. Huse, [Phys. Rev. B](#) **90**, 064203 (2014).
- [457] D. A. Huse, R. Nandkishore, V. Oganesyan, A. Pal, and S. L. Sondhi, [Phys. Rev. B](#) **88**, 014206 (2013).
- [458] Y. Bahri, R. Vosk, E. Altman, and A. Vishwanath, [Nat Commun](#) **6** (2015).
- [459] A. Chandran, V. Khemani, C. R. Laumann, and S. L. Sondhi, [Phys. Rev. B](#) **89**, 144201 (2014).
- [460] B. Bauer and C. Nayak, [J. Stat. Mech.](#) **2013**, P09005 (2013).
- [461] R. Vosk and E. Altman, [Phys. Rev. Lett.](#) **112**, 217204 (2014).
- [462] R. Vosk and E. Altman, [Phys. Rev. Lett.](#) **110**, 067204 (2013).
- [463] M. Serbyn, Z. Papić, and D. A. Abanin, [Phys. Rev. Lett.](#) **111**, 127201 (2013).
- [464] V. Ros, M. Müller, and A. Scardicchio, [Nuclear Physics B](#) **891**, 420 (2015).
- [465] A. Chandran, I. H. Kim, G. Vidal, and D. A. Abanin, [Phys. Rev. B](#) **91**, 085425 (2015).
- [466] M. Žnidarič, T. Prosen, and P. Prelovšek, [Phys. Rev. B](#) **77**, 064426 (2008).
- [467] A. Pal and D. A. Huse, [Phys. Rev. B](#) **82**, 174411 (2010).

- [468] J. H. Bardarson, F. Pollmann, and J. E. Moore, [Phys. Rev. Lett. \*\*109\*\*, 017202 \(2012\)](#).
- [469] A. D. Luca and A. Scardicchio, [EPL \*\*101\*\*, 37003 \(2013\)](#).
- [470] D. J. Luitz, N. Laflorencie, and F. Alet, [Phys. Rev. B \*\*91\*\*, 081103 \(2015\)](#).
- [471] V. Oganesyan and D. A. Huse, [Phys. Rev. B \*\*75\*\*, 155111 \(2007\)](#).
- [472] R. Mondaini and M. Rigol, [arXiv:1508.02722 \(2015\)](#).
- [473] M. Schreiber, S. S. Hodgman, P. Bordia, H. P. Lüschen, M. H. Fischer, R. Vosk, E. Altman, U. Schneider, and I. Bloch, [Science \*\*349\*\*, 842 \(2015\)](#).
- [474] S. Iyer, V. Oganesyan, G. Refael, and D. Huse, [Phys. Rev. B \*\*87\*\*, 134202 \(2013\)](#).
- [475] J. A. Kjäll, J. H. Bardarson, and F. Pollmann, [Phys. Rev. Lett. \*\*113\*\*, 107204 \(2014\)](#).
- [476] C. R. Laumann, A. Pal, and A. Scardicchio, [Phys. Rev. Lett. \*\*113\*\*, 200405 \(2014\)](#).
- [477] T. Grover and M. P. A. Fisher, [J. Stat. Mech. \*\*2014\*\*, P10010 \(2014\)](#).
- [478] W. De Roeck and F. Huveneers, [Phys. Rev. B \*\*90\*\*, 165137 \(2014\)](#).
- [479] M. Schiulaz, A. Silva, and M. Müller, [Phys. Rev. B \*\*91\*\*, 184202 \(2015\)](#).
- [480] N. Y. Yao, C. R. Laumann, J. I. Cirac, M. D. Lukin, and J. E. Moore, [arXiv:1410.7407 \(2014\)](#).
- [481] P. Ponte, Z. Papić, F. Huveneers, and D. A. Abanin, [Phys. Rev. Lett. \*\*114\*\*, 140401 \(2015\)](#).
- [482] D. Pekker, G. Refael, E. Altman, E. Demler, and V. Oganesyan, [Phys. Rev. X \*\*4\*\*, 011052 \(2014\)](#).
- [483] Y. Huang and J. E. Moore, [Phys. Rev. B \*\*90\*\*, 220202 \(2014\)](#).

- [484] R. Vasseur, A. C. Potter, and S. A. Parameswaran, [Phys. Rev. Lett. \*\*114\*\*, 217201 \(2015\)](#).
- [485] M. Friesdorf, A. H. Werner, W. Brown, V. B. Scholz, and J. Eisert, [Phys. Rev. Lett. \*\*114\*\*, 170505 \(2015\)](#).
- [486] A. Chandran, J. Carrasquilla, I. H. Kim, D. A. Abanin, and G. Vidal, [Phys. Rev. B \*\*92\*\*, 024201 \(2015\)](#).
- [487] D. Pekker and B. K. Clark, [arXiv:1410.2224 \(2014\)](#).
- [488] V. Khemani, F. Pollmann, and S. L. Sondhi, [arXiv:1509.00483 \(2015\)](#).
- [489] X. Yu, D. Pekker, and B. K. Clark, [arXiv:1509.01244 \(2015\)](#).
- [490] M. L. Mehta, *Random matrices*, Vol. 142 (Academic press, 2004).
- [491] E. Cuevas, M. Feigel'man, L. Ioffe, and M. Mezard, [Nat Commun \*\*3\*\*, 1128 \(2012\)](#).
- [492] M. Serbyn and J. E. Moore, [arXiv:1508.07293 \(2015\)](#).
- [493] C. Monthus, [arXiv:1510.03711 \(2015\)](#).
- [494] C. Monthus, [arXiv:1510.08322 \(2015\)](#).
- [495] T. Grover, [arXiv:1405.1471 \(2014\)](#).
- [496] A. Chandran, C. R. Laumann, and V. Oganesyan, [arXiv:1509.04285 \(2015\)](#).
- [497] C. Gogolin and J. Eisert, [arXiv:1503.07538 \(2015\)](#).
- [498] D. N. Page, [Phys. Rev. Lett. \*\*71\*\*, 1291 \(1993\)](#).
- [499] J. Sato, B. Aufgebauer, H. Boos, F. Göhmann, A. Klümper, M. Takahashi, and C. Trippe, [Phys. Rev. Lett. \*\*106\*\*, 257201 \(2011\)](#).
- [500] V. Alba, [Phys. Rev. B \*\*91\*\*, 155123 \(2015\)](#).



- [501] J. P. Keating, N. Linden, and H. J. Wells, *Commun. Math. Phys.* **338**, 81 (2015).
- [502] D. M. Kennes and C. Karrasch, [arXiv:1511.02205](#) (2015).
- [503] T. Devakul and R. R. P. Singh, *Phys. Rev. Lett.* **115**, 187201 (2015).
- [504] S. P. Lim and D. N. Sheng, [arXiv:1510.08145](#) (2015).
- [505] C. Nadal, S. N. Majumdar, and M. Vergassola, *Phys. Rev. Lett.* **104**, 110501 (2010).
- [506] R. Vosk, D. A. Huse, and E. Altman, *Phys. Rev. X* **5**, 031032 (2015).
- [507] Z.-C. Yang, C. Chamon, A. Hamma, and E. R. Mucciolo, [arXiv:1506.01714](#) (2015).
- [508] S. Leiman, A. Eisenbach, and R. Berkovits, [arXiv:1507.06177](#) (2015).
- [509] A. Feiguin, S. Trebst, A. W. W. Ludwig, M. Troyer, A. Kitaev, Z. Wang, and M. H. Freedman, *Phys. Rev. Lett.* **98**, 160409 (2007).
- [510] R. Vasseur, A. J. Friedman, S. A. Parameswaran, and A. C. Potter, [arXiv:1510.04282](#) (2015).
- [511] A. Polkovnikov, K. Sengupta, A. Silva, and M. Vengalattore, *Rev. Mod. Phys.* **83**, 863 (2011).
- [512] P. Calabrese and J. Cardy, *J. Stat. Mech.* **2005**, P04010 (2005).
- [513] G. D. Chiara, S. Montangero, P. Calabrese, and R. Fazio, *J. Stat. Mech.* **2006**, P03001 (2006).
- [514] V. Alba and F. Heidrich-Meisner, *Phys. Rev. B* **90**, 075144 (2014).
- [515] V. Eisler and I. Peschel, *J. Stat. Mech.* **2007**, P06005 (2007).
- [516] H. Kim and D. A. Huse, *Phys. Rev. Lett.* **111**, 127205 (2013).

- [517] S. Bravyi, M. B. Hastings, and F. Verstraete, [Phys. Rev. Lett. \*\*97\*\*, 050401 \(2006\)](#).
- [518] J. Eisert and T. J. Osborne, [Phys. Rev. Lett. \*\*97\*\*, 150404 \(2006\)](#).
- [519] C. K. Burrell and T. J. Osborne, [Phys. Rev. Lett. \*\*99\*\*, 167201 \(2007\)](#).
- [520] F. Iglói, Z. Szatmári, and Y.-C. Lin, [Phys. Rev. B \*\*85\*\*, 094417 \(2012\)](#).
- [521] A. Nanduri, H. Kim, and D. A. Huse, [Phys. Rev. B \*\*90\*\*, 064201 \(2014\)](#).
- [522] K. Agarwal, E. Demler, and I. Martin, [Phys. Rev. B \*\*92\*\*, 184203 \(2015\)](#).
- [523] F. Andraschko, T. Enss, and J. Sirker, [Phys. Rev. Lett. \*\*113\*\*, 217201 \(2014\)](#).
- [524] M. Serbyn, Z. Papić, and D. A. Abanin, [Phys. Rev. Lett. \*\*110\*\*, 260601 \(2013\)](#).
- [525] M. Pino, [Phys. Rev. B \*\*90\*\*, 174204 \(2014\)](#).
- [526] N. Y. Yao, C. R. Laumann, S. Gopalakrishnan, M. Knap, M. Müller, E. A. Demler, and M. D. Lukin, [Phys. Rev. Lett. \*\*113\*\*, 243002 \(2014\)](#).
- [527] M. Serbyn, M. Knap, S. Gopalakrishnan, Z. Papić, N. Y. Yao, C. R. Laumann, D. A. Abanin, M. D. Lukin, and E. A. Demler, [Phys. Rev. Lett. \*\*113\*\*, 147204 \(2014\)](#).
- [528] P. Jurcevic, B. P. Lanyon, P. Hauke, C. Hempel, P. Zoller, R. Blatt, and C. F. Roos, [Nature \*\*511\*\*, 202 \(2014\)](#).
- [529] K. Agarwal, S. Gopalakrishnan, M. Knap, M. Müller, and E. Demler, [Phys. Rev. Lett. \*\*114\*\*, 160401 \(2015\)](#).
- [530] Y. Bar Lev, G. Cohen, and D. R. Reichman, [Phys. Rev. Lett. \*\*114\*\*, 100601 \(2015\)](#).
- [531] E. J. Torres-Herrera and L. F. Santos, [Phys. Rev. B \*\*92\*\*, 014208 \(2015\)](#).

- [532] D. J. Luitz, N. Laflorencie, and F. Alet, [arXiv:1511.05141](#) (2015).
- [533] A. Leroze, V. K. Varma, F. Pietracaprina, J. Goold, and A. Scardicchio, [arXiv:1511.09144](#) (2015).
- [534] A. C. Potter, R. Vasseur, and S. A. Parameswaran, [Phys. Rev. X \*\*5\*\*, 031033 \(2015\)](#).
- [535] S. Gopalakrishnan, K. Agarwal, D. A. Huse, E. Demler, and M. Knap, [arXiv:1511.06389](#) (2015).
- [536] R. B. Griffiths, [Phys. Rev. Lett. \*\*23\*\*, 17 \(1969\)](#).
- [537] M. Ovadia, D. Kalok, I. Tamir, S. Mitra, B. Sacépé, and D. Shahar, [Scientific Reports \*\*5\*\*, 13503 \(2015\)](#).
- [538] J. Smith, A. Lee, P. Richerme, B. Neyenhuis, P. W. Hess, P. Hauke, M. Heyl, D. A. Huse, and C. Monroe, [arXiv:1508.07026](#) (2015).
- [539] P. Bordia, H. P. Lüschen, S. S. Hodgman, M. Schreiber, I. Bloch, and U. Schneider, [arXiv:1509.00478](#) (2015).
- [540] R. Islam, R. Ma, P. M. Preiss, M. Eric Tai, A. Lukin, M. Rispoli, and M. Greiner, [Nature \*\*528\*\*, 77 \(2015\)](#).
- [541] D. Petz and C. Ghinea, [Quantum Probability and Related Topics \*\*27\*\*, 261 \(2011\)](#).
- [542] M. Pino, B. L. Altshuler, and L. B. Ioffe, [arXiv:1501.03853](#) (2015).
- [543] W. D. Roeck and F. Huveneers, [Commun. Math. Phys. \*\*332\*\*, 1017 \(2014\)](#).
- [544] M. Schiulaz and M. Müller, [AIP Conference Proceedings \*\*1610\*\*, 11 \(2014\)](#).
- [545] J. M. Hickey, S. Genway, and J. P. Garrahan, [arXiv:1405.5780](#) (2014).
- [546] M. van Horssen, E. Levi, and J. P. Garrahan, [Phys. Rev. B \*\*92\*\*, 100305 \(2015\)](#).

- [547] Z. Papić, E. M. Stoudenmire, and D. A. Abanin, [Annals of Physics](#) **362**, 714 (2015).
- [548] O. G  hne and G. T  th, [Physics Reports](#) **474**, 1 (2009).
- [549] Y. Makhlin, G. Sc  hn, and A. Shnirman, [Nature](#) **398**, 305 (1999).
- [550] A. J. Berkley, H. Xu, R. C. Ramos, M. A. Gubrud, F. W. Strauch, P. R. Johnson, J. R. Anderson, A. J. Dragt, C. J. Lobb, and F. C. Wellstood, [Science](#) **300**, 1548 (2003).
- [551] S. Ghosh, T. F. Rosenbaum, G. Aeppli, and S. N. Coppersmith, [Nature](#) **425**, 48 (2003).
- [552] H. H  ffner, W. H  nsel, C. F. Roos, J. Benhelm, D. Chek-al kar, M. Chwalla, T. K  rber, U. D. Rapol, M. Riebe, P. O. Schmidt, C. Becher, O. G  hne, W. D  r, and R. Blatt, [Nature](#) **438**, 643 (2005).
- [553] L. Childress, M. V. G. Dutt, J. M. Taylor, A. S. Zibrov, F. Jelezko, J. Wrachtrup, P. R. Hemmer, and M. D. Lukin, [Science](#) **314**, 281 (2006).
- [554] S. Bertaina, S. Gambarelli, A. Tkachuk, I. N. Kurkin, B. Malkin, A. Stepanov, and B. Barbara, [Nat Nano](#) **2**, 39 (2007).
- [555] P. C. E. Stamp and A. Gaita-Ari  o, [J. Mater. Chem.](#) **19**, 1718 (2009).
- [556] S. Simmons, R. M. Brown, H. Riemann, N. V. Abrosimov, P. Becker, H.-J. Pohl, M. L. W. Thewalt, K. M. Itoh, and J. J. L. Morton, [Nature](#) **470**, 69 (2011).
- [557] H. Bernien, B. Hensen, W. Pfaff, G. Koolstra, M. S. Blok, L. Robledo, T. H. Taminiau, M. Markham, D. J. Twitchen, L. Childress, and R. Hanson, [Nature](#) **497**, 86 (2013).
- [558] F. Dolde, I. Jakobi, B. Naydenov, N. Zhao, S. Pezzagna, C. Trautmann, J. Meijer, P. Neumann, F. Jelezko, and J. Wrachtrup, [Nat Phys](#) **9**, 139 (2013).

- [559] J. J. Pla, K. Y. Tan, J. P. Dehollain, W. H. Lim, J. J. L. Morton, F. A. Zwanenburg, D. N. Jamieson, A. S. Dzurak, and A. Morello, [Nature](#) **496**, 334 (2013).
- [560] W. Pfaff, B. J. Hensen, H. Bernien, S. B. v. Dam, M. S. Blok, T. H. Taminiau, M. J. Tiggelman, R. N. Schouten, M. Markham, D. J. Twitchen, and R. Hanson, [Science](#) **345**, 532 (2014).
- [561] S. Pirandola, J. Eisert, C. Weedbrook, A. Furusawa, and S. L. Braunstein, [Nature Photonics](#) **9** (2015).
- [562] F. Verstraete, M. Popp, and J. I. Cirac, [Phys. Rev. Lett.](#) **92**, 027901 (2004).
- [563] Č. Brukner, V. Vedral, and A. Zeilinger, [Phys. Rev. A](#) **73**, 012110 (2006).
- [564] D. Das, H. Singh, T. Chakraborty, R. K. Gopal, and C. Mitra, [New J. Phys.](#) **15**, 013047 (2013).
- [565] H. Singh, T. Chakraborty, D. Das, H. S. Jeevan, Y. Tokiwa, P. Gegenwart, and C. Mitra, [New J. Phys.](#) **15**, 113001 (2013).
- [566] N. B. Christensen, H. M. Rønnow, D. F. McMorrow, A. Harrison, T. G. Perring, M. Enderle, R. Coldea, L. P. Regnault, and G. Aeppli, [PNAS](#) **104**, 15264 (2007).
- [567] A. Candini, G. Lorusso, F. Troiani, A. Ghirri, S. Carretta, P. Santini, G. Amoretti, C. Muryn, F. Tuna, G. Timco, E. J. L. McInnes, R. E. P. Winpenny, W. Wernsdorfer, and M. Affronte, [Phys. Rev. Lett.](#) **104**, 037203 (2010).
- [568] D.-J. Choi, R. Robles, S. Yan, J. A. J. Burgess, S. Rolf-Pissarczyk, J.-P. Gauyacq, N. Lorente, M. Ternes, and S. Loth, [arXiv:1507.04785](#) (2015).
- [569] R. A. Cowley, [J. Phys.: Condens. Matter](#) **15**, 4143 (2003).

- [570] M. Cramer, M. B. Plenio, and H. Wunderlich, [Phys. Rev. Lett. \*\*106\*\*, 020401 \(2011\)](#).
- [571] M. Cramer, A. Bernard, N. Fabbri, L. Fallani, C. Fort, S. Rosi, F. Caruso, M. Inguscio, and M. B. Plenio, [Nature Communications \*\*4\*\* \(2013\)](#).
- [572] C. H. Bennett and D. P. DiVincenzo, [Nature \*\*404\*\*, 247 \(2000\)](#).
- [573] S. Bose, [Phys. Rev. Lett. \*\*91\*\*, 207901 \(2003\)](#).
- [574] M. Christandl, N. Datta, A. Ekert, and A. J. Landahl, [Phys. Rev. Lett. \*\*92\*\*, 187902 \(2004\)](#).
- [575] T. J. Osborne and N. Linden, [Phys. Rev. A \*\*69\*\*, 052315 \(2004\)](#).
- [576] L. Campos Venuti, C. Degli Esposti Boschi, and M. Roncaglia, [Phys. Rev. Lett. \*\*99\*\*, 060401 \(2007\)](#).
- [577] L. Trifunovic, F. L. Pedrocchi, and D. Loss, [Phys. Rev. X \*\*3\*\*, 041023 \(2013\)](#).
- [578] J. E. Lorenzo, L. P. Regnault, C. Boullier, N. Martin, A. H. Moudden, S. Vanishri, C. Marin, and A. Revcolevschi, [Phys. Rev. Lett. \*\*105\*\*, 097202 \(2010\)](#).
- [579] S. Sahling, G. Remenyi, C. Paulsen, P. Monceau, V. Saligrama, C. Marin, A. Revcolevschi, L. P. Regnault, S. Raymond, and J. E. Lorenzo, [Nat Phys \*\*11\*\*, 255 \(2015\)](#).
- [580] D. Loss and E. V. Sukhorukov, [Phys. Rev. Lett. \*\*84\*\*, 1035 \(2000\)](#).
- [581] G. Burkard, D. Loss, and E. V. Sukhorukov, [Phys. Rev. B \*\*61\*\*, R16303 \(2000\)](#).
- [582] N. M. Chtchelkatchev, G. Blatter, G. B. Lesovik, and T. Martin, [Phys. Rev. B \*\*66\*\*, 161320 \(2002\)](#).
- [583] C. Beenakker and C. Schönenberger, [Physics Today \*\*56\*\*, 37 \(2003\)](#).

- [584] A. Crépieux, R. Guyon, P. Devillard, and T. Martin, [Phys. Rev. B \*\*67\*\*, 205408 \(2003\)](#).
- [585] A. N. Jordan and M. Büttiker, [Phys. Rev. Lett. \*\*92\*\*, 247901 \(2004\)](#).
- [586] D. Dasenbrook and C. Flindt, [Phys. Rev. B \*\*92\*\*, 161412 \(2015\)](#).
- [587] L. S. Levitov and G. B. Lesovik, [JETP \*\*58\*\*, 230 \(1993\)](#).
- [588] M. Esposito, U. Harbola, and S. Mukamel, [Rev. Mod. Phys. \*\*81\*\*, 1665 \(2009\)](#).
- [589] D. Kambly, C. Flindt, and M. Büttiker, [Phys. Rev. B \*\*83\*\*, 075432 \(2011\)](#).
- [590] K. Okamoto and K. Nomura, [Physics Letters A \*\*169\*\*, 433 \(1992\)](#).
- [591] F. Alet, I. P. McCulloch, S. Capponi, and M. Mambrini, [Phys. Rev. B \*\*82\*\*, 094452 \(2010\)](#).
- [592] S. Eggert, I. Affleck, and M. Takahashi, [Phys. Rev. Lett. \*\*73\*\*, 332 \(1994\)](#).
- [593] M. A. Cazalilla, R. Citro, T. Giamarchi, E. Orignac, and M. Rigol, [Rev. Mod. Phys. \*\*83\*\*, 1405 \(2011\)](#).
- [594] F. D. M. Haldane, [Phys. Rev. Lett. \*\*47\*\*, 1840 \(1981\)](#).
- [595] W. Krauth, [Phys. Rev. B \*\*44\*\*, 9772 \(1991\)](#).
- [596] G. G. Batrouni and R. T. Scalettar, [Phys. Rev. B \*\*46\*\*, 9051 \(1992\)](#).
- [597] V. F. Elesin, V. A. Kashurnikov, and L. A. Openov, [JETP Lett. \*\*60\*\*, 177 \(1994\)](#).
- [598] V. A. Kashurnikov, A. V. Krasavin, and B. V. Svistunov, [JETP Lett. \*\*64\*\*, 99 \(1996\)](#).
- [599] N. Elstner and H. Monien, [Phys. Rev. B \*\*59\*\*, 12184 \(1999\)](#).
- [600] T. D. Kühner, S. R. White, and H. Monien, [Phys. Rev. B \*\*61\*\*, 12474 \(2000\)](#).

- [601] J. Zakrzewski and D. Delande, in *AIP Conference Proceedings*, Vol. 1076 (AIP Publishing, 2008) pp. 292–300.
- [602] G. Roux, T. Barthel, I. P. McCulloch, C. Kollath, U. Schollwöck, and T. Giamarchi, *Phys. Rev. A* **78**, 023628 (2008).
- [603] S. Ejima, H. Fehske, and F. Gebhard, *EPL* **93**, 30002 (2011).
- [604] I. Danshita and A. Polkovnikov, *Phys. Rev. A* **84**, 063637 (2011).
- [605] M. Gerster, M. Rizzi, F. Tschirsich, P. Silvi, R. Fazio, and S. Montangero, [arXiv:1510.01074](#) (2015).
- [606] G. Gershon, Y. Bomze, E. V. Sukhorukov, and M. Reznikov, *Phys. Rev. Lett.* **101**, 016803 (2008).
- [607] Q. Le Masne, H. Pothier, N. O. Birge, C. Urbina, and D. Esteve, *Phys. Rev. Lett.* **102**, 067002 (2009).
- [608] N. Ubbelohde, C. Fricke, C. Flindt, F. Hohls, and R. J. Haug, *Nat Commun* **3**, 612 (2012).
- [609] J. J. García-Ripoll and J. I. Cirac, *New J. Phys.* **5**, 76 (2003).
- [610] O. Mandel, M. Greiner, A. Widera, T. Rom, T. W. Hänsch, and I. Bloch, *Nature* **425**, 937 (2003).
- [611] P. Zoller, J. I. Cirac, L. Duan, and J. J. Garcia-Ripoll, [arXiv:quant-ph/0405025](#) (2004).
- [612] P. Treutlein, T. Steinmetz, Y. Colombe, B. Lev, P. Hommelhoff, J. Reichel, M. Greiner, O. Mandel, A. Widera, T. Rom, I. Bloch, and T. Hänsch, *Fortschr. Phys.* **54**, 702 (2006).
- [613] I. Bloch, J. Dalibard, and W. Zwerger, *Rev. Mod. Phys.* **80**, 885 (2008).
- [614] I. Bloch, *Nature* **453**, 1016 (2008).
- [615] P. Horodecki and A. Ekert, *Phys. Rev. Lett.* **89**, 127902 (2002).



- [616] P. Zanardi, C. Zalka, and L. Faoro, [Phys. Rev. A \*\*62\*\*, 030301 \(2000\)](#).
- [617] D. A. Abanin and E. Demler, [Phys. Rev. Lett. \*\*109\*\*, 020504 \(2012\)](#).
- [618] A. J. Daley, H. Pichler, J. Schachenmayer, and P. Zoller, [Phys. Rev. Lett. \*\*109\*\*, 020505 \(2012\)](#).
- [619] A. K. Ekert, C. M. Alves, D. K. L. Oi, M. Horodecki, P. Horodecki, and L. C. Kwek, [Phys. Rev. Lett. \*\*88\*\*, 217901 \(2002\)](#).
- [620] C. Moura Alves and D. Jaksch, [Phys. Rev. Lett. \*\*93\*\*, 110501 \(2004\)](#).
- [621] W. S. Bakr, J. I. Gillen, A. Peng, S. Fölling, and M. Greiner, [Nature \*\*462\*\*, 74 \(2009\)](#).
- [622] J. F. Sherson, C. Weitenberg, M. Endres, M. Cheneau, I. Bloch, and S. Kuhr, [Nature \*\*467\*\*, 68 \(2010\)](#).
- [623] D. F. V. James, P. G. Kwiat, W. J. Munro, and A. G. White, [Phys. Rev. A \*\*64\*\*, 052312 \(2001\)](#).
- [624] L. Mazza, D. Rossini, R. Fazio, and M. Endres, [New J. Phys. \*\*17\*\*, 013015 \(2015\)](#).
- [625] T. Fukuhara, S. Hild, J. Zeiher, P. Schauß, I. Bloch, M. Endres, and C. Gross, [arXiv:1504.02582 \(2015\)](#).
- [626] X.-G. Wen, [International Scholarly Research Notices \*\*2013\*\*, 198710 \(2013\)](#).